A DROPLET-BASED MICROFLUIDIC SCHEME FOR COMPLEX CHEMICAL REACTIONS

Dissertation

zur Erlangung des Grades
des Doktors der Naturwissenschaften
der Naturwissenschaftlich-Technischen Fakultät II
- Physik und Mechatronik -
der Universität des Saarlandes

von

Venkatachalam Chokkalingam

Saarbrücken

2010

Tag des Kolloquiums: 15.12.2010

Dekan: Univ.-Prof. Dr. rer. nat. Helmut Seidel

Mitglieder des Prüfungsausschusses:

Vorsitzender: Univ.-Prof. Dr. rer. nat. Helmut Seidel

Gutachter: Univ.-Prof. Dr. rer. nat. Ralf Seemann
Univ.-Prof. Dr. rer. nat. Albrecht Ott

Akademischer Mitarbeiter: Dr. Oliver Bäumchen

ABSTRACT

In the present work, a novel droplet-based microfluidic scheme is developed to perform chemical reactions. The chemical reactants are dispensed with precise volume control into pairs of droplets produced via step-emulsification. The reaction is activated by merging the pairs of droplets by a geometrical constriction and fast mixing inside the merged droplets. Furthermore, the post-processing of the chemical products is also included within the microfluidic device.

This microfluidic reaction scheme allows performing precisely volume controlled reactions with long and stable operation conditions without any clogging even if precipitates or sticky gels are formed during the reaction. We demonstrate the potential of our microfluidic scheme by producing mesoporous silica particles from a rapid gelation optimized sol-gel synthesis route. The produced silica particles have a superior surface area of about 820 m^2g^{-1} and a narrow pore radius distribution around 2.4 nm. This microfluidic scheme is quite universal and therefore, only the chemical recipe needed slight modifications to produce platinum doped silica catalysts with superior catalytic behavior than commercially available catalysts.

KURZZUSSAMENFASSUNG

In der hier vorliegenden Doktorarbeit wird ein neues, auf Tröpfchen basierenden, mikrofluidisches Verfahren präsentiert, um chemische Reaktionen durchzuführen. Die Reaktionspartner werden in Tropfenpaaren dispergiert, deren Volumen präzise eingestellt werden kann. Diese Tropfenpaare werden mittels einer Stufen-Emulgierung erzeugt. Die chemische Reaktion wird ausgelöst durch die Vereinigung der Tropfenpaare an einer geometrischen Engstelle. Homogene Reaktionsbedingungen werden durch das nachfolgende schnelle Durchmischen der vereinigten Tropfen erzielt. Darüber hinaus ist eine Nachbehandlung der chemischen Produkte in den mikrofluidischen Prozess mit eingeschlossen.

Dieses mikrofluidische Verfahren erlaubt die Durchführung präziser volumenkontrollierter Reaktionen mit langen und stabilen Operationsbedingungen, sogar wenn Ausfällungen oder klebrige Gele durch die Reaktion entstehen, ohne das sonst übliche Problem der Verstopfung der mikrofluidischen Kanäle. Wir demonstrieren das große Potential unseres mikrofluidischen Verfahrens durch die Herstellung mesoporöser Silica-Partikel mittels eines schnellen Sol-Gel-Verfahrens. Die hergestellten Silica-Partikel haben eine sehr große innere Oberfläche von ungefähr 820 m^2 g^{-1} und eine schmale Porenradienverteilung von etwa 2.4 nm. Diese Werte sind deutlich oberhalb üblicher Volumenverfahren und anderer mikrofluidischer Verfahren. Das tropfenbasierte Verfahren erscheint also ideal geeignet, um auch Platin dotierte Silica-Partikel für die heterogene Katalyse herzustellen. Da das entwickelte mikrofluidische Verfahren universell einsetzbar ist, musste hierzu einzig die chemische Rezeptur leicht modifiziert werden. Die erzeugten Platin dotierten Silica-Partikel weisen, wie erwartet, eine größere Oberfläche und eine größere katalytische Aktivität als kommerziell erhältliche Katalysatoren auf.

CONTENTS

LIST OF FIGURES

LIST OF TABLES

INTRODUCTION

In recent years, one of the important scientific developments is the progressive miniaturization of chemical and biological processes. This is achieved by manipulating very small volumes of fluid (micro-, nano-, pico- and even femto-liter volumes) with precise control using a technique known as "microfluidics". With the help of microfluidics, typical desktop laboratory procedures are miniaturized to a single "Lab-on-a-Chip" device [1-3]. The idea is to realize every process necessary e.g. sampling, sample pretreatment, reaction, separation, detection and analysis in one integrated device [4-6]. Also, handling sub microliter volume quantities is very important for many rare or expensive or toxic substances. With such an integrated microfluidic device, for example, minute volume blood samples might be sufficient to determine the exact levels of red and white blood cells as well as other blood components [7,8]. Due to the small sample size this analysis can be done within a very short time.

The simple linear downscaling of reaction vessels is not sufficient since the behavior of the fluids on the microfluidic scale differs significantly from the behavior of fluids on the macrofluidic scale. Flow in microfluidic devices typically occurs at low Reynolds numbers, such that the flow is purely laminar [9-11]. Due to this laminar flow, two or more streams flowing side-by-side will mix only by diffusion. Such a mixing is very slow to perform chemical reactions within the length scales typically used in microfluidic systems [9,12,13]. Due to the parabolic flow profile, dispersion along the microfluidic channel (Taylor dispersion [14]) is also a problem associated with the laminar flow.

One way to overcome these typical microfluidic obstacles is to use multiphase flows within microchannels. In order to avoid the axial dispersion, e.g. continuous phase liquid samples or reagents in form of slugs can be produced within microfluidic channels with gas as the separating dispersed phase [15-17]. Fast mixing is achieved within the liquid slug due to the friction induced recirculation motion [18-20]. Axial dispersion is eliminated because the liquid sample is not dispersed along the whole microfluidic channel but restricted within the volume of the liquid slug. But the liquid slug is directly in contact with the microfluidic channel walls and therefore, cross-contaminations and sticking of samples or reagents to the microchannel walls is unavoidable in this gas-liquid microfluidic system.

Alternatively, the reagents can be compartmented in droplets rather than in the continuous phase. This approach is termed as "droplet-based" microfluidic systems [21,22]. Here, the produced droplets in the form of emulsion are not in contact with the microchannel walls and therefore, cross-contaminations and the sticking of reagents inside the droplet to the microfluidic channel walls is avoided [23]. The other major advantages like fast mixing and no axial dispersion within the droplets to perform chemical reactions with different reagents remain unchanged [24]. The reagents for the reaction are already touching and reactive at the inlet nozzle even before being dispersed into droplets. This method where the reagents are in contact (reactive) at the inlet nozzle is not suitable for fast reactions where a gel or precipitate is formed. This will result in channel clogging [25-27] and therefore, long and stable operation conditions are not possible. This problem can be avoided only by initiating the reaction inside the microfluidic droplet. Due to its superior potential to control the process parameters, this type of droplet-based microfluidics have a large potential when combined with techniques to manipulate [28,29], redistribute [30] and split droplets [28,31].

In this thesis, we developed a droplet-based microfluidic scheme to perform fast chemical reactions without channel clogging with precise volume and process control. This microfluidic scheme enables the device to function for long operation times with stable conditions. For that every microfluidic processing step will be considered and adapted to meet the experimental requirements. We demonstrated this scheme explicitly for the production of mesoporous silica particles and platinum doped silica particles from a sol-gel synthesis route for heterogeneous catalysis.

The topic of this thesis focuses on microfluidic part as well as the sol-gel chemistry part and is organized as follows: In the first chapter, the theoretical background of microfluidics, the behavior of liquids at small length scales together with the background information on surfactants and emulsions. The fabrication of microfluidic devices and the chemicals used for emulsion droplet formation are described in the second chapter. In the third chapter, the droplet-based microfluidic scheme that will be used for sol-gel reactions will be outlined. Here, we explore droplet production, detection, merging and sorting methods. Since we will demonstrate this microfluidic scheme for performing sol-gel reactions to synthesize silica particles in the fifth chapter, we introduce the required background information on the sol-gel chemistry in the fourth chapter along with the required analyzing techniques.

1. MICROFLUIDIC BACKGROUND

1.1 Physics of liquids at small length scales

The characteristics of fluids at the microscale differ from macrofluidic behavior. The surface energies are dominant over the effect of gravity at small length scale. In order to understand and work with microfluidics, one must first understand the physical phenomena at microscale dimensions and this is discussed in the following sections.

1.1.1 Low Reynold's number hydrodynamics

The basic equation for the dynamics of an incompressible, uniform-viscosity, Newtonian fluid is the Navier-Stokes equations [32]:

$$\rho\left(\frac{\partial u}{\partial t} + \left(u \cdot \nabla\right)u\right) = -\nabla p + \eta\nabla^2 u + f \tag{1.1}$$

where ρ is the fluid density, u the fluid velocity, p the pressure, and η the fluid viscosity. Since fluids are continuum materials, the Navier-Stokes equation essentially represents the continuum version of Newton's law $F = ma$. Forces per unit volume on the right-hand side are balanced by

inertial acceleration terms on the left-hand side. *f* represents body force densities. To determine the relative effect of viscous to inertial forces, the dimensionless Reynold's number can be considered:

$$Re = \frac{\rho u l}{\eta} = \frac{inertial\ forces}{viscous\ forces} \qquad (1.2)$$

where *l* is a typical length scale of the observed system. On macroscopic dimensions, where turbulences are governing the flow behavior, Reynolds numbers of *10^3* or higher are found. Because of the small size of microchannels the Reynolds number in microfluidic system hardly exceeds unity and thus the flow is almost always laminar. In a typical channel with a diameter between 100 nm and 100 µm, where $\eta(H_2O) = 1.025 \times 10^{-3}$ Pa s, $\rho(H_2O) = 1000$ kg/m^3 and $u = 1$ cm/s, *Re* lies between 1 and 10^{-3}. One consequence of the laminar flow is that two or more streams flowing in contact with each other will not mix except by diffusion.

1.1.2 Diffusion and mixing in microfluidics

Mixing is a physical process required for many biological, chemical, and physical applications with the goal of achieving a uniform distribution of different components in a mixture, usually within a short period of time. Mixing is one of the main goals to achieve in microfluidics but occurs only by diffusion. Transport by diffusion is caused by random molecular motion that leads to homogenous distribution of all compounds. The difference in concentration is the driving force in the process. This is given by Fick's law [10, 32]:

$$j = -D\frac{dC}{dx} \qquad (1.3)$$

where *j* is the flux per area [moles/s/m^2], D is the diffusion coefficient [cm^2/s], C is the concentration [mg/dL] and *x* is the diffusion distance. The solute diffuses from the higher

concentration (C_1) into the less concentrated solution (C_2). If the concentration on both sides is known, the equation becomes:

$$j = \frac{D}{l} \cdot (C_1 - C_2) \tag{1.4}$$

where l is the known distance [m]. Typical values for the diffusion coefficient D are $10^{-4} - 10^{-5}$ m²/s for gases, 10^{-8} - 10^{-9} m²/s for self-diffusion in liquids, 10^{-9} - 10^{-11} m²/s for molecules in liquids e.g. depending on molecular weight. Due to the typical length scale of microfluidic devices, the time for this diffusive mixing often exceeds typical microfluidic processing times which is supposed to be faster for other steps, e.g. transport and analysis. For instance, small solutes with diffusion coefficients on the order of $D = 10^{-9}$ m²/s, mixing by diffusion across a 500 μm wide channel would result in a mixing time of several minutes. For larger solutes such as proteins ($D = 10^{-11}$ m²/s), the time needed for diffusive mixing becomes several hours or days. This large time scale is a hindrance for high-throughput microfluidic applications.
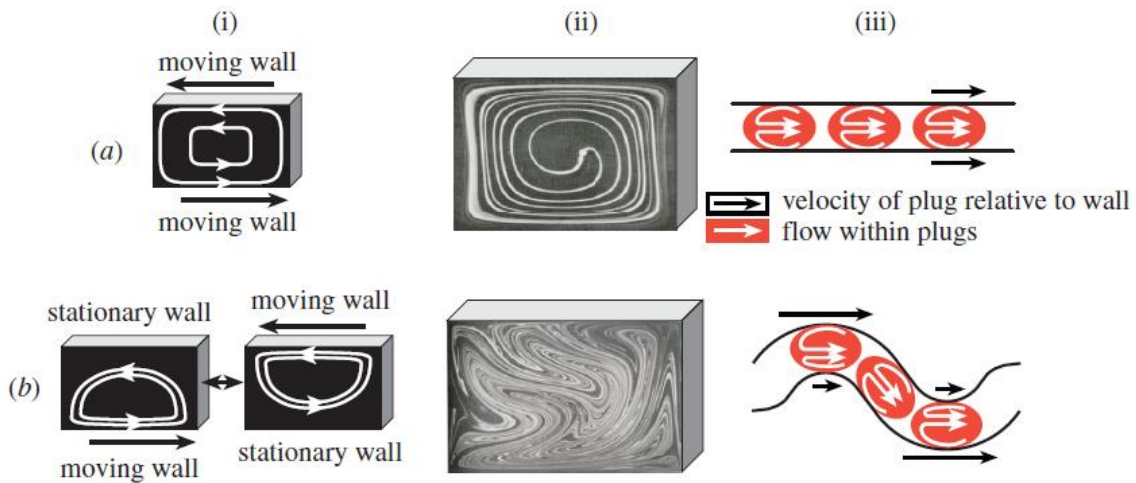
Figure 1. *Comparing mixing in flow cavities and in plugs moving through microchannels. Mixing by (a) steady, recirculating flow and (b) chaotic advection. (i) Mixing represented by schemes of flow in a flow cavity; (ii) images of flow in a flow cavity and (iii) schemes of flow in plugs moving through (a) a straight and (b) a winding channel. Images are taken from ref. 34.*

In droplet-based microfluidics, rapid internal mixing can be achieved within individual droplets, and is found to proceed quite efficiently where special channel geometries [18,33,34] are used. When a droplet moves through a straight channel, a recirculating flow is generated due to the friction with the side walls in each half of the droplet that touches the channel wall. Fluids within each half of the droplet are mixed, but the halves remain unmixed and separated from each other (see Fig. 1a). To enhance internal mixing within droplets, special channel geometries are used to create chaotic advection to fold and stretch the droplet contents [18,33-35] (see Fig. 1b). As the droplet travels through a winding channel, the halves of the droplet experience unequal recirculating flows. One half of the droplet is exposed to the inner arc of the winding channel, a shorter channel section, and thus a smaller recirculating flow is generated compared to the other droplet half which is exposed to a longer channel section. The irregular motion along the walls promotes chaos and crossing of fluid streams since the fluid vortexes of each half are asymmetrical. The droplets achieve an alternating asymmetric flow pattern through the serpentine microchannels. The sharp turns also help to reorient the droplet so that it becomes thoroughly mixed as it goes through a series of stretching, reorientation, and folding [35,36]. An advantage of this design is that the degree of mixing is determined by the length of the channel. These properties make the droplet-based microfluidics ideal to perform chemical or biological reactions.

1.2   Surface tension

In the case of droplet-based microfluidics, surface tension between two liquid phases is important especially for the formation and stability of emulsions. The attractive forces between molecules in bulk liquids are uniform in all directions resulting in a zero net force. However, at the liquid surface the molecules cannot form uniform interaction because the molecules on the gas phase are widely spaced and the molecular interactions are dominated by the surface molecules and the subsurface liquid molecules (non-zero net force). As a result, the molecules at the liquid surface have larger free energies than the molecules in the bulk liquid. This excess free energy per unit area is defined as surface tension, γ. Surface tension represents the amount of minimum work required per unit area to create a larger surface area i.e., the free energy per unit area of the surface between two phases (J/m^2) which can be also written as the force per unit length (N/m). Due to this force, a liquid

surface has a tendency to occupy a minimum surface area. The surface energy between two phases 1 and 2, γ_{12}, is expressed by:

$$\gamma_{12} = \gamma_1 + \gamma_2 - 2\psi_{12}$$ (1.5)

where γ_1, γ_2 and ψ_{12} are surface energy of phase 1, surface energy of phase 2, and interaction energy between 1 and 2 per unit area, respectively. Due to this surface tension, pressure difference exists across any curved liquid surface, with the pressure being greater on the concave side i.e., on the inside of a droplet or bubble. Consider an interface between phase A, in a droplet, and phase B, surrounding the droplet. These will have pressures P_A and P_B. If the principal radii of curvature are r_1 and r_2 then, the magnitude of this pressure differential is given by the Young–Laplace equation:

$$\Delta p = P_A - P_B = \gamma \left(\frac{1}{r_1} + \frac{1}{r_2} \right)$$ (1.6)

For spherical droplets or bubbles of radius r in an emulsion having $r = r_1 = r_2$,

$$\Delta p = P_A - P_B = \frac{2\gamma}{r}$$ (1.7)

so that Δp varies with the radius, r. The Young-Laplace equation shows that when $P_A > P_B$, then the pressure on the concave side i.e. inside a droplet or bubble exceeds the outside pressure.

1.2.1 Pendant drop method

There exist a number of different methods to measure the surface tension between two phases. Which method is preferred depends upon the nature of the phase being measured, the conditions under which the surface tension is to be measured, and the stability of its surface when it is

deformed. The pendant drop method involves the determination of the profile of a drop of a denser liquid being suspended from a syringe tip (see Fig. 2a) in another phase (air or liquid) at mechanical equilibrium. Gravity acts to elongate the drop while interfacial tension opposes elongation because of the associated increase in interfacial area. The profile of a drop of liquid suspended in another is thus determined by the balance between gravity and surface forces. If a droplet is imaged in a 2D projection, to get a reliable result, first, the drop has to be symmetric about a central vertical axis; this means it is irrelevant from which direction the drop is viewed. Second, the drop is not in motion in the sense that viscosity or inertia is playing a role in determining its shape; this means that surface tension and gravity are the only forces shaping the drop.
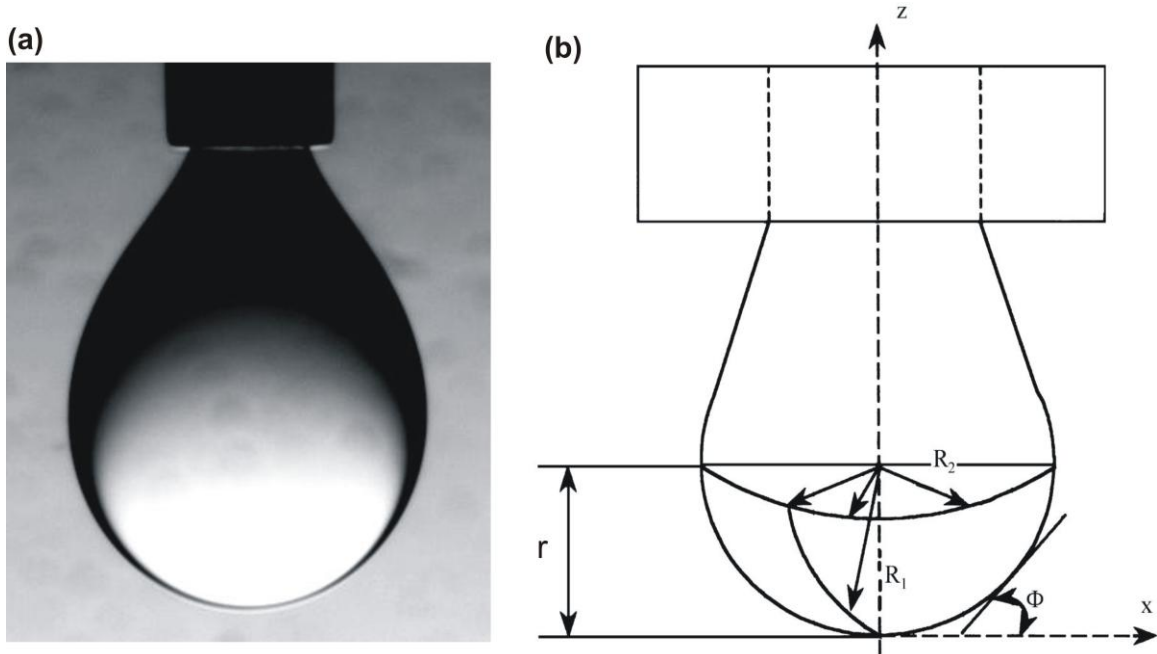
Figure 2. *(a) Oil drop hanging from a needle surrounded by water. (b) Sketch of the pendant drop geometry with parameters need to solve equation 1.8.*

In this case, the equation of Bashforth and Adams [37] which is based on Laplace's equation, relates the drop profile to the interfacial tension through a nonlinear differential equation which is given below:

$$\frac{1}{\left(\dfrac{R_1}{r}\right)} + \frac{\sin\phi}{\left(\dfrac{x}{r}\right)} = -B \cdot \left(\frac{z}{r}\right) + 2 \tag{1.8}$$

where B is given by

$$B = \frac{r^2\, g\, \Delta\rho}{\gamma} \tag{1.9}$$

where r is the radius of curvature at the apex of the drop, x, z, ϕ are the cylindrical coordinates as indicated in Fig. 2b and R_1 is the radius of curvature at the point with coordinates (x,z), $\Delta\rho$ is the difference between the densities of the two liquids in contact, g is the gravitational constant and γ is the surface tension between two liquids.

1.3   Contact angle

At the inlets where the liquids are injected into the microfluidic device and at the regions where the emulsion droplets are formed, wettability of the microfluidic channel walls has a significant impact. The wettability can be quantified by the 'contact angle' the liquid forms with the substrate. In the present section, the behavior of a liquid when it comes into contact with a solid surface will be discussed. One important factor for a two-phase microfluidic environment is the wetting property of the liquids with respect to each other and the substrate. In particular for droplet formation, the wetting principle involves how the fluids interact with the substrate. The contact angle, θ is the angle at which a fluid/fluid interface contacts a solid surface. Figure 3 shows a schematic diagram of three wetting cases. At the three phase contact line of a droplet, in equilibrium with the surface, the three horizontal components of the surface tensions (γ_{SL}, γ_{SV} *and* γ_{LV} each with a tendency to minimize their surface area) should be in balance [38-42]. Partial wetting occurs when θ is any value between 0° and 180°. Perfect wetting ($\theta = 0°$) describes the scenario in which one liquid wets the surface and the other liquid is separated from the surface by a thin film of the first and perfect

non-wetting occurs for $\theta = 180°$. The contact angle, θ is defined by balancing these three interfacial tensions and can be written in a form which is known as Young-Dupre equation (Eqn. 1.10) [43].

$$\gamma_{SV} - \gamma_{SL} = \gamma_{LV} \cos\theta \qquad (1.10)$$

(a) $\theta = 0°$ complete wetting

(b) $0° < \theta < 180°$ partial wetting

(c) $\theta = 180°$ non-wetting
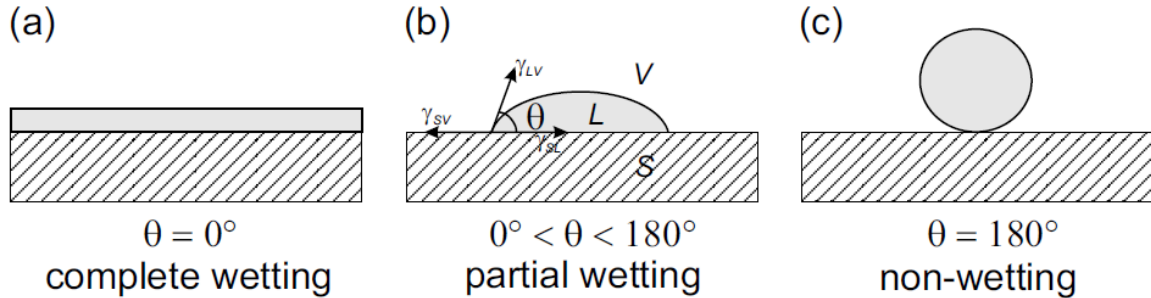
Figure 3. *Contact angle schematic for a solid liquid interface. The contact angle θ is determined by a force balance of the three surface tensions γ_{SL}, γ_{SV} and γ_{LV}. S, L and V denote the solid, liquid and vapor phase respectively.*

1.4   Emulsion science

In droplet-based microfluidics, some fundamental knowledge on emulsions is important to understand the generation and stabilization of droplets in microfluidic systems which will be discussed in this section. Normally, two immiscible liquids cannot form a stable emulsion. To allow for a suspension of one liquid in another to be stable enough to be classified as an emulsion, typically a third component of surface active agents must be present to stabilize the system. When an emulsion is formed, liquid droplets (the dispersed phase) are dispersed in a liquid medium (the continuous phase) via creation of an interface. The practical application of emulsions and emulsion technology is considerable, and includes dairy products [44], pharmaceutical preparations [45] and cosmetics [46]. High-pressure homogenization [47] is industrially used for producing emulsions. It consists of forcing two fluids or a coarse premix to flow through an inlet valve, into a mixing chamber, under the effect of a very high pressure. These techniques do not lead to homogeneous droplet sizes and are thus not applicable for microfluidic emulsion systems. Depending on the size

of the droplet, an emulsion is classified into three different groups namely macroemulsion, mini-emulsion and microemulsion. A macroemulsion is thermodynamically unstable but can be kinetically stabilized by surfactant and the droplet sizes typically range from a few to hundreds of microns. Using co-surfactant/surfactant systems droplet sizes down to about 100 nm may be produced and the resulting emulsions are referred to as miniemulsions [48]. Co-surfactants can be added to increase the stability of mini-emulsions and must be soluble in the dispersed phase. Another term for co-surfactant is co-stabilizer because of co-surfactant has no surface active properties. The role of the co-stabilizer, as the name suggests, is to act together with the surfactant to provide stability to the droplets. If interfacial tensions are reduced to very low levels though due to the larger amount of surfactant, even emulsions with a droplet sizes down to about 10 nm can be produced and the emulsion appears transparent due to the small size of the dispersed phase droplets. Such systems represent thermodynamically stable phases and are termed microemulsions [49]. In most of the emulsions, one of the phases is aqueous and the other is (in the widest sense of the term) hydrocarbon and referred to as oil. Two types of emulsion are readily distinguished in principle: if the oil is the dispersed phase, the emulsion is termed oil-in-water (O/W) emulsion and if the aqueous medium is the dispersed phase, the emulsion is termed water-in-oil (W/O) emulsion.

1.4.1 Surfactants and HLB

Two immiscible liquids cannot form a stable emulsion on storage. This breakdown of emulsions may proceed through two distinct mechanisms: Ostwald ripening [44,50] and coalescence [51]. Ostwald ripening is the expression given to the process whereby the droplet size distribution in an emulsion progressively shifts towards larger sizes. The smaller droplets have higher Laplace pressure than their larger counterparts. As a result, molecules of the dispersed phase diffuse from the high-pressure regions to the low-pressure ones, that is, the small droplets shrink and the larger ones grow as the material is transferred by diffusion through the continuous phase [49,52,53]. Coalescence refers to the process of thinning and rupturing of the thin liquid film that forms between two adjacent droplets resulting in the fusion of two or more droplets to form larger droplets. To avoid this emulsion breakdown and to prepare stable emulsions, a third component – an emulsifying surface active agent (surfactant) must be present typically (not true for surface ordering compounds like alkanes or liquid crystals at the right temperature or pickering emulsions).

The role of the surfactant is to reduce the interfacial tension between two phases by adsorbing at the liquid-liquid (or liquid/air) interface as an oriented interfacial film stabilizing the droplet. Surfactant molecules are amphiphilic compounds whose molecules contain polar (hydrophilic) head and non-polar (hydrophobic or lipophilic) tail parts (see Fig. 4a). They position at the interface, with the hydrophobic portion oriented towards the hydrophobic phase (air or oil) and the hydrophilic portion oriented towards the hydrophilic phase (water) (see Fig. 4b).

(a)

Hydrophilic Part
(or polar head)

Hydrophobic part

(b)

oil

water drop

surfactant molecule
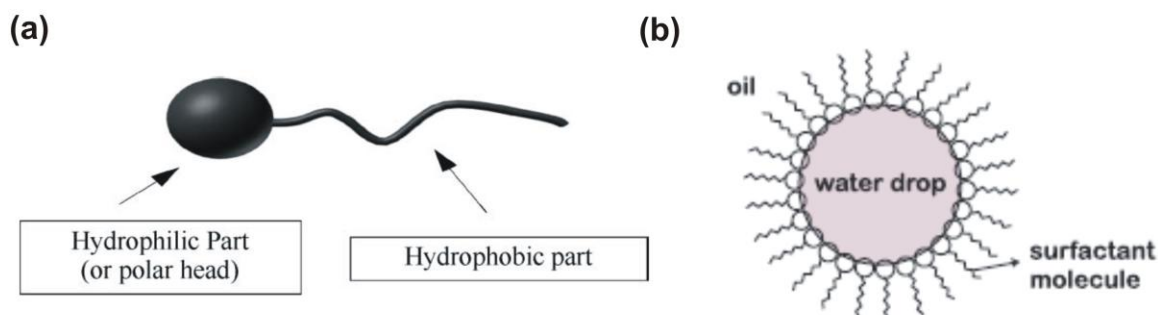
Figure 4. *(a) Diagram of a surfactant molecule. b) W/O emulsion stabilized by surfactant.*

As a result of surfactant adsorption, the surface tension of water/air interface is reduced from its value of 72 mN/m before adsorption to typically around 30–40 mN/m. Similarly, the surface tension for oil/water systems decreases from a value of 50 mN/m (for an alkane oil) before adsorption to a value of 1–10 mN/m, depending on the nature of the surfactant [54,55]. The nature of the surfactant can determine the type of the emulsion, i.e. which liquid will be dispersed as droplets and which will form the continuous phase. The surfactants which are more soluble in water tend to make oil-in-water (O/W) emulsions and surfactants more soluble in oil tend to make water-in-oil (W/O) emulsions. The balance between hydrophilic and lipophilic (hydrophobic) functional groups greatly influences the emulsion type [49,54,55]. However, there was no quantitative measure of this balance until 1949, when Griffin introduced the concept of the HLB, the Hydrophile-Lipophile Balance, as a way of predicting the emulsion type from the molecular composition of the surfactant. The HLB number is defined in terms of numerical values from their chemical formulae assigned to the chemical groupings in the surfactant, as follows:

$$HLB = 7 + \sum (\text{hydrophilic group numbers}) - \sum (\text{lipophilic group numbers})$$

The HLB characterizes the relative oil and water solubility of surfactants. The group numbers assigned by Davies and Rideal [54-57] are given in Table 1. The dimensionless scale ranges from 0 - 20 for non-ionic surfactants; a low HLB number indicates a more hydrophobic surfactant and a high HLB number indicates a more hydrophilic surfactant. Thus, W/O and O/W emulsions are favored for low and high HLB numbers, respectively. Most ionic surfactants have HLB values greater than 20, for example, sodium dodecyl sulfate (SDS) has an HLB of 40. For the microfluidic approaches to be discussed in the next chapters we will use water in oil emulsions to be able to adapt this system to many chemical or biological reactions.

Type	Chemical group	Group number
Lypophilic	$-CH-$	0.475
	$=CH-$	0.475
	$-CH_2-$	0.475
	CH_3-	0.475
Hydrophilic	$-SO_4Na$	38.7
	$-COOK$	21.1
	$-COONa$	19.1
	$-SO_3Na$	11.0
	$=N-$	9.4
	Ester (sorbitan ring)	6.8
	Ester (free)	2.4
	$-COOH$	2.1
	$-OH$ (free)	1.9
	$-O-$	1.3
	$-OH$ (sorbitan ring)	0.5

Table 1. *HLB numbers for various chemical groups.*

2. MATERIALS AND EXPERIMENTAL SET-UP

In the previous chapter we discussed the theoretical background that is important for droplet-based microfluidics. In this chapter, we will introduce and discuss the particular emulsion systems used for the various experiments and the techniques applied for the fabrication and operation of microfluidic devices.

2.1   Emulsion systems

Water-in-oil (W/O) emulsions are good candidates for applications where aqueous phase chemical reactions are required and are used throughout this thesis. We used the following types of emulsion systems in our microfluidic devices, depending on the experimental aim. To explore and test the properties of the microfluidic devices, we used a low cost, stable and easy to handle system consisting of an aqueous dispersed phase (Millipore^{TM} water) dispensed in the low viscosity oil (Isopar$^{™}$ M, Exxon Mobil, $\eta = 2.1$ mPas) as continuous phase. Non-ionic surfactant, 2 wt. % Span 80 ($C_{24}H_{44}O_6$, sorbitan monooleate), which has a HLB value of 4, was added to the continuous phase to stabilize the single droplets from merging. Figure 5 shows the molecular structure of the amphiphilic Span 80 where the hydrophilic sorbitan group acts as the polar head and the hydrophobic oleic acid group acts as the nonpolar tail. This emulsion is very stable allowing for long observation times in the microchannels. The surface tension of this system is obtained by the

pendant drop technique discussed in section 1.2.1 and is around 4.8 mN/m. This system performs very well for channels made of poly (methylmethacrylate) (PMMA) and SU-8 but could not be extended to channels made of poly (dimethylsiloxane) (PDMS) since Isopar™ M oil swells PDMS and could not be used for long time emulsion production. To overcome this swelling problem, aqueous phase (Millipore^{TM} water) was dispensed in a fluorinated oil e.g. FC-40 (ABCR GmbH, Germany), perfluorodecalin (PFD) ($C_{10}F_{18}$, ABCR GmbH, Germany) as the continuous oil phase. Besides, neither the aqueous phase nor the organic compounds are soluble in the fluorinated oils. This emulsion system is stabilized by suitable surfactants.
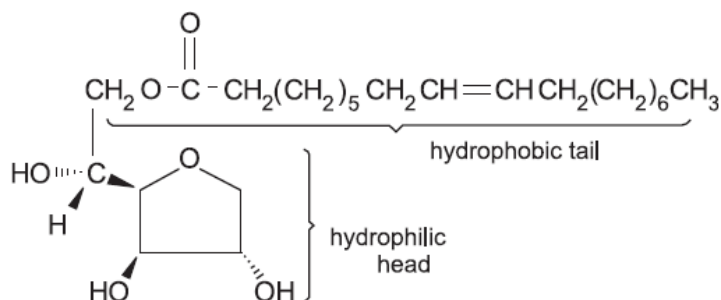
Figure 5. *Molecular structure of Span 80, showing the hydrophilic head (sorbitan) and hydrophobic tail (oleic acid) parts.*

For FC-40 oil phase, 2.5 wt. % Krytox® 157 FSL (DuPont, Germany) which is a surfactant made of the carboxylic acid forms of the perfluorinated polyether (PFPE) is added. This system results in very stable droplet production up to high dispersed phase volume fraction (similar to the Isopar™ M and Span 80 system) and merging of the droplets can only be achieved through electro-coalescence as will be discussed in section 3.4. For PFD oil phase, 20 wt.% of the penta decaflouoro-1-octanol ($C_8H_3F_{15}O$, ABCR GmbH & Co. KG), which is a oil-soluble fluorinated surfactant is added. This system results in droplet production but with less stability such that the drops merge when they pass through geometrical constrictions or densely packed. We used this PFD system to produce stable drops from the dispersed phases consisting of methanol and water (in chapter 5) to achieve the sol-gel chemistry inside microfluidic channels. Figure 6 shows the water/PFD and the water + methanol/PFD interfacial tension as function of the penta decaflouoro-1-octanol surfactant concentration using the pendant drop analyzer (Data Physics GmbH, Germany)

as described in section 1.2.1. Interestingly, the presence of the methanol lowers the surface tension and also the stability of the emulsion droplets significantly.
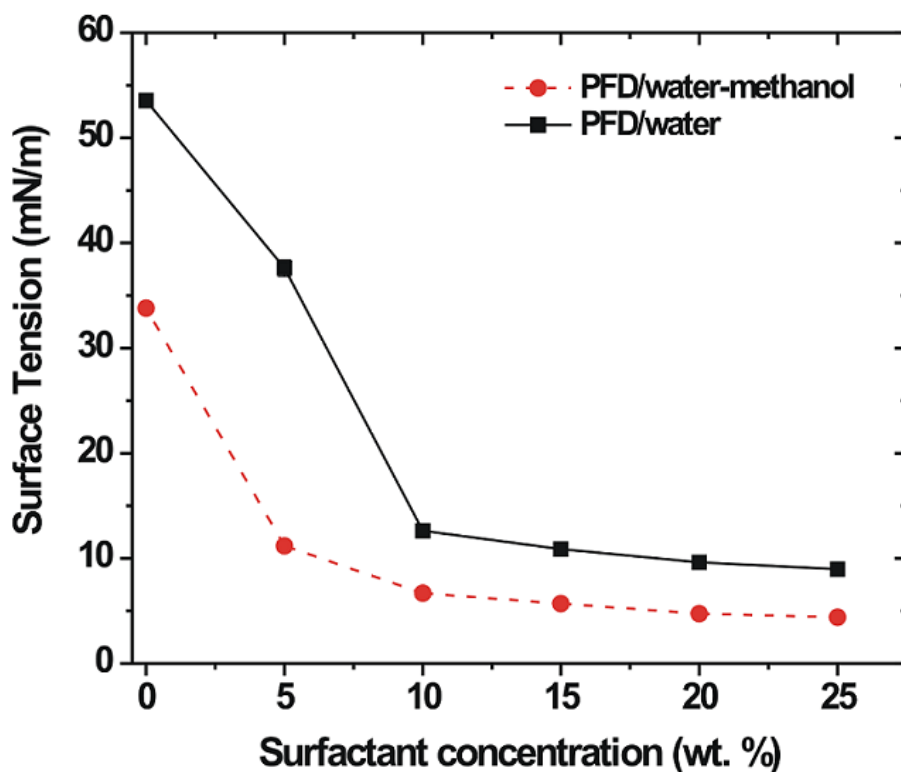
Figure 6. *Interfacial tension of the perfluorodecalin oil/water and the perfluorodecalin oil /methanol-water (60/40 v/v as used for sol-gel reactions discussed in chapter 5) mixture as function of the surfactant concentration (penta decaflouoro-1-octanol).*

2.2   Microfluidic device fabrication

The fabrication of microfluidic devices has become a subspecialty of micro-electro-mechanical systems (MEMS). Silicon microfabrication was well-established already in integrated circuit (IC) processes and therefore first microfluidic systems applied silicon as a material for the devices [1-3]. Glass has been the traditional material for chemical analysis and reactions and therefore it was also a natural choice for microchips. However, microfabrication in glass and silicon substrates is not

simple due to several fabrication steps for e.g. etching, wafer bonding *etc*. Polymer microfabrication techniques were developed later to reduce fabrication time and increase fabrication volumes [58-60]. Wide selection of polymeric materials and fabrication techniques gives suitable methods and materials for most applications. Therefore, we only used polymeric devices in this thesis, which will be explained in the following. For droplet-based microfluidics, the channel material used should have a suitable chemical resistance and wettability for stable droplet generation. In the following, two methods for fabricating microfluidic channels used in this thesis will be presented. Depending on the dimensions of the channels, the devices are fabricated using either micro-machining (section 2.2.1) or photolithographic methods (section 2.2.2). For the larger channel dimensions (critical dimension larger than 200 µm), the channels could be directly micro-machined in a PMMA block. For channel dimensions less than 200 µm, we developed photolithographic methods and a bonding technique to form channels in polymer materials. Depending on the ease of fabrication and the polymeric material needed for the microfluidic channel wall, this photolithographic method is also extended for soft-lithography fabrication as will be discussed in this section.

2.2.1   Direct micro-machining

Poly (methylmethacrylate) (PMMA) is one of the typical materials for polymer microchannel fabrications with the features of good chemical resistance, wettability together with low cost, high transparency and excellent mechanical properties [61,62]. Microfluidic device design and dimensions were drawn using Solid Edge^{TM} which is a 2D/3D CAD software. Later, this design is fabricated by micromachining in a PMMA block (Lutze GmbH & Co. AG) and sealed with another 2 mm thick PMMA cover block using metal screws (see Fig. 7). One end of the polytetrafluoroethylene (PTFE) tubing (inner diameter of 0.8 mm, outer diameter of 1.6 mm) (VWR, Germany) is shaped with a flange tool and fitted into the thread of the PMMA element through plastic screws (Novodirect GmbH, Germany). This connection can be used for high pressure applications due to the perfect transition between the tube and microchannel. Furthermore, this device was reusable after cleaning with ethanol and drying under nitrogen flow. This reuse was possible because the cover block can be removed and sealed again.
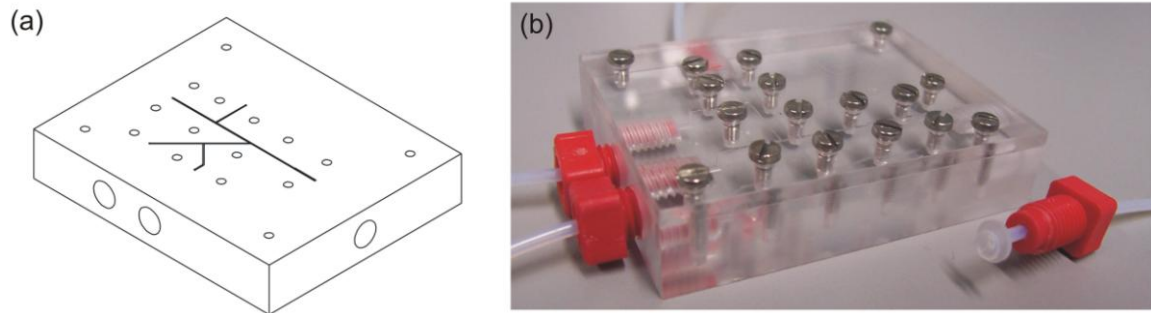
Figure 7. *(a) Schematic of the device designed with Solid Edge (b) Micromachined PMMA device connected with tubing.*

2.2.2 Photolithographic fabrication

In order to scale down our devices, photolithographic fabrication was employed. We used SU-8 photoresist for our fabrication purpose. SU-8 is an epoxy photoresist developed by IBM and is one of the most widely used materials for microfluidic structures [63-66]. SU-8 is a negative photoresist, which means that the exposed portions of the films are crosslinked rendering them insoluble to the developer solution (mr-Dev600, Micro Resist Technology GmbH, Germany) [1,64,67]. The oligomers in SU-8 have high density of epoxy groups that can form tightly cross-linked structure during curing. SU-8 has been shown to be hydrophobic [66,68] and compatible with most chemicals applied in analytical applications [69,70]. SU-8 is also mechanically strong and optically transparent for wavelengths above 350 nm. These properties enable patterning of thick layers with high aspect ratios and vertical walls. Layer thicknesses over 2 mm have been demonstrated and with proper optimization aspect ratios greater than 1:18 can be obtained with UV-exposure of SU-8 [71]. Hence structures similar to silicon Deep Reactive Ion Etching (DRIE) can be fabricated with SU-8 photolithography process.

In this thesis, we could fabricate microchannels directly in SU-8 photoresist (Micro Resist Technology GmbH, Germany) for channel widths down to 10 μm (for transparency masks) with a single ultra-violet (UV) exposure step. The device fabrication (see Fig. 8) starts with creating a design in an AutoCAD® program. A high resolution commercial image setter then prints this design on a transparency (JD Photo tools, UK). This transparency serves as the photomask in contact

photolithography to produce a negative relief in photoresist on a glass substrate. A round glass disk with 50 mm diameter (VWR, Germany) is pre-coated with Omnicoat for better adhesion of SU8 to glass. Then a 5 μm thick underlayer of SU8-2005 was applied to ensure homogeneous wetting behaviour on all channel walls, and exposed to UV without mask to crosslink the underlayer. The crosslinked layer was treated with oxygen plasma (Diener electronic GmbH, Germany) for 30 s to render the surface hydrophilic for improved spin-coating of the following coating. Afterwards, either SU8-100 photoresist (viscosity of 52407 cSt) or SU8-50 photoresist (viscosity of 14953 cSt) for 80-120 μm deep channels or 20-50 μm deep channels respectively were spun onto the wafer.

Spin coating parameters were optimized to achieve the desired film thickness, e.g. to prepare 120 μm deep channels, 1500 rpm for 30 s with 5 s ramping time was used. Subsequently, the sample was soft baked (drying of the photoresist film and improving photoresist adhesion to the wafer) in order to evaporate the solvent and densify the film. Soft baking times were based on the film thickness. For 120 μm layer thickness, the samples were baked for 13 min at 65°C and 37 mins at 95°C. Then, the samples were exposed to UV light ($\lambda = 365$ nm) in the mask aligner (ABM Inc., Model 60 Exposure systems, USA) for 30 s through the photomask. Upon exposure, the cross-linking proceeds in-two-steps; the formation of a strong acid during the exposure process is followed by an acid-initiated, thermally driven epoxy cross-linking step during the post exposure bake. After exposure, the sample is post-baked for a time which depends on the thickness of the photoresist (1 min at 65°C and 7 min at 95°C for 120 μm thick resist; 1 min at 65°C and 2 min at 95°C for 30-50 μm thick resist). The samples were rinsed with developer to remove the non-crosslinked regions, which were shaded by the mask. For high aspect ratio channels a few seconds of ultrasonication in the developer solution is needed to fully develop the channels. Thus the fabrication of the SU-8 structures was accomplished on a glass disk. This disk can be used directly in order to have SU-8 material as channel wall which we will refer to as 'SU-8 devices' or this disk can be alternatively used as a mold or master for soft-lithographic technique [72-74] to have PDMS channel walls referred as 'PDMS devices'.
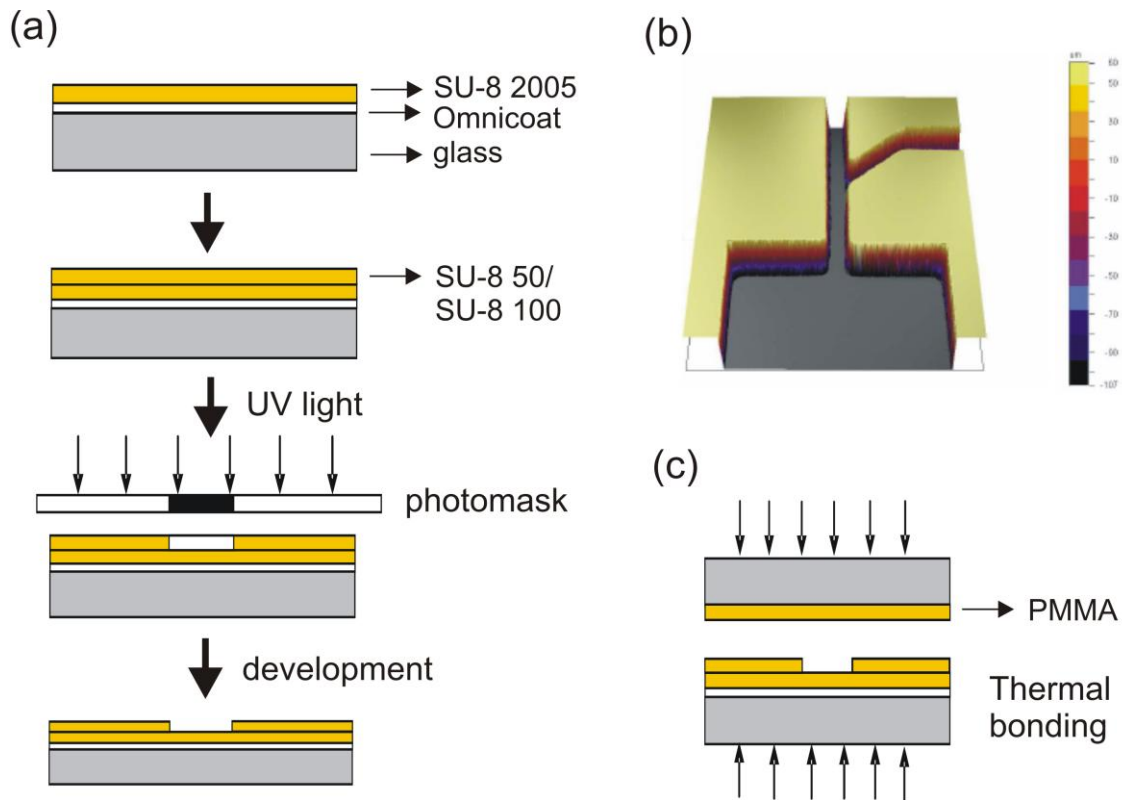
Figure 8. *Schematic overview of the microfluidic device fabrication by photolithography. (a) Fabrication of the SU-8 microfluidic channels. (b) Channel cross section captured by white light interferometry. (c) Thermal bonding to cover the microfluidic channels.*

In order to have SU-8 devices, holes were drilled into the supporting glass substrate to have inlets and outlets in the structured SU-8 photoresist. The channels were closed by thermally bonding a second glass disk coated with a 10 μm thick PMMA layer at 160°C using a mechanical press. To perform electro-coalescence in the microfluidic device, prior to bonding, gold electrodes with an underlying chromium adhesion layer were thermally vapour deposited at 10^{-6} mbar onto the cover glass. Wires were glued to the electrodes using electrically conducting epoxy resin (ITW Chemtronics®) to contact the evaporated electrodes prior to the PMMA layer. Teflon tubing was connected to the microfluidic device via Nanoports^{TM} (Up-Church), which were bonded to the device as shown in Fig. 9. The detailed photolithographic fabrication recipes for different channel depths are given in the appendix.
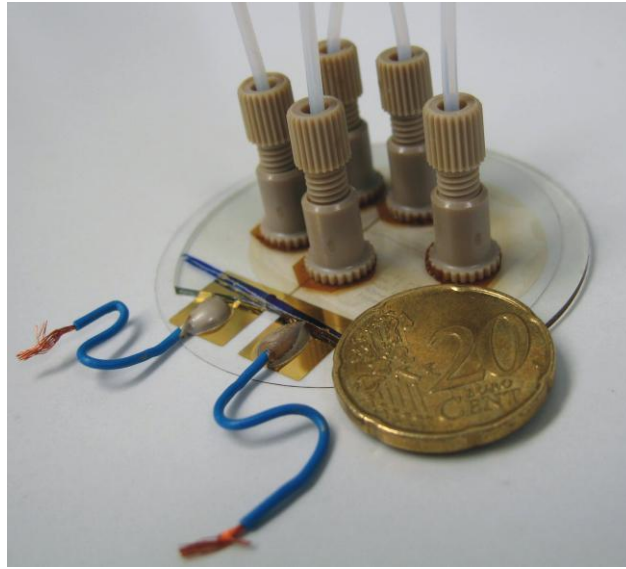
Figure 9. *Image of a completed device with fluid and electrode connections.. The diameter of the glass disks is 50 mm and the channel width is typically 20-100 μm. The teflon tubing are connected to the device via Nanoports^{TM}.*

In addition to low costs associated with producing PDMS devices, one could fabricate several PDMS devices from a single SU-8 master which is not the case with SU-8 channel wall devices. Within the framework of this thesis, to fabricate PDMS devices, soft lithography technique was employed. An elastomeric block with patterned relief structures on its surface is the key to soft lithography. PDMS has a unique combination of properties resulting from the presence of an inorganic siloxane backbone and organic methyl groups attached to silicon. They have very low glass transition temperatures and hence are fluids at room temperature. These liquid materials can be readily converted into solid elastomers by cross-linking. The PDMS elastomer Sylgard™ 184 (Dow Corning GmbH, Germany) was used for microfluidic device fabrication. It comes in two parts: a liquid silicone rubber base (i.e. a vinyl-terminated PDMS) and a catalyst or curing agent (i.e. a mixture of a platinum complex and copolymers of methylhydrosiloxane and dimethylsiloxane). A photo-lithographically prepared SU-8 structure on silicon wafer was used as the master with inversed pattern structure. The main steps in fabricating are sketched in Fig. 10a.
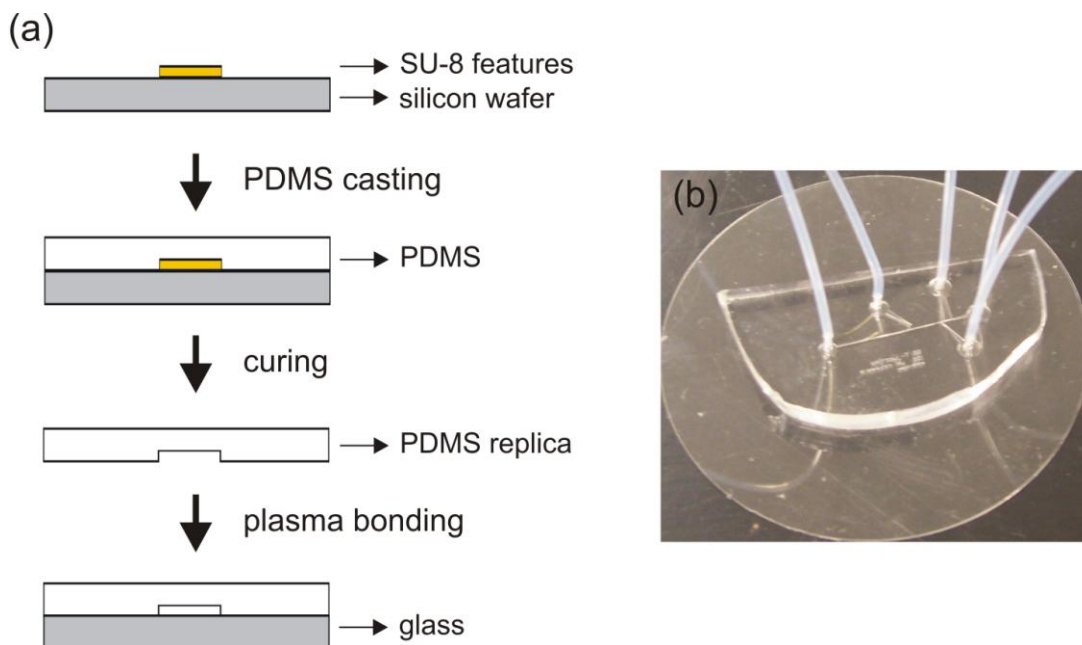
Figure 10. *(a) Schematic of PDMS Device Fabrication. (b) PDMS device connected with tubing.*

PDMS base and curing agent was mixed in a ratio of 10:1 w/w, degassed and decanted onto the SU-8 master. Once mixed, poured over the master and heated to elevated temperatures, the liquid mixture becomes a solid, cross-linked elastomer in a few hours via the hydrosilylation reaction between vinyl ($SiCH=CH_2$) groups and hydrosilane (SiH) groups [72]. The multiple reaction sites on both the base and crosslinking oligomers allow for three-dimensional crosslinking. After thermal curing overnight in an oven at 65 °C, the PDMS has a low surface energy which usually facilitates easy peeling of the PDMS structure from the SU-8 master. In order to use these PDMS structures as microfluidic devices, inlet holes need to be punched and the channels need to be sealed by another glass slide. Although different techniques have been reported for PDMS-glass bonding surface activation by oxygen plasma is the most commonly used technique [75,76] and we used the same technique (Diener electronic GmbH, Germany). The plasma treatment makes the channels hydrophilic. In order to produce aqueous droplets in oil within microchannels, the surfaces of the bonded devices were rendered back to hydrophobic nature by heating the devices to 60 °C for at least 6 hours. Teflon tubing was connected to the punched holes (Fig. 10b) and the other end of the tubing was connected to gas tight precision glass syringes (Hamilton Bonaduz AG, Switzerland) connected to custom-made syringe pumps as will be discussed in the subsequent section.

2.3   Experimental set-up

A Leica Z16 APO optical microscope with a Leica L5 FL light source (Fig. 11a), was typically used to monitor the microfluidic processes. Images and movies were recorded using a high resolution CCD camera (PCO 1600 hs, PCO AG, Germany) through the CamWare software. When needed, a high speed CMOS camera (PCO 1200 hs, PCO AG, Germany) which is able to capture more than 600 frames per second was used. Typical exposure times ranged from 500 µs to 50 ms, depending on flow velocity. The flow rates were adjusted using custom-made syringe pumps (Fig. 11b) driven by dc motors with decoder and controlled by programs written in LabView (National Instruments Corporation). Using glass syringes (Hamilton) with various diameters, flow rates between 10 µl/h and 1 ml/h could be achieved. Image analysis was done using softwares: Image-Pro Plus 6.3 (Media Cybernetics, Inc., USA) and ImageJ 1.42 (National Institute for Health, USA).
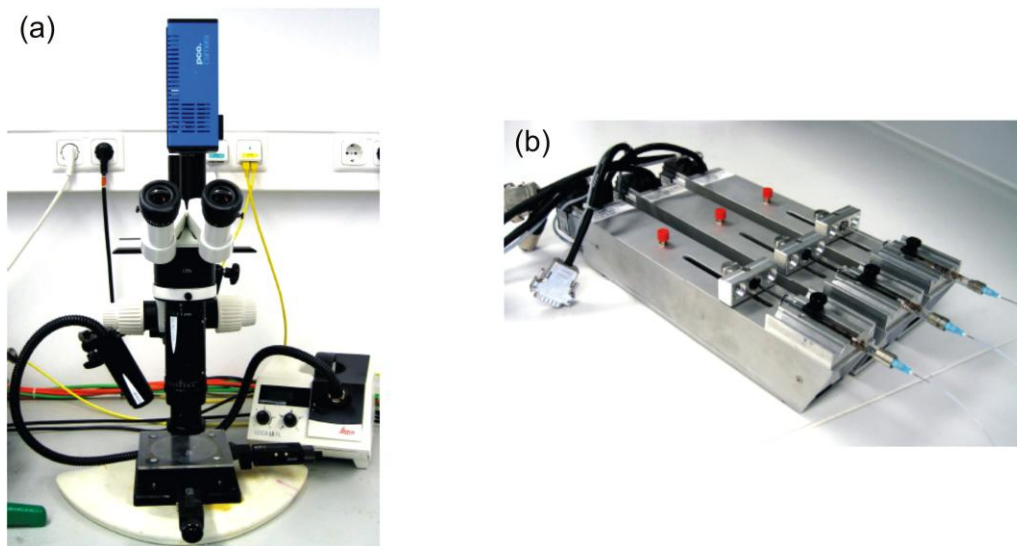
Figure 11.   *a) Z16 APO Leica microscope with a Leica L5 FL light source and camera. b) pumps with glass syringes (Hamilton).*

3. DROPLET-BASED MICROFLUIDIC SCHEME

3.1 Droplet generation

For many of the droplet-based microfluidic applications, it is desirable to generate monodisperse emulsion droplets directly in a microfluidic device with adjustable volume, volume fraction and production rate. A variety of techniques have been developed for controlled generation of droplets in a microfluidic system based on the geometry of microchannels [77-81]. In this section, we will focus on: the most important microfluidic designs for droplet generation that were already existing (T-junction – section 3.1.1, hydrodynamic flow-focusing – section 3.1.2) and designs we developed during the framework of this thesis (step-emulsification – section 3.1.3) to meet the requirements of this project.

3.1.1 T-junction emulsification

Due to its simplicity the most common microfluidic geometry used for the generation of droplets is the T-junction geometry (see Fig. 12) [82-84] and this can also be used for the formation of bubbles [18,85] and double emulsions [86,87] in a host of analytical applications [35,88,89]. In the T-junction configuration, the inlet channel containing the dispersed phase intersects the main channel which contains the continuous phase. Here, the dispersed aqueous phase enters the main channel

and flows until the continuous oil phase forces the dispersed phase to elongate in the downstream direction, while the neck at the entrance to the main channel begins to thin. Eventually the neck breaks, creating a droplet that travels down the main channel and the remaining dispersed phase retreats towards the inlet.
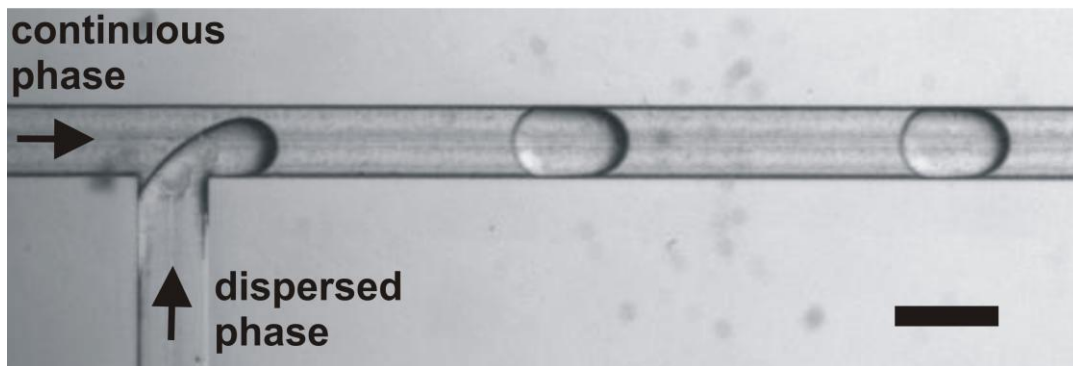
Figure 12. *Droplet generation in a T-junction microfluidic device. Scale bar: 100 μm.*

The size of the droplets is determined solely by the ratio of the volumetric rates of flow of the two immiscible fluids (i.e. aqueous and oil phases). This characteristic leads to a simple scaling law [90] for the size of the discrete fluid segments:

$$L/w = 1 + \alpha * (Q_d/Q_c) \qquad (3.1)$$

where L is the length of the droplet, w is the width of the channel, Q_d is the flow rate of the dispersed fluid, Q_c is the flow rate of the carrier fluid and α is a constant that depends on the geometry of the T-junction. Although the system remains at low Reynolds number, the flow is nonlinear because of interactions on the boundary between the two fluids. Here, the boundary is not static and that the motion of one fluid can carry along the other [91]. The resulting instability that drives droplet formation is due to the competition between surface tension and shear forces [92]. The size of the produced droplets can be varied in a wide range by altering the fluid flow rates, the channel dimensions or by changing the relative viscosity between the two phases.

T-Junctions are not limited to single inlets as more complicated schemes have been used for performing chemical reactions [88,93], and forming gas plugs [18,88] and droplets of alternating composition [89]. However, the limited range of volume fraction and the critical flow velocity needed for droplet break-up, polydispersity and difficulty to change the production frequency without changing the droplet size are the drawbacks of the T-junction method. Within the framework of this thesis, we used a simple T-junction device to test different combinations of surfactants and oils for stable droplet generation since it allows varying the produced droplet sizes within a very large range.

3.1.2   Hydrodynamic flow-focusing

A second commonly used microfluidic design that produces monodisperse droplets is a flow-focusing device which has a very high droplet production frequency (several thousands of droplets per second) and excellent monodispersity [94-96].

A flow-focusing device contains two lateral channels and a main channel. The main channel carries the aqueous dispersed phase, while the lateral channels carry the oily continuous phase (see Fig. 13). The two phases are forced to flow through a small orifice downstream of the channels. The continuous phase from the lateral channels exerts pressure and viscous stresses that forces the dispersed phase into a narrow thread while flowing through the orifice. This narrow thread breaks off inside or downstream of the orifice. It is a Rayleigh-Plateau type instability where the flow rates of the continuous and dispersed liquids, the ratio of the flow rates, the width of the channels and the size of the orifice determine the size of the droplets. The droplet size is not limited by the orifice size, i.e. droplets can be much smaller or larger than the orifice size and can be adjusted by changing the relative flow velocities of the two fluid phases.

The droplet generation in the flow-focusing design can be achieved without surfactants, although their use might support stable and monodisperse droplet generation. The device geometry is more complicated than the T-junction geometry. Moreover, flow-focusing design needs many tubings at the inlets because of the presence of two lateral channels for the continuous phase and one main channel for the aqueous phase. Many variations of the basic flow focusing design have

been developed to facilitate more complex applications [97]. Flow focusing channels may be fabricated using different methods including soft lithography, the insertion of capillary sheathes into microdevices [87], incorporating pneumatically controlled walls to widen or narrow the flow focusing region [98] and electrical control of flow-focusing droplet generation [99].
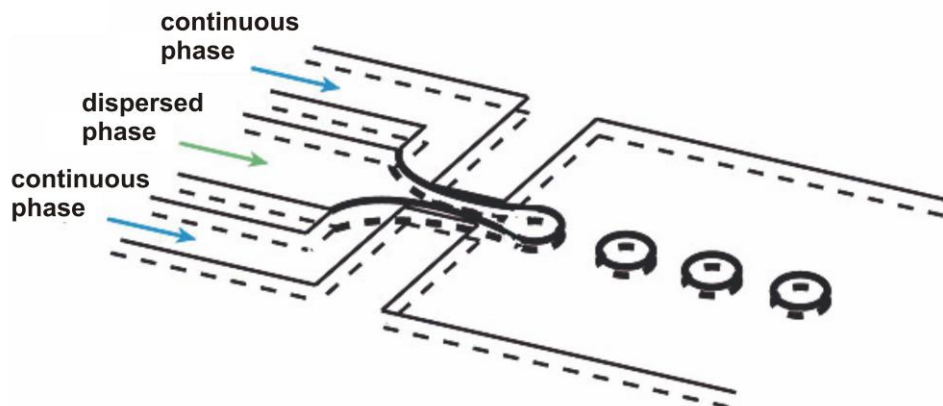
Figure 13. *(a) A schematic diagram of a flow-focusing microfluidic design. In a microfluidic flow-focusing device, streams of continuous phase pinch off a dispersed phase thread to produce monodisperse droplets. The flow rate of the phases controls the size of the droplets, and the frequency with which they form. Image adopted from ref. 96.*

3.1.3   Step-emulsification

A simple to handle device to produce emulsions in a large parameter range and with excellent monodispersity was introduced by Priest *et al.* as 'step-emulsification' (see Fig. 14) [100]. Priest *et al.* directly micromachined the microfluidic channels into PMMA (as described in section 2.2.1) which allows for the fabrication of a topographic step. This microfluidic design consists of a T-junction at a shallow rectangular channel connected to a three-dimensional channel. The dispersed phase is injected into the continuous phase where it is guided in a shallow channel and stabilized by the surrounding continuous phase and channel geometry where fluctuations of a fine liquid thread are effectively suppressed. When the stream enters to the deep channel at the topographic step, the continuous stream of the dispersed phase breaks-up into extremely monodisperse droplets (Coefficient of Variance (CV) in droplet diameter < 1.2%). It offers an adjustable droplet

production frequency from several tenths up to several hundred droplets per second, with excellent monodispersity, whereas the volume fraction (φ) of the dispersed phase might be up to 96%. But the PMMA micromachining of these devices clearly sets a lower limit for the channel dimensions.
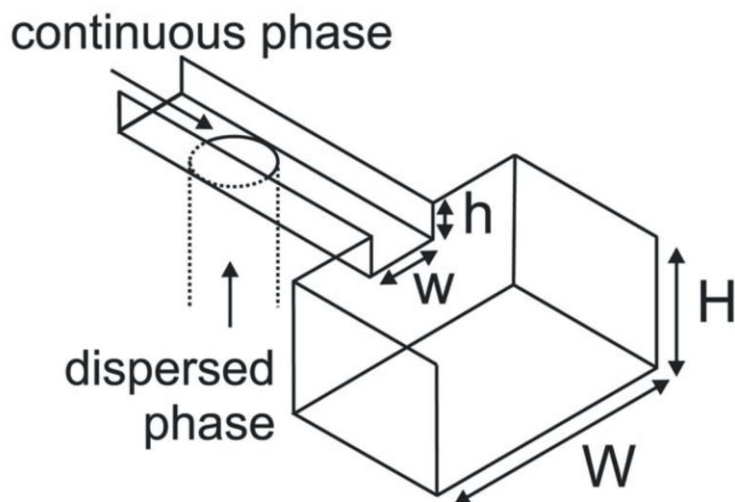
Figure 14. *Schematic of a step-emulsification device fabricated by micromachining in PMMA. (w = 200 μm and* h *= 10, 22, or 43 μm, while* H = W *= 250 μm).*

To downscale the channel size compared to the micromachined PMMA devices, within the framework of this thesis, we optimized the geometry of the step-emulsification to be fabricated in a single photolithographic exposure step as described in the section 2.2.2. To achieve this, we rotated the device geometry as introduced by Priest et al. [100] by 90 degrees to be in the plane of the photoresist. A schematic of our device is shown in Fig. 15. Identical to the behavior found for the step-emulsification device that was micro-machined into PMMA [100] we found that the drop formation proceeds via three mechanisms: shear at the inlet, where the droplets are produced by the inlet acting as a simple *T*-junction (Fig. 16a), via step-emulsification i.e. droplet formation directly at the transition from the high aspect channel to the low aspect ratio channel (Fig. 16b) or injection of a liquid jet in the wider channel (Fig. 16c).
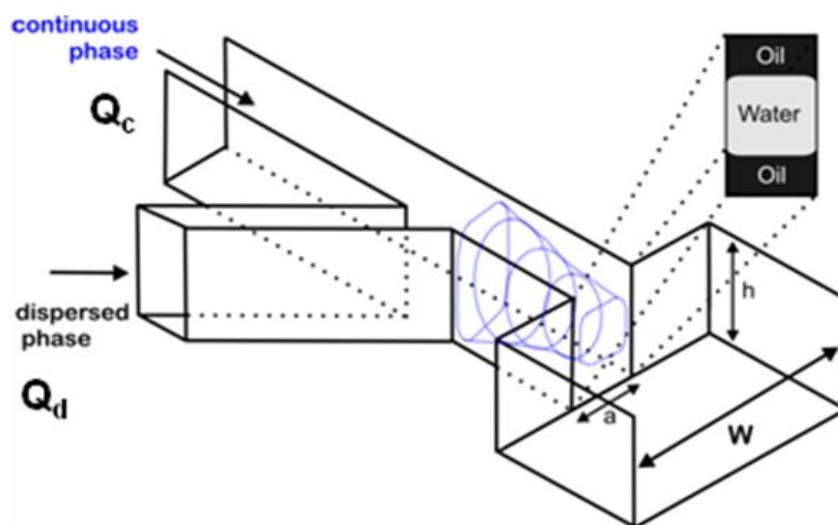
Figure 15. *Schematic of a step-emulsification device fabricated by photolithography. The formation of the dispersed phase liquid into the high aspect ratio channel is indicated with blue dotted lines together with the cross section of the stream right before reaching the low aspect ratio channel. (a = 35 μm, h =120 μm and W = 160 μm).*
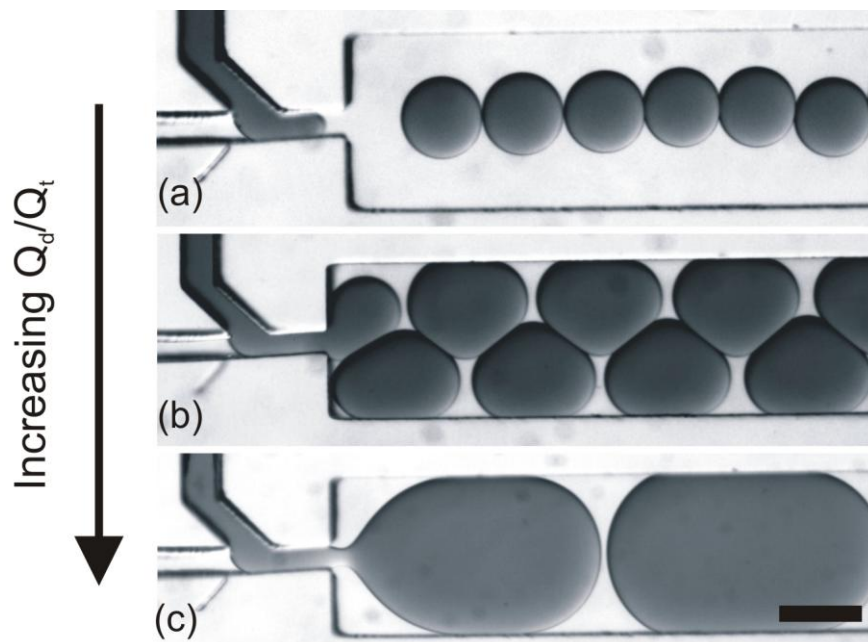
Figure 16. *Optical micrographs of the droplet formation via the three different mechanisms occurring at a step-emulsification device: (a) T-junction, (b) step- and (c) jet- emulsification mechanisms. The dispersed water phase is colored with nile blue for better visibility. Scale bar: 150 μm.*

Figure 17 clearly shows the boundaries between the three different production mechanisms as function of the total volumetric flow rate Q_t (sum of the volumetric flow rates of the continuous phase Q_c and the dispersed phase Q_d). When the flow rate of the dispersed phase, Q_d, is smaller than about half of the total flow rate, Q_t, emulsification occurs at the *T*-junction where the two liquids meet (see Fig. 16a). For intermediate Q_d/Q_t, the dispersed and continuous phases enter the high-aspect ratio channel ($h/a \geq 4$ where h and a are the height and width of the channel at the step), where the dispersed phase forms a fine liquid stream (indicated by the blue dotted lines in Fig. 15). This liquid stream of dispersed phase decays into droplets right at the step ($h/a >> h/W$ where W is the width of the wider channel) and the droplets are generated via the step emulsification (see Fig. 16b). The step emulsification is directly induced by the abrupt change in aspect ratio, where the narrow channel merges into the wide channel. The physical reason for this transition is that the flow profile is effectively two-dimensional in the narrow channel, but is three-dimensional in the broader channel. This minimizes the impact of fluctuations, yielding rather well controlled droplet sizes.
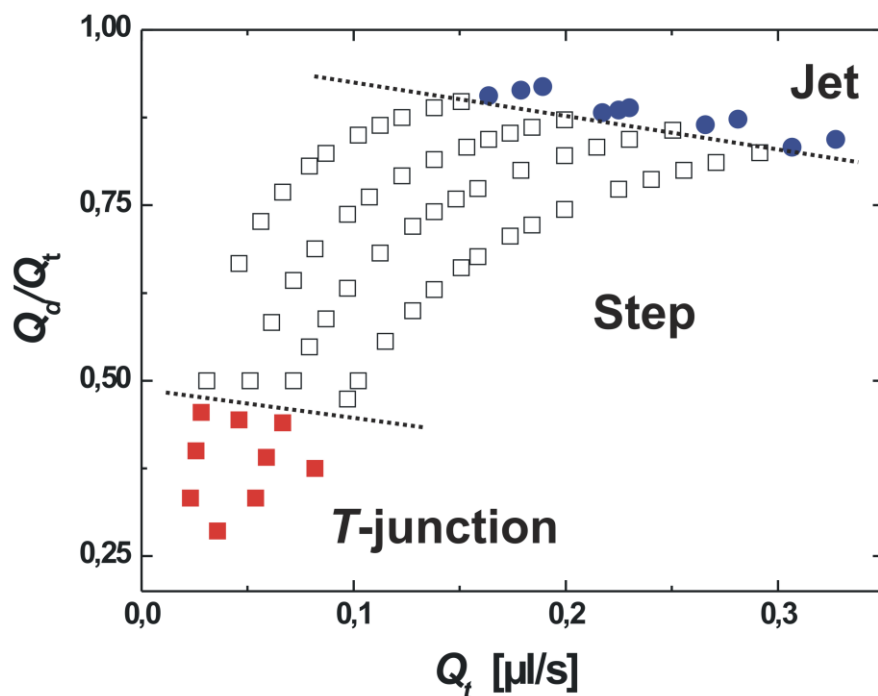
Figure 17.   *Different mechanisms for drop production: T-junction (red solid squares), step emulsification (open squares), and jet instability (blue solid circles). The dashed lines are guidelines to the eye indicating different regimes. Scale bars: 100 µm.*

At high relative flow rates, Q_d/Q_t, however, the instability at the step is not fast enough and a liquid jet is injected into the low aspect ratio channel and Rayleigh-Plateau type instability develops downstream from the step i.e. jet emulsification and the droplets produced are larger and unstable (see Fig. 16c). Using step emulsification we are able to prepare largely disordered emulsions to highly ordered gel emulsions by adjusting flow conditions in a single device. As the dispersed phase volume fraction increases, the droplet arrangements become increasingly ordered. At the highest fractions, the droplets self-assemble into highly ordered "foamlike" arrangements. Operating this device in the step-emulsification regime, emulsions with very high dispersed phase volume fraction up to 96 %, monodispersity better that 1.2% and variable droplet production frequencies could be obtained.

The frequency of the droplet production depends solely on the total flow rate ($v \propto Q_t$) and can be varied from a few to several 100 Hz. Curiously, the drop volume V_d is insensitive to the total flow rate, Q_t, provided the relative flow rate Q_d/Q_c is constant [100]. As a result, the production rate can be adjusted independent of the drop volume by varying Q_t with Q_d/Q_c fixed. This will be discussed in detail in section 3.3. Moreover, this important feature of droplet size insensitive to the total flow rate (with Q_d/Q_c = constant) makes the step-emulsifiaction devices much preferred to the the other standard microfluidic droplet generators for many Lab-on-a-Chip applications. The changed device geometry fabricated with a single photolithographic exposure step shows absolutely the same behavior that was found in the previous publication by Priest *et al.* [100]. Such an emulsification technique not only allows for standard device fabrication using soft-lithography and an enormous technical improvement but also for precise volume controlled droplet-based microfluidic chemical reactions.

3.2   Generation of two kinds of droplets using step-emulsification

To perform chemical reactions by merging or coalescing droplets inside a microfluidic device or to synthesize particles it is not just enough to produce one kind of monodisperse droplets we rather have to produce two types of monodisperse droplets (with appropriate reagents) in a strictly alternating manner. Figure 18 gives a simple idea of our microfluidic design. The droplets of

aqueous phases A and B containing different reagents are produced at two single step-emulsification units (section 3.1.3). Due to the very stable droplet production frequency of the single step-emulsification units, alternating droplets containing two different reagents can be produced by synchronizing two individual production units at a Y-junction. In this case, the exact synchronization could be either done 'manually' by repeatedly recording short sequences of the droplet production using a microscope and high speed camera or by direct optical detection as will be discussed in the following.
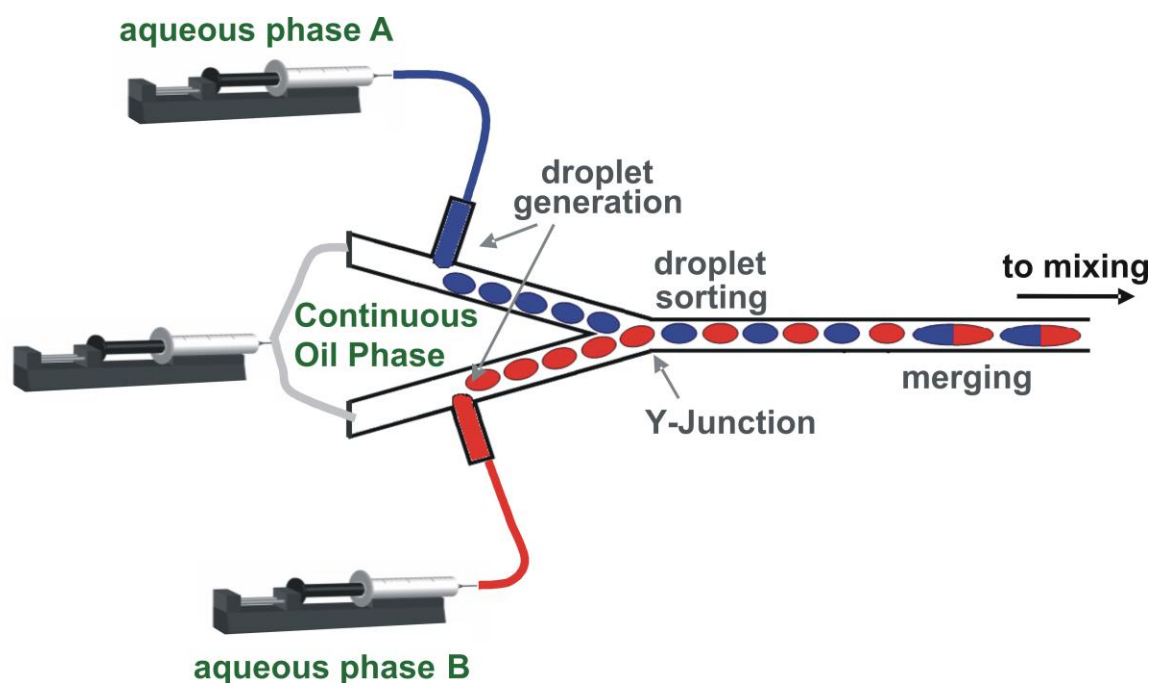
Figure 18. *Microfluidic design with two individual droplet generation units, sorting and merging regions.*

The direct optical detection is performed in a plane perpendicular to that of the microfluidic device. IR-transmitter and a photodiode setup [101,102] are chosen because of the possibility to have very small active detecting area equal to the size of the droplets that are produced. With this setup whose active area was reduced to an active length of only about 100 μm only, the droplet production frequency can be monitored (Fig. 19). Depending on the refractive index difference between the water and oil phases used (here, refractive index of water and oil are 1.33 ad 1.43,

respectively), the intensity signals are detected. The voltage output of the photodiode is directly proportional to the light intensity incident on the photodiode. The intensity of the transmitted light varies as the droplets pass the photo diode. Now, the flow rates at the individual droplet production units can be adjusted *in-situ* while monitoring the production frequency, mainly for a direct and easy controlling and therefore for faster adjustment of experimental parameters. With this system, emulsification units with droplet production frequency to about 30 Hz can be synchronized effectively downstream.
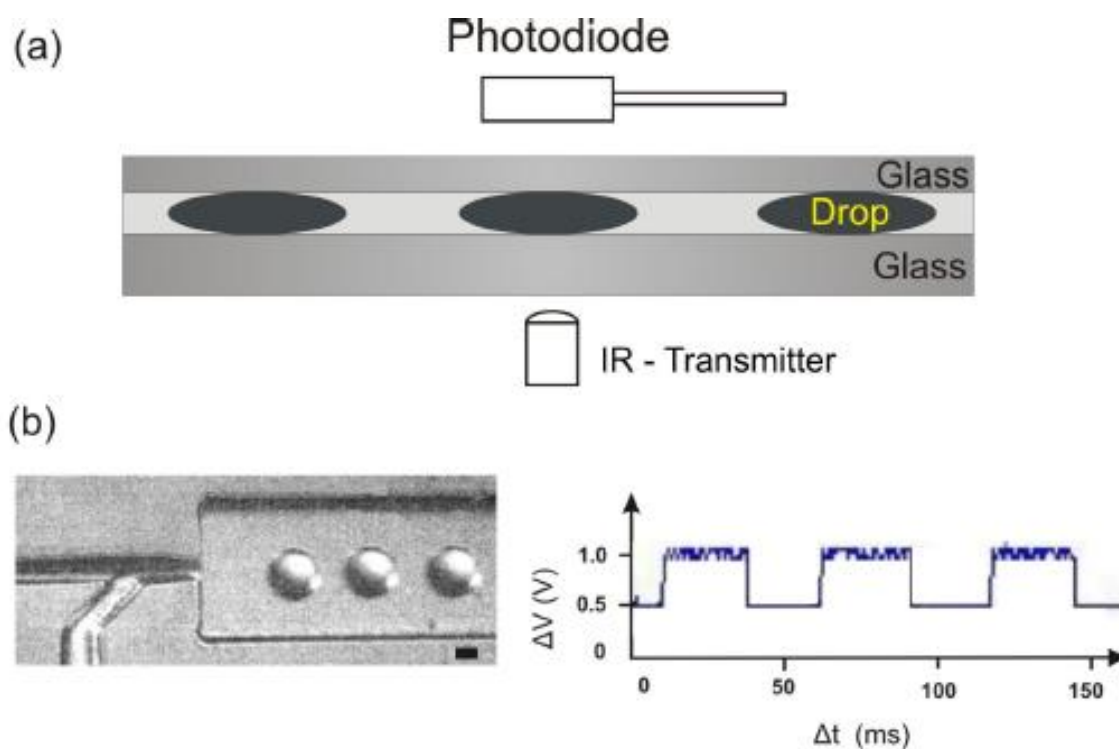
Figure 19.   *In-situ monitoring of the droplet production: (a) Sketch of the vertical cross-section of the micro-channel along with the IR-LED and the photodiode. (b) right: Typical intensity signal detected when the droplets (left) passed the photodiode. Scale bar: 50 μm.*

3.3   Double step-emulsification

Using the diode monitoring technique as explained above droplet pairs can be produced to perform chemical reactions. However, their application in droplet-based microfluidics to produce special materials is very limited due to the low production which results from the manual synchronization. A much higher production rate is required and would be highly beneficial if the individual production units automatically produce synchronized droplet pairs. For that, we combined two single step-emulsification units into one device (see Fig. 20). The resulting double-step-emulsification device thus consists of two single step-emulsification units combined to a common outlet channel (hereafter referred to as the main channel), which are fed by a common upstream channel containing the continuous phase.
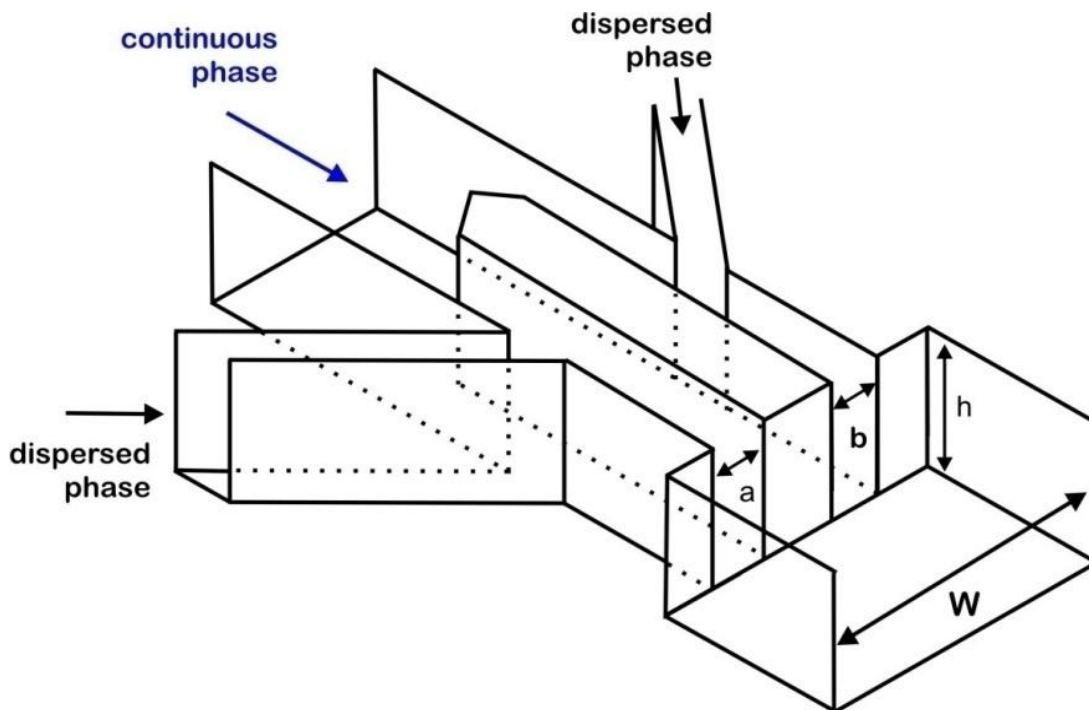
Figure 20.   *Schematic of the double step-emulsification device. The formation of the liquid stream of dispersed phase in each unit is similar to what was shown in Figure 15. The dimensions typically used in our experiments:* a, b = *35 μm,* h =*120 μm and* W = *160 - 420 μm.*

A time series of the droplet formation process is shown in Fig. 21: When a droplet forms in one production unit (e.g. bottom channel in Fig. 21a), the Laplace pressure of the forming drop decreases as its radius increases. This results in a pressure drop redirecting the continuous phase flow towards this production unit (bottom channel in Fig. 21b,c). Simultaneously, the pressure in the main channel increases due to the injected dispersed phase pushing the already formed stream of dispersed phase back into the other channel (top channel in Fig. 21b,c). After the droplet pinched-off into the main channel, the Laplace pressure changes rapidly and the stream of the dispersed phase retracts into the bottom channel (Fig. 21d). This, in turn, accelerates the dispersed phase in the top channel (Fig. 21e). Next, a droplet will be formed at this channel outlet and the cycle is repeated. This pressure cross talk between the individual production units synchronizes the drop production and leads to strictly alternating pairs of droplets (see Fig. 22a). This alternating droplet production is very robust even up to about 300 droplets and works up to a dispersed phase volume fraction of about 96% (see Fig. 22b).
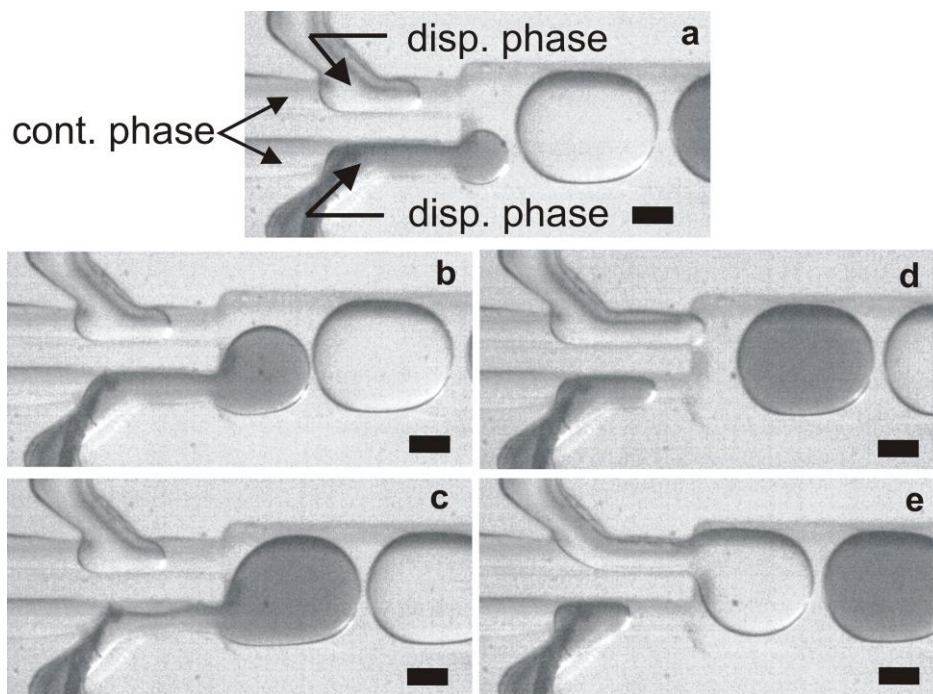
Figure 21. *Time series of optical images displaying the droplet formation mechanism using a double step-emulsification device. For clarity, the aqueous phase entering the bottom production unit is dyed with nile blue. Scale bar: 50 μm.*
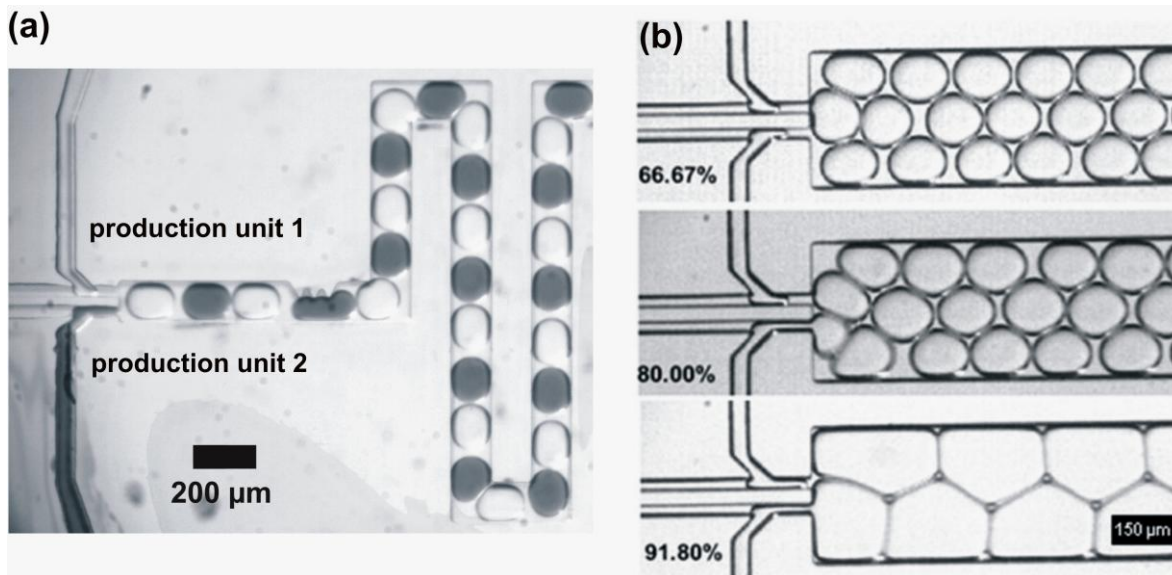
Figure 22. *(a) Strictly alternating droplet generation with $d_1/d_2 = 1:1$; $v_1/v_2 = 1:1$ and $\varphi = 55\,\%$. (b) Droplet arrangement as a function of increasing dispersed phase volume fraction.*

If we set the volumetric flow rates of the dispersed phases at the production units 1 and 2 equal ($Q_{d1} = Q_{d2}$), the corresponding droplet production frequencies, v_1 and v_2, at the production units 1 and 2, respectively, are equal. The coefficient of variance of the droplet diameters (d_1 and d_2) was always less than 1.2%, exhibiting the same excellent monodispersity as observed for a single step-emulsification device in section 3.1.3 (Fig. 23a) [100]. The synchronization mechanism of the double step-emulsification device is so robust that even different volumetric flow rates of the two dispersed phases Q_{d1} and Q_{d2} result in a strictly alternating droplet production. But as a result of the different flow rates, the mean size of the two droplet families becomes different, still maintaining excellent monodispersity within each droplet type (variance < 1.2%) (see Fig. 23b). As we increase the difference of the volumetric flow rates Q_{d1} and Q_{d2} ($Q_{d2} \approx 1.19\,Q_{d1}$), the two corresponding peaks in the displayed histogram can be clearly distinguished (see Fig. 23b). But even here, the production frequencies are strictly the same. Further increase in Q_{d2} results in different production frequencies with a fixed ratio of 1:2 (here, $v_1 = 2v_2$ for $Q_{d2} \approx 1.32\,Q_{d1}$) (see Fig. 23c) [103]. This self-synchronization is achievable even up to a fixed ratio of 1:4 after which system becomes unstable possibly due to fluctuations created by the pumps.
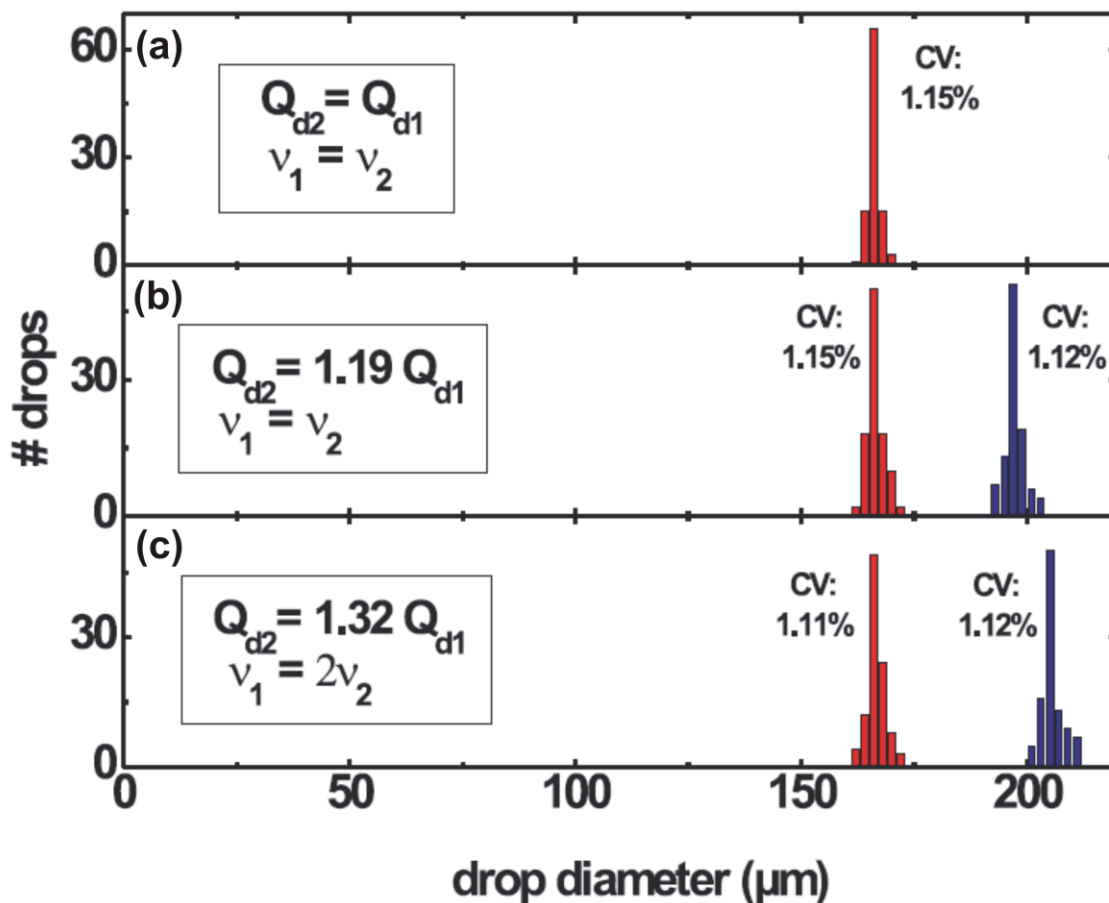
Figure 23. *Histograms for variable flow rates (a) $Q_{d2} = Q_{d1}$, (b) $Q_{d2} = 1.19\ Q_{d1}$ and (c) $Q_{d2} = 1.32\ Q_{d1}$.*

As discussed before in section 3.1.3, the production rate of the step-emulsification device can be adjusted independent of the drop volume by varying Q_t with Q_d/Q_c fixed. This is demonstrated also for a double step-emulsification device for three different main channel widths, W, at constant relative flow, $Q_d/Q_c = 1$ (see Fig. 24). Interestingly, it is observed that wider the main channels, smaller the droplets and larger the production frequency. To understand this effect in more detail, the width of the main channels (W) of double step-emulsification devices was varied from 160 μm through 420 μm. We altered the volumetric flow rates of the dispersed phases keeping the volumetric flow rate of continuous phase constant while the droplet production was always maintained in the step-emulsification regime.
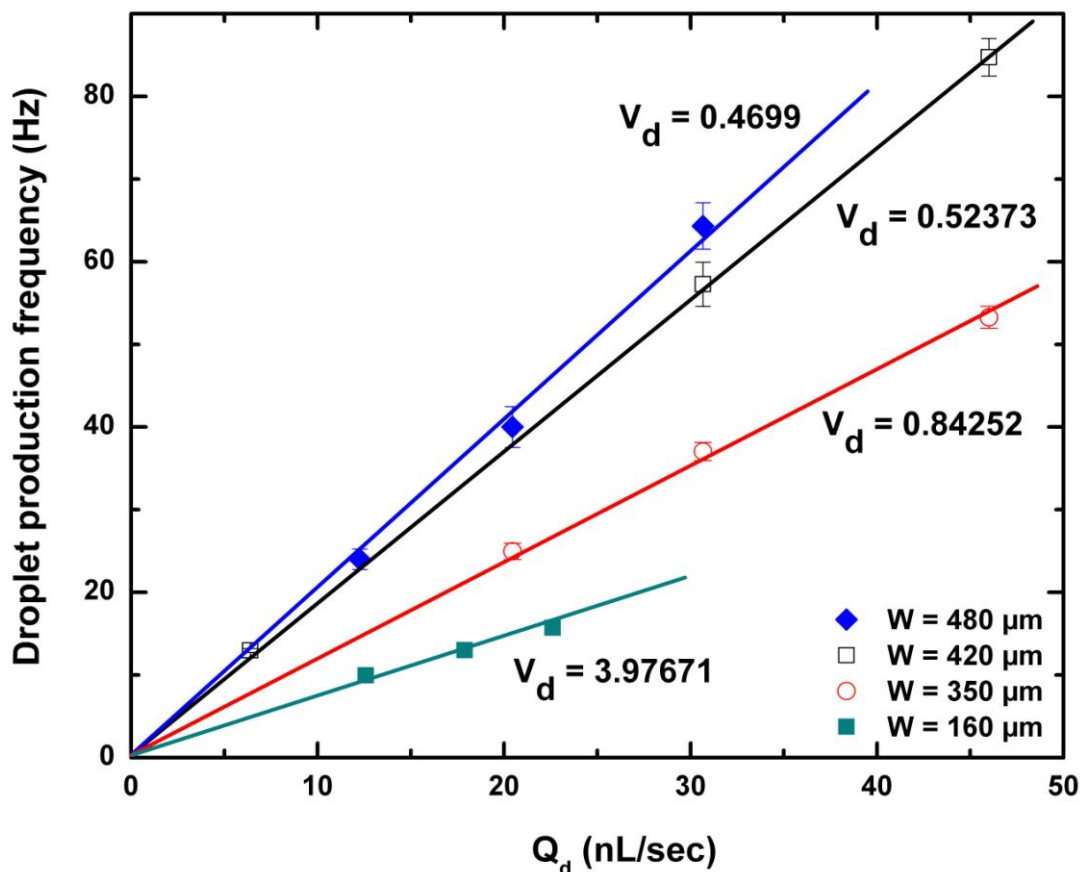
Figure 24. *The drop production frequency increases linearly for the flow fraction $Q_d/Q_c=1$ for several main channel widths* W.

As shown by the red closed circles in Fig. 25, for a 160 μm channel, for volume fraction (Q_d/Q_t) < 0.45, monodispersed droplets were produced with a fairly large inter droplet distance in the main channel (see Fig. 25a). Now the volumetric flow rates of the dispersed phase are increased at both the production units. Also, the droplet production frequency increased. After a certain dispersed phase volume fraction, $Q_d/Q_t > 0.45$, the produced droplets arranges in a bamboo pattern (see Fig. 25b) with increasing droplet volume but decreasing droplet production frequency (see the sharp kink in Fig. 25). This behavior of reduction in droplet production frequency may be understood as an effect of the increased flow resistance created within the microfluidic channel when the droplets become bigger to feel significant confinement of the channel [104]. Further increase in the dispersed phase flow rate significantly reduced the droplet production frequency.
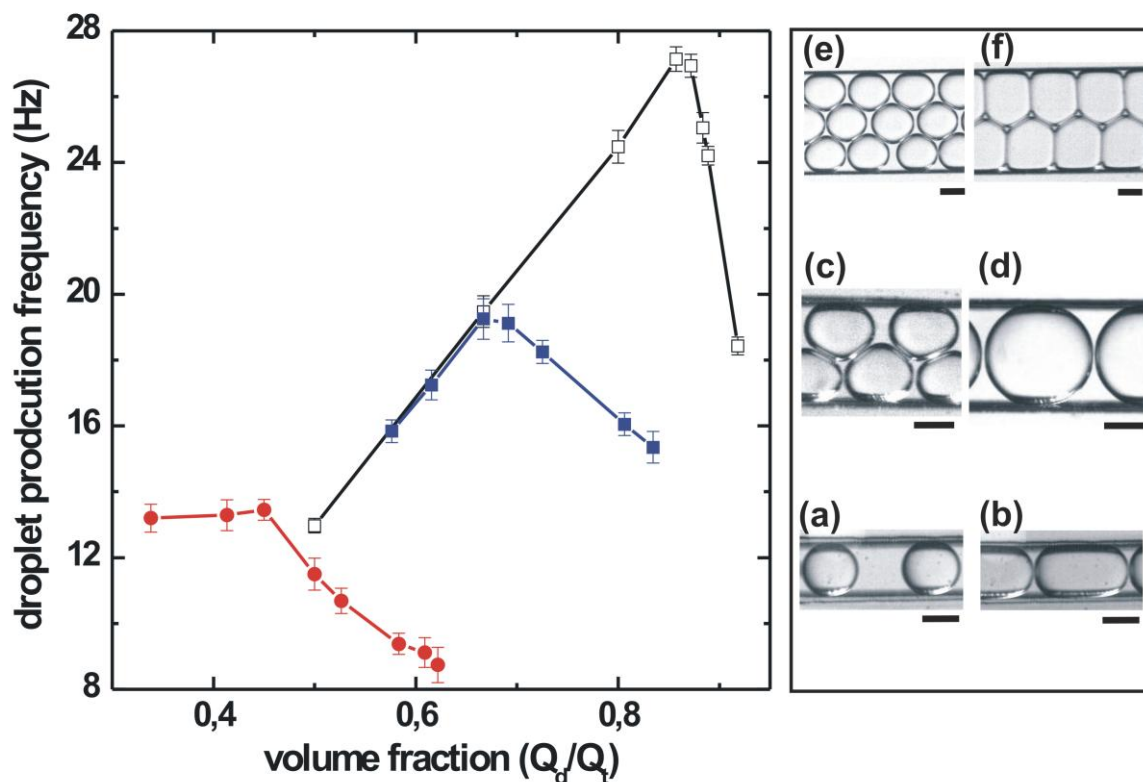
Figure 25. *Droplet production frequency as a function of volume fraction Q_d/Q_t displaying the shift in droplet production frequency at higher dispersed phase volume fractions. Black, blue and red lines indicate the behavior in 420 μm, 320 μm and 160 μm width channels, respectively. Scale bar: 100 μm.*

For larger channel widths, as observed before, the number of rows in which droplets were produced increased with increasing channel width. The blue closed squares in Fig. 25, for a 320 μm channel, for volume fraction $Q_d/Q_t < 0.65$ (see Fig. 25c), the droplets were produced in a 3-row pattern in the main channel. After a dispersed phase volume fraction, $Q_d/Q_t > 0.65$ (see Fig. 25d), the produced droplet assembly shifts from a 2-row pattern to a 1-row pattern with increase in droplet volume but decrease in droplet production frequency (see the sharp kink in Fig. 25). This behavior of reduction in droplet production frequency may be understood as an effect due to the increased flow resistance created within the microfluidic channel. Further increase in the dispersed phase volume fraction i.e. at the highest volume fractions, the droplets self-assemble into "foamlike" gel emulsions. This variation in droplet production frequency and self-assembly of

droplets due to flow resistance is also well observed for other main channel width of 420 μm as shown in Fig. 25e,f.

Thus, in a double step-emulsification device, monodisperse and bidisperse pairs of droplets were generated if the volumetric flow rates of the dispersed phases differ. The system is stable in both the monodisperse and the bidispersed regime with excellent monodispersity (Coeff. of Variance in diameter < 1.2 %) with drop volume insensitive to the total flow rate. All these characteristics along with strictly alternating droplet production makes the double step-emulsification device ideal for many complex microfluidic chemical or biological processing.

3.4   Droplet merging

To perform chemical reactions, the regular stream of droplets A and B has to be merged in a controlled way to initiate the chemical reaction within the merged droplet C (see Fig. 26). This merging can be achieved via either electro-coalescence or via a geometrical constriction as will be discussed in the following. Subsequent mixing of the reagents inside the merged droplets is very fast and effective as already discussed in section 1.1.2.

Electro-coalescence

Electro-coalescence of droplet pairs has been demonstrated in capillaries using AC potential, where the droplets were initially well-separated [105]. Here, electro-coalescence occurs in three steps: droplet approach, film thining, and rupture. As film rupture is characteristically rapid, the rate of coalescence is largely governed by the approach and film thinning steps.

When droplets are separated by only thin lamellae, the electro-coalescence is rapid and requires only a very small applied voltage, allowing for numerous coalescence events per second. For this reason, electro-coalescence is an excellent candidate for droplet merging within microfluidic channels. Figure 26 demonstrates electro-coalescence of droplet pairs in a microchannel using an applied potential of only 1 V between gold electrodes (dark regions) separated by 100 μm. One

electrode remained grounded at all times. Here, aqueous droplets are produced in Isopar M oil phase with span 80 as surfactant. The mechanism of electro-coalescence has been explained as an electric field induced dynamic instability of the thin oil lamella separating two aqueous droplets [106]. The occurring instability of the thin dielectric lamella between the droplets can be understood in terms of the spinodal instability of a thin film in the presence of an electric field [107]. The required electrical potential (U) is proportional to the lamella thickness (d), $U \propto d$ and is widely independent of the aqueous phase conductivities for typical aqueous phases. If the droplet separation or the flow velocity is large the applied voltage has to be increased.
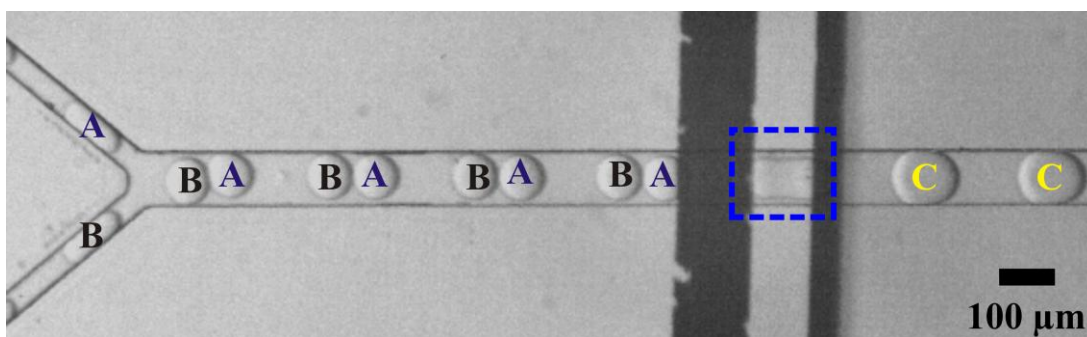
Figure 26. *Optical micrograph showing droplets merging via electro-coalescence. Droplets A and B merge as they pass through the electrodes (dark regions), resulting in a merged droplet C.*

Electro-coalescence works very effectively both for surfactant enabled as well as for non-surfactant stabilized systems. To perform electro-coalescence in the microfluidic device, more fabrication steps like electrode deposition, bonding wires and PMMA layer coating on cover glass are involved (as described in section 2.2.2 and Fig. 9). Thus, performing electro-coalescence has high demands on device fabrication and operation. Therefore, other techniques having reduced demands on device fabrication are desired.

Geometrical constriction

To account for the experimental needs, we developed a technique where the aqueous droplet pairs can also be merged when they wanted to pass through a geometrical constriction. Such a

merging technique works very effective for a system not stabilized with surfactants or with less effective surfactants i.e. surfactants that do not stabilize the emulsion very well (see Fig. 6, section 2.1). When the droplet pairs reach a geometrical constriction, the merging of the two droplets is induced by slowing down the leading droplet at the constriction. This technique has the lowest demands on the device fabrication and operation. As already discussed, downstream mixing of the reagents proceeds very efficiently due to the twisty flow pattern inside the droplets (section 1.1.2) [34,36,108] generated by the flow induced friction of the surfactant lamellae with the channel walls.

Due to the particular concentration gradient present in case of merged droplets the mixing in the droplet is particularly fast as we will explain in the following. In case of a chemical gradient perpendicular to the flow direction mixing can be accelerated by repeatedly altering the symmetry of the flow pattern by back fold channel geometry [34] (section 1.1.2). However, in the situation considered here, where two droplets are combined that are flowing behind each other, the resulting chemical gradient is along the flow direction and the symmetry of the concentration gradient does not need to be destroyed by a back fold or winding channel geometry. In this geometry the elongation of the merged droplet at the constriction and the followed expansion in the wider channel also promotes faster mixing.

In our experiments, two kinds of droplets were produced with different volumes and not touching the sidewalls for the sake of the subsequent drop coalescence (see Fig. 27). Due to the parabolic flow profile, small droplets move to the center of the channel where they experience a larger mean flow velocity and travel faster than larger ones [104, 108]. Accordingly, at a small distance downstream from the production unit, we find clearly separated droplet pairs where the larger droplet is leading and the smaller droplet is trailing behind. The coalescence occurs at the constriction as explained earlier.
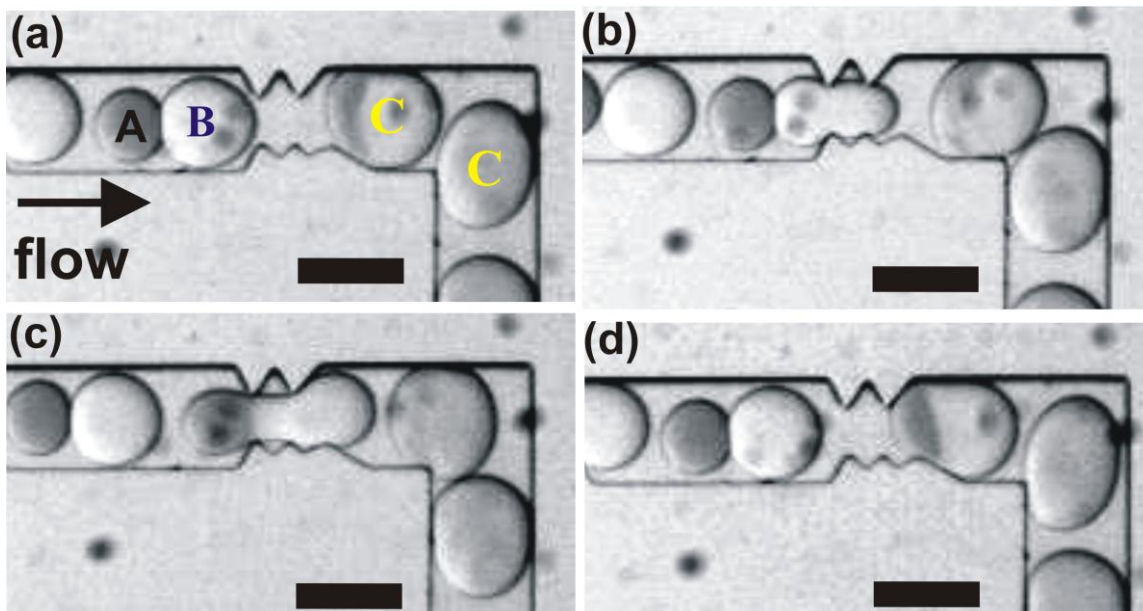
Figure 27. *Time series of snapshots of droplets merging via a geometrical constriction. Droplets A and B merge as they pass through the constriction, resulting in a merged droplet C. Scale bar: 200 μm.*

3.5 Microfluidic scheme

We replaced the two single step-emulsification droplet generation units and a Y-Junction sorting region in the microfluidic scheme sketched in Fig. 18 with a double step-emulsification unit. The schematic of the microfluidic scheme with a double step-emulsification droplet generation unit is shown in Fig. 28. The droplet pairs produced can be effectively merged to initiate any complex chemical or biological processing, with one of the techniques mentioned in section 3.4 with the right choice of surfactants. If needed, delay lines or post-processing units within the microfluidic device just before the outlet could be added to the microfluidic scheme depending on the requirements of the chemical or biological process to be investigated. In chapter 6, we describe how we successfully use the developed microfluidic techniques to produce mesoporous silica particles by sol-gel chemistry.
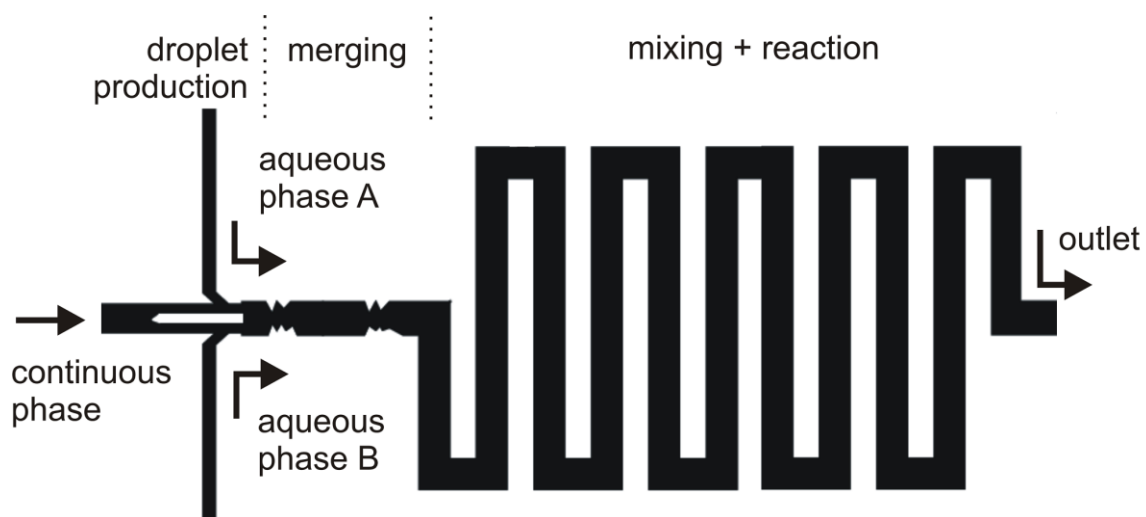
Figure 28. *Microfluidic scheme for complex chemical or biological reactions indicating the different functional units.*

4. SOL-GEL CHEMISTRY: BACKGROUND AND METHODS

4.1 Mesoporous silica

Porous materials play an important role as catalysts, catalyst supports, filters and therefore used for efficient reaction and separation. The pore size and structure of the matrix are crucial variables for the application along with the chemical composition of the solid matrix. While porous materials have been used in the chemical industry since its inception, there are increasing efforts to precisely control the size and shape of the pores in inorganic materials. The International Union of Pure and Applied Chemistry (IUPAC) have divided porous inorganic solids into three main classifications. Materials that contain pores with diameters of less than 2 nm are considered 'microporous' materials, those with pore diameters in the range of 2 - 50 nm are defined as 'mesoporous' materials, and materials with pores greater than 50 nm in diameter are termed as 'macroporous'. Mesoporous materials with pores of 2 - 50 nm possess a potential combination of high surface areas and pore sizes that make them ideal candidates to be used in catalysis and separation of complex molecules. High surface area porous silica is primarily produced through sol-gel processing (section 4.1.1) and in our microfluidic approach, we will follow the same route, which will therefore be explained in the following.

4.1.1 Sol-Gel process

The most common starting point of the sol-gel process is the mixing of alkoxides (any organic compound derived from an alcohol by replacement of a hydrogen atom with a metal or other species) in a hydrolyzing environment (a chemical reaction of a compound with water). Gelation of the initial alkoxide solution occurs via a two-step process. Alkoxides are ideal chemical precursors for sol-gel synthesis because they react readily with water. The reaction is called hydrolysis, because a hydroxyl ion becomes attached to the silicon atom as follows:

$$Si(OR)_4 + H_2O \rightarrow HO\text{-}Si(OR)_3 + R\text{-}OH$$

where R represents CH_3, C_2H_5, or C_3H_7. Depending on the amount of water and catalyst present, hydrolysis may proceed to completion, so that all of the OR groups are replaced by OH groups, as follows:

$$Si(OR)_4 + 4\ H_2O \rightarrow Si(OH)_4 + 4\ R\text{-}OH$$
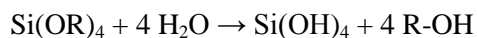
Any intermediate species $[(OR)_2\text{–}Si\text{-}(OH)_2]$ or $[(OR)_3\text{–}Si\text{-}(OH)]$ would be considered the result of partial hydrolysis. In addition, two partially hydrolyzed molecules can link together in a condensation reaction to form a siloxane [Si–O–Si] bond:

$$(OR)_3\text{–}Si\text{-}OH + HO\text{–}Si\text{-}(OR)_3 \rightarrow [(OR)_3Si\text{–}O\text{–}Si(OR)_3] + H\text{-}O\text{-}H \qquad \text{(or)}$$

$$(OR)_3\text{–}Si\text{-}OR + HO\text{–}Si\text{-}(OR)_3 \rightarrow [(OR)_3Si\text{–}O\text{–}Si(OR)_3] + R\text{-}OH$$
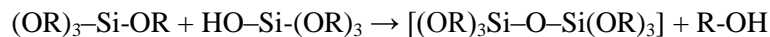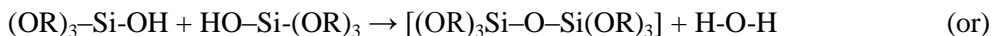
Condensation liberates a small molecule, such as water or alcohol. This type of reaction can continue to build larger and larger silicon-containing molecules. The hydrolysis of the alkoxide may be catalyzed by both acids and bases, but the condensation step generally occurs more slowly under acidic conditions. The hydrolysis and polycondensation reactions initiate at numerous sites within the precursor and H_2O solution as mixing occurs. When sufficient interconnected Si-O-Si bonds are formed in a region, they respond cooperatively as colloidal (submicrometer) particles or a sol. The

size of the sol particles and the cross-linking within the particles depend upon the pH and molar ratio r $(r = [H_2O]/[Si(OR)_4])$ [109]. With time the colloidal particles and condensed silica species link together to become a three-dimensional network.

The physical characteristics of the gel network depend greatly upon the size of the formed particles and extent of cross-linking prior to gelation. At gelation, the viscosity increases sharply and results in a solid object. The gel is allowed to condense further during the following aging step (also called syneresis, involves maintaining the gel for a period of time, hours to days) in order to increase crosslinking in the metal oxide network, and thereby to increase the strength and structural stability of the gel. After aging, the gel still contains excess water not used in hydrolysis of the alkoxide, alcohol produced during hydrolysis, and other additives present in the starting mixture. So the gel must be dried under atmospheric conditions to remove these solvents. After drying, gels are frequently calcined in temperatures above 500 °C in order to burn off the left-over organics and surface absorbed species. After this processing, the physical properties like surface morphology, pore size, pore volume of the synthesized silica can be analyzed using the techniques which will be explained in the following sections.

4.2   Scanning electron microscopy

Hitachi S-4500 Scanning Electron Microscopy (SEM) was used in this thesis for high magnification imaging of the surface structure of the produced mesoporous particles. For that, the silica particles are fixed to an electrically conducting carbon bed stuck to the SEM sample holder and then coated with thin gold layer to avoid charging effects. The accelerating voltage used in the measurements was 10 kV. SEM resources were used in the group of Prof. U. Hartmann (Experimental Physics, Saarland University).

During SEM inspection, a beam of electrons is focused on a spot volume of the specimen, resulting in the transfer of energy to the spot. These bombarding electrons, also referred to as primary electrons, dislodge electrons from the specimen itself. The dislodged electrons, also known as secondary electrons, are attracted and collected by a positively biased grid or detector, and then

translated into a signal. To produce the SEM image, the electron beam is scanned across the inspected area, producing many such signals. These signals are then amplified, analyzed and translated into images of the topography. Finally, these images are shown on a cathode ray tube and recorded.

4.3   Measuring surface area by physisorption

The porosity of the produced silica can be analyzed by 'physisorption'. The term 'physisorption' or 'physical adsorption' refers to the phenomenon of gas molecules adhering to a surface at a pressure less than the vapour pressure. The attraction between the adsorbed molecules and the surface are relatively weak. The energy of adsorption is approximately 20 kJ/mol which is insufficient to break bonds and therefore the adsorbed molecules retain their identities. This is done by cautiously varying the partial pressure of the gas and the resulting measurement curve is called adsorption isotherm. The adsorption isotherm is the measurement of amount adsorbed versus adsorptive pressure at constant temperature. The most widely used analysis of dealing with multilayer adsorption was derived by Stephen **B**runauer, Paul **E**mmet and Edward **T**eller, and is called the **BET** isotherm [109-111]. Here, if the initial adsorbed layer on the solid surface can act as a substrate for further adsorption then, instead of the isotherm leveling off to some saturated value at high pressures (Langmuir isotherm [112]), it can expected to rise indefinitely.

The BET isotherm is expressed as the extent of surface coverage θ [113]:

$$\theta \; = \; \frac{n_a}{n_m} = \frac{cx}{(1-x)\;[1+(c-1)\,x]} \tag{4.1}$$

where n_a is the adsorbed amount, n_m is the amount of gas required to form a monolayer of the adsorbate on the surface, x is the relative pressure, P/P_o (where P and P_0 are the equilibrium and the saturation pressure of the adsorbates i.e., the vapor pressure of the adsorbates at the temperature of

adsorption) and c is the dimensionless BET constant (equation 4.2) which is greater than one and depending on temperature.

$$c \approx \exp\left[\frac{\left(\Delta H_{des} - \Delta H_{vap}\right)}{RT}\right]$$

(4.2)

This constant c represents the relative strengths of adsorption to the surface and condensation of the pure adsorbate where ΔH_{des} and ΔH_{vap} are the enthalpies of desorption from the monolayer and of vaporization of the liquid adsorbate, respectively. Practically, the number of moles adsorbed as a function of equilibrium pressure is measured. Practically, one measures the number of moles adsorbed as a function of equilibrium pressure, i.e. one does not directly measure the surface coverage θ. Algebraic rearrangement of the BET isotherm (equation 4.3) is usually applied to experimental data. This equation implies an adsorption isotherm and can be plotted as a straight line with x ($=P/P_o$) on the x-axis and $x/n_a (1\text{-}x)$ on the y-axis according to the experimental results (see Fig. 29). This plot is called a BET plot.

$$\frac{x}{n_a (1-x)} = \frac{1}{n_m c} + \frac{(c-1) x}{n_m c}$$

(4.3)

From an experimentally derived BET plot, the value of the slope A and the y-intercept I of the line are used to calculate the monolayer adsorbed gas quantity n_m and the BET constant c. The following equations can be used to calculate n_m and c:

$$n_m = \frac{1}{A + I}$$

$$c = 1 + \frac{A}{I}$$

(4.4)
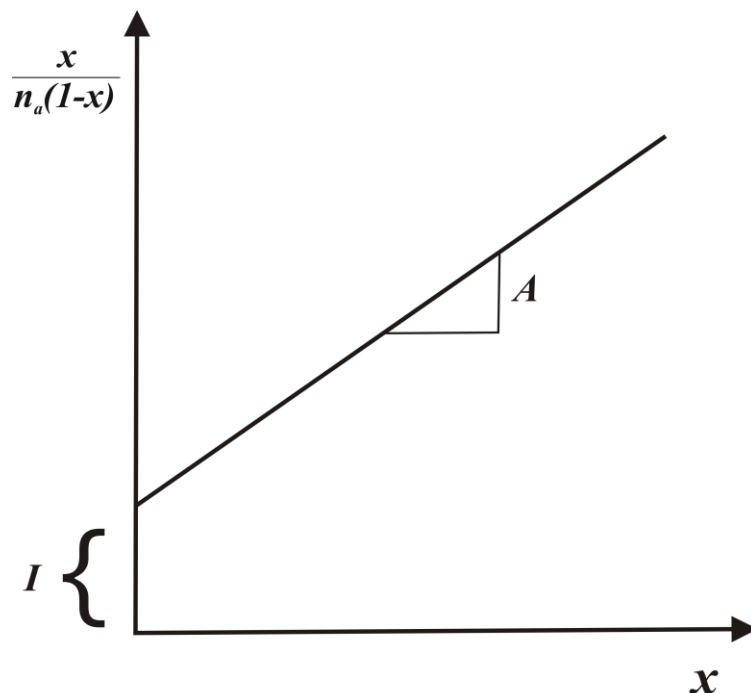
Figure 29. *A BET plot representing an adsorption isotherm.*

Knowing the area occupied by one adsorbate molecule σ, (the molecular area of the adsorbate N_2 is taken to be 15.8 $\mathring{A}^2$), the Specific Surface Area (SSA) of the material can be determined from the isotherm with the recorded mass change during the adsorption.

$$SSA = \frac{N_A n_m \sigma}{m} \tag{4.5}$$

Here, N_A is Avogadro's number, and m is the mass of the sample. The adsorption process is generally taken as completely reversible, but, under some conditions the isotherm may exhibit a different shape upon desorption as compared to adsorption. This is called hysteresis and can be used to determine the structure and size of pores in the absorbent using the classical pore size model developed by Barrett, Joyner and Halenda (BJH) [114] in 1951, which is most widely used for calculations of the Pore Size Distribution (PSD). It is the distribution of pore volume with respect to pore size which is obtained from the desorption branch of the isotherm. It is plotted by the

software with BET analyzer based on the Kelvin equation [115] and corrected for multilayer adsorption.

In our experiments, the specific surface area (m^2/g) and pore volumes (cm^3/g) of the solid materials was measured by a Brunauer-Emmet-Teller (BET) multipoint technique using an automated gas adsorption analyzer (Carlo Erba Sorptomatic 1990). The produced samples (at least 200 mg to reduce the signal to noise ratio) were loaded and degassed at 200 °C for 2 h in vacuum, followed by analysis at the temperature of liquid nitrogen (77 K) with N_2 as the adsorbate gas.

4.4   Catalytic activity measurements

In the course of this thesis the silica spheres with larger surface area are also used as support for catalytically active materials like platinum. The catalytic activities of those metal doped silica spheres can be determined by two techniques: emissivity corrected infrared thermography (ecIRT) for fast screening and conventional fixed bed reactor for quantitative analysis. The primary idea of the ecIRT measurement was to display temperature differences on a library [116-118] which are considered to be proportional to catalytic activity. The principal parts of the IR thermography setup are the IR camera, the reactor, gas supply, gas flow controller and temperature controller. The camera was controlled and operated by the multi purpose software program and attached to a tripod over the reactor and adjusted to full library view. The data were transmitted digitally to the measurement computer by a RS 422 interface. The A/D converter was integrated within the detector head. The exposure and also the display of live images, single images or image sequences were controlled by a software program, which worked at up to 50 frames per second. For the IR thermographic investigation, the catalyst powders were manually transferred into hexagonally positioned wells of a slate library plate (see Fig. 30a) and the library plate was inserted in a gas flow reactor with an IR transparent sapphire window on the top (see Fig. 30b), allowing IR imaging of the library surface with an IR camera (PtSi crystal detector with 256×256 pixel, Thermosensorik Corp.). The whole experimental setup, including gas dosing, temperature, and IR camera control, was managed automatically with custom made software.
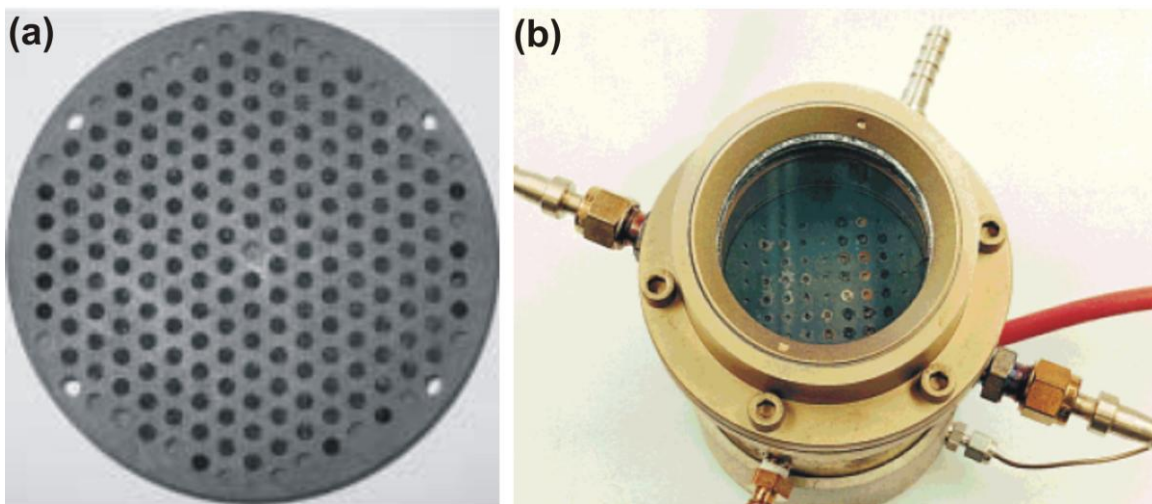
Figure 30.   *a) Catalyst plate library. b) Reactor for IR-thermography with catalyst plate library, the sapphire window, gas inlets and outlets.*

Prior to the measurement, the library was pretreated at 380 °C for 30 min in synthetic air (O_2 and N_2 only) at 50 ml/min to evaporate water and oxidize volatile organic combustion residues if present. After that, a six-point temperature calibration was carried out in a range of 10 K in the area of -4 to +6 K around each specific reaction temperature and images were taken. To examine the catalytic activity of the library samples (for e.g. propane oxidation), the reactor was held constant at a fixed temperature and different reaction gas mixtures passed successively through the system with a constant flow rate of 50 ml/min. The resulting differential temperature was calculated by the software based on the Stefan-Boltzmann-law:

$$T = \frac{M}{\varepsilon \sigma} \tag{4.6}$$

where T is the absolute temperature, ε is the emissivity dependent on temperature, σ is the Stefan-Boltzmann-constant and M is the emissive power. Different materials exhibit different radiated intensity of surface at the same temperature. The intensity change depends on the temperature change, therefore a correlation $I(T)$ using 6 point calibration was determined. This calibration

essentially subtracts the images taken before the reaction, and only the temperature differences are recorded. Such ecIRT enables to measure even very low temperature differences. This temperature difference correlates to the catalytic activity of the samples in the plate library.

To understand and validate the catalytic activity, the active samples were tested in a conventional fixed bed reactor. The schematic representation of the conventional test reactor unit is shown in Fig. 31. The premixed reaction gas and synthetic air enters the conventional gas flow reactor with a total feed flow rate of 50 ml/min where about 100 mg of sampled is stored. A suitable operating temperature range for the reaction is selected and temperature of the catalyst is controlled by a thermo-element during the combustion (reaction). The product gas is analyzed for the exit concentrations using gas sensors.
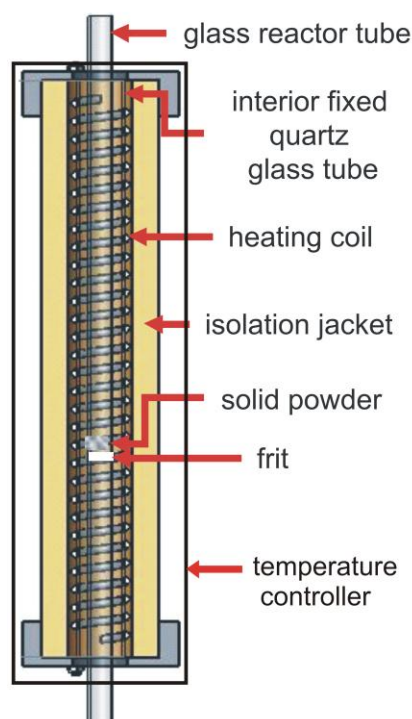
Figure 31. *Reactor unit in a conventional fixed bed reactor.*

5. MICROFLUIDIC SOL-GEL SYNTHESIS

In this chapter, we demonstrate the potential of our microfluidic reaction scheme developed in chapter 3 by producing mesoporous silica particles from complex sol-gel precursor solutions with properties suitable for heterogeneous catalytic activities. The long and stable operation conditions of this reaction scheme allow producing sufficient quantities of the silica particles for quantitative analysis of their surface area and pore size. Furthermore, we characterize the microfluidically produced silica particles using the techniques presented in chapter 4 and compare them to bulk synthesized and commercially available products.

5. 1   Microfluidic synthesis of silica particles

To produce silica particles by microfluidic routes, we started by optimizing the sol-gel recipe to allow for typical processing time of few seconds and to perform reactions without clogging the channels with reactant solutions at appropriate pH. The applied microfluidic sol-gel synthesis scheme is sketched in Scheme 1 and the different steps involved are explained one after the other as follows: Two kinds of droplets from aqueous phases A and B were pair wise dispensed in a strictly alternating fashion (see Fig. 32) using the presented double step-emulsification device (section 3.3) into the microfluidic device made of PDMS (section 2.2.2). The droplets are merged into droplets C and the content is mixed down the channel. After the mixing, droplets are given sufficient residence

time in the microfluidic device before they are collected outside the microfluidic device, calcined and characterized.
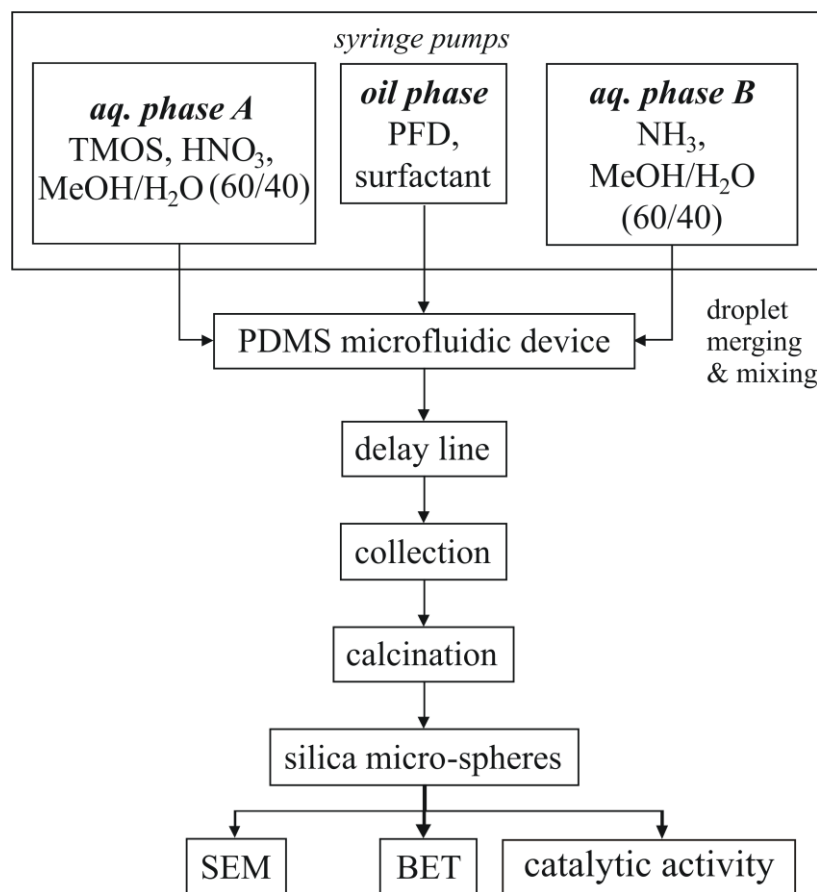
Scheme 1. *Synthesis route.*

One type of droplets from aqueous phase A consists of a 1.57 M acidified solution of the silica precursor tetramethoxysilane, TMOS (*Si(OCH₃)₄*, ABCR GmbH & Co. KG) in a mixture of methanol (Merck KGaA, Darmstadt, Germany) and water (Millipore™) at a volumetric ratio of 60/40. The second type of droplets from aqueous phase B contains ammonia (Merck KGaA, Darmstadt, Germany) based on the same solvent having the same volumetric content (methanol/water, 60/40). As continuous phase perfluorodecalin (PFD, *C₁₀F₁₈*, ABCR GmbH & Co. KG) oil with 20 wt.% fluorinated surfactant, penta decaflouoro-1-octanol (*C₈H₃F₁₅O*, ABCR GmbH

& Co. KG) (as explained in section 2.1, Fig. 6) was used, where, none of the dispersed phase reagents is soluble. Furthermore, PFD oil does not swell microfluidic channels made of PDMS which can be fabricated easily through soft lithography techniques (Section 2.2.2, Fig. 10). Before starting an experiment, the microchannels were rendered fluorophilic by flushing the microchannels for about one hour with a PFD solution containing 40 wt. % of the selected surfactant to achieve appropriate wetting properties as discussed in section 1.3.
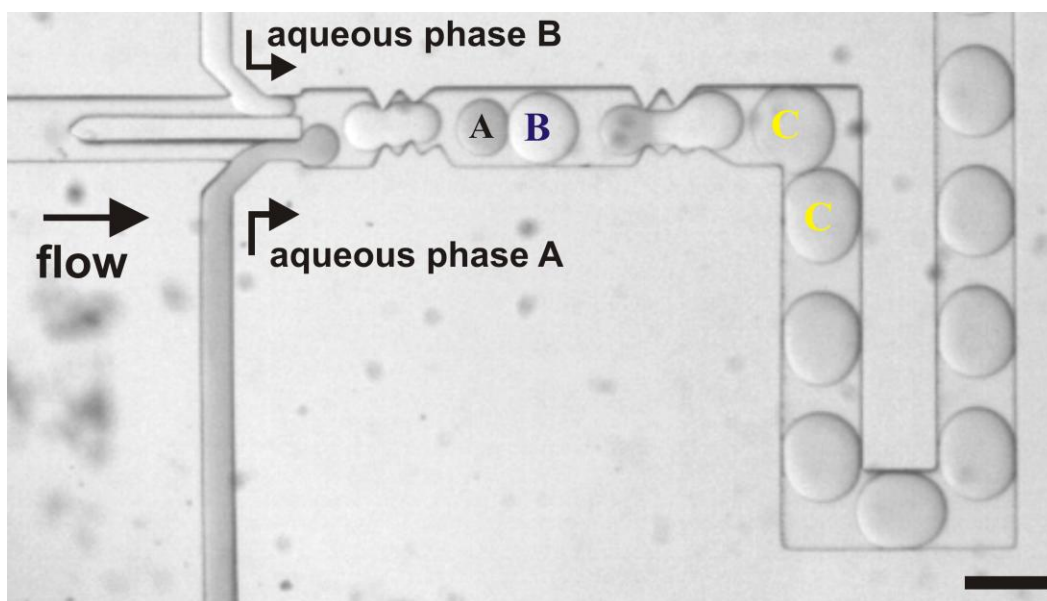
Figure 32. *Optical micrograph showing the self-synchronized pair-wise production of different kinds of monodisperse droplets using a double step-emulsification device and the subsequent formation of separated droplet pairs and merging of two droplets at a geometrical constriction. The aqueous phase injected from the bottom channel is colored with nile blue for clarity. Scale bar: 200 μm.*

The two kinds of monodisperse droplets A and B were produced with different volumes (see Fig. 33) for the sake of the subsequent droplet merging (droplet C) at the geometrical constriction as explained in section 3.4. A rapid acid catalyzed hydrolysis of TMOS occurs in the aqueous solution A even before dispensing it into droplets A at pH 1-2. Because of the high molar ratio of $Si:H_2O$ (r > 10) and the nearly nonexistent retarding effect of the methoxide group on the hydrolysis rate, a rapid and nearly quantitative hydrolysis of the precursor to silicic acid can be assumed within a few

minutes [119]. The formation of the silica gel, however, is very slow at this pH range. To accelerate the condensation of silicic acid in our microfluidic synthesis route, we combined the TMOS containing droplets A with the ammonia containing droplets B to form droplets C and thereby adjust the pH to be between 6 and 7, above the iso-electric point of silica (pH > 3), where the gelation time is minimum [109].

As shown in Fig. 32, mixing within the merged droplet C is performed within a travel distance of 500 μm, which corresponds to about twice the drop length within about 100 ms at a typical flow velocity of about 8 mm/s. The final molar ratio was TMOS/methanol/HNO$_3$/NH$_3$/H$_2$O = 1/17.8/0.13/0.33/34.3. The condensation reaction starts with the deprotonation of silanols by reacting with hydroxyl ions. The condensation of deprotonated silanols combined with the aggregation of the condensed species leads to a continual growth of the formed gel up to a point where the silica particles become too large to be solvated. Apart from condensation, the dissolution of silica by means of alcoholysis and hydrolysis of siloxane bonds (reverse reactions of condensation) also exhibits a strong pH-dependence which increases by more than three orders of magnitude between pH 3 and 8 in aqueous solution [109,120-122]. Due to the large methanol concentration in the merged final droplet C, a rather low dissolution rate can be assumed since the solubility of silica in methanol is much lower than in water.
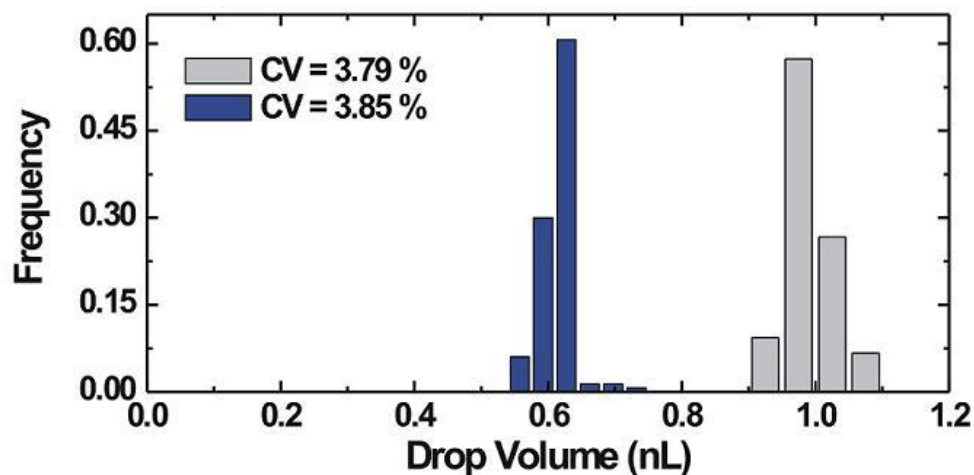
Figure 33. *Histogram of the two kinds of droplets that were generated with the self-synchronizing double step-emulsification device.*

During the merging and mixing of droplets inside the microfluidic device, none of the reactive mixture gets in contact with the microfluidic channels which avoid any precipitation or sticking to channel walls. Figure 34 shows the histogram of the volume of the merged gel drops C collected outside the microfluidic device with a coefficient of variance of CV in volume < 4 %. For a better judgment of the dispersing precision, we give here the monodispersity in volume percentage and not in radius as done in section 3.1.3. Volume of droplets is calculated as follows: If the radius R of the projected droplet area is smaller or equal than the height of the microfluidic channel, the droplet is spherical and its volume equal to $V = 4/3 \ \pi R^3$. If the size of the droplets exceeds the height of the channel h the droplets are assumed as disk shaped droplets and their volume is calculated by $(\pi/12) \cdot [2D^3 - (D - h)^2 (2D + h)]$ where D is the diameter of the disk.
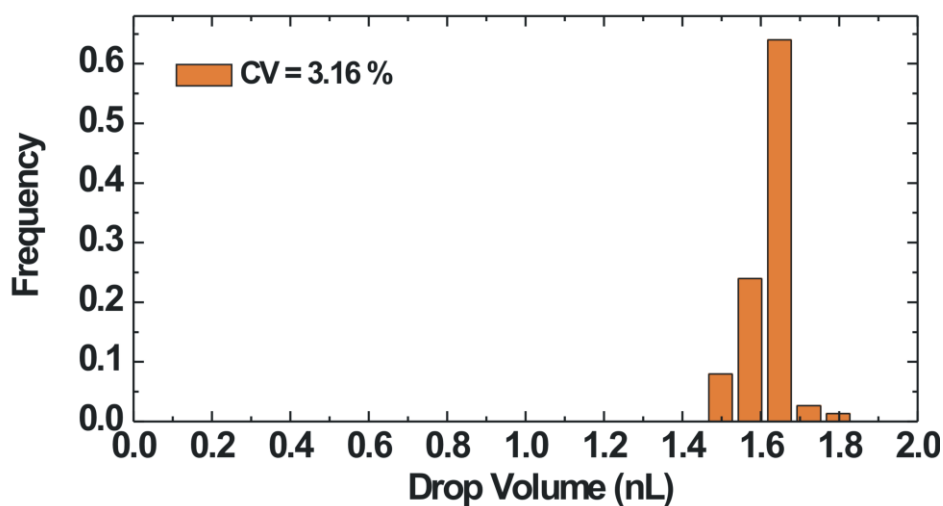
Figure 34. *Histogram of the gel droplet volume after merging and before calcination as collected in the continuous phase outside the microfluidic device.*

To ensure that the pH of the droplets is not influenced by the large concentration of the fluoroalkyl groups of the surfactant [121], which might be also slightly soluble in the aqueous phase, we performed control experiments using the same microfluidic scheme, whereas a pH indicator was added to one of the droplets [Methyl red: red at pH below 4.4, yellow at pH over 6.2, and orange in between (Fig. 35a). Bromothymol blue: yellow at pH below 6, blue at pH over 7.6 and dark green in between (Fig. 35b)]. With these reactions we could confirm that the pH for our

sol-gel reaction is in fact between 6.2 and 7.6 which is desired for faster gelation and can exclude a significant pH change by the large concentration of surfactant.
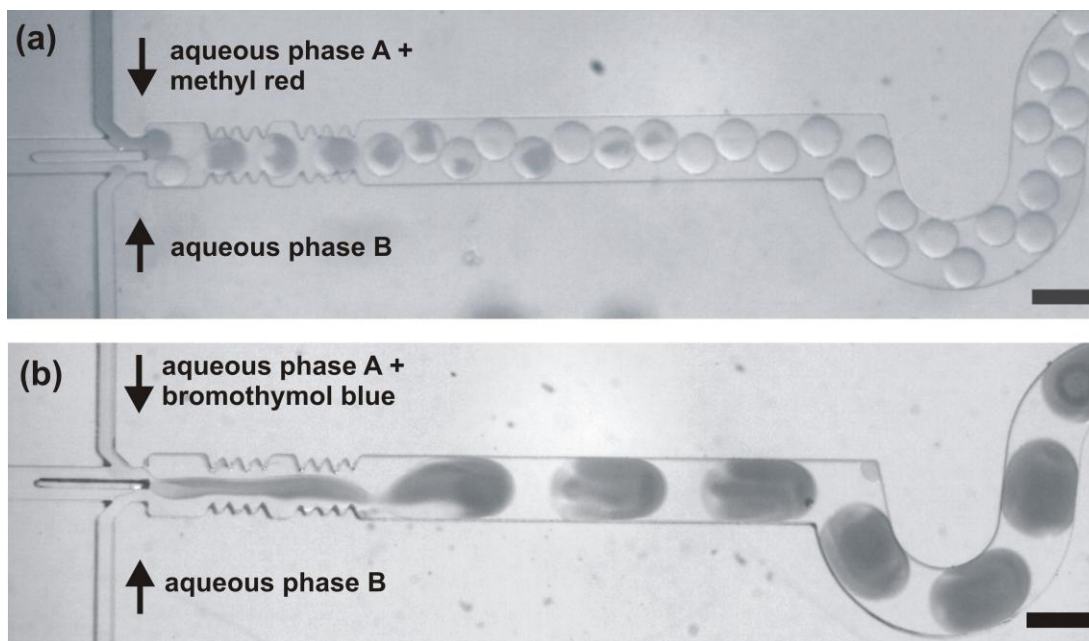
Figure 35. *Control experiments to confirm that the pH of the droplets is in the desired range of pH 6 to 8 where the gel formation time is minimal and not influenced by the large concentration of the surfactant. Scale bar: 150 μm. (pH indicator: (a) methyl red (pH > 6.2), (b) bromothymol blue (pH < 7.6)).*

The merged droplets C are subsequently given some time to develop the gel network in a delay line. In order to avoid the formation of clumps of silica gel at the rear side of the droplets [123] due to the motion induced twisty flow pattern (as described in section 1.1.2) inside the droplets, we reduce the flow velocity of the droplets with a delay line and the flow induced flow pattern since the droplets do not touch the side walls of the delay line. This is achieved by increasing the microfluidic channel width and guiding the gel particles into Teflon tubing with a cross sectional area which is more than ten times larger than that of the microfluidic channel width. Also, to adapt our microfluidic scheme for this sol-gel synthesis and to ensure that the droplets do not undergo any unwanted coalescence events in the delay line or sticking to each other, the distance between the

merged droplets C is increased by adding a small percentage of continuous oil phase after the back fold channels (see Fig. 36), before entering the Teflon tubing delay line.
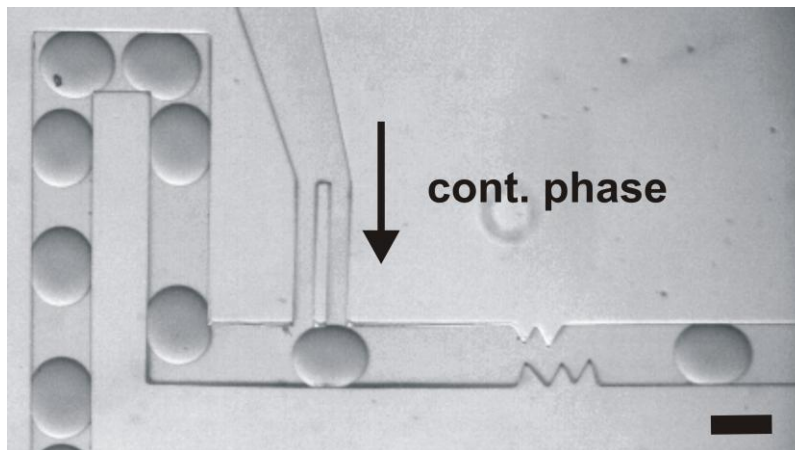
Figure 36. *End of the back fold channel geometry with a side channel to inject continuous phase to increase the inter droplet distance. Scale bar: 150 μm.*

The Teflon tubing is about 1 m in length and coiled up in a temperature controlled chamber at 65 °C, accelerating the gel formation and the removal of the solvent from the droplets. After a residence or flow time of about 20 min in the Teflon tubing, the monodisperse silica-gel particles are collected outside of this microfluidic device in a beaker containing the same perfluorinated continuous phase, which is also kept at the same temperature. In this beaker, the gel particles remain under continuous stirring for another 2 h, to ensure that the network formation has been completed and to gently evaporate remaining solvent. The collected gel particles are removed from the beaker and subsequently stored at room temperature for about 48 hours. To remove the remaining organics and surface absorbed species, the gel particles are calcined at an elevated temperature.

To determine the calcination temperature required for the synthesized silica gel particles a thermo-gravimetric analysis was performed using a TGA/DSC1 (Mettler-Toledo GmbH, Germany). It is important to determine an optimum temperature that is as high as needed to remove all organics but as low as possible not to densify the porous silica. The silica particles were filled into an alumina cup and heated at ramp rates of 10 °C/min from ambient temperature to 800 °C. The

reference material was an empty alumina cup. A flow of synthetic air (O_2 and N_2 only) of 40 ml/min, was maintained during the experiment. Evolving gases were monitored online with a Balzers ThermoStar GSD 300 T quadrupole mass spectrometer. Figure 37 shows the recorded TGA curve. With mass spectrometer signals, the mass loss of the samples was mainly divided into two temperature regions: from ambient temperature to 120 °C water was evolved and between 120 to 550 °C perfluorodecalin (PFD) oil passed out at the lower temperatures (small peak between 120 °C to 250 °C in Fig. 37) and combusted at higher temperatures leading to CO_2 desorption (small peak between 300 °C to 420 °C in Fig. 37). As a result, a minimum temperature of about 500 °C is required for calcination to expel all volatile organic components completely out of the silica gel particles. Accordingly, all the collected gel particles that were used for the analysis were calcined at a temperature of 550 °C.
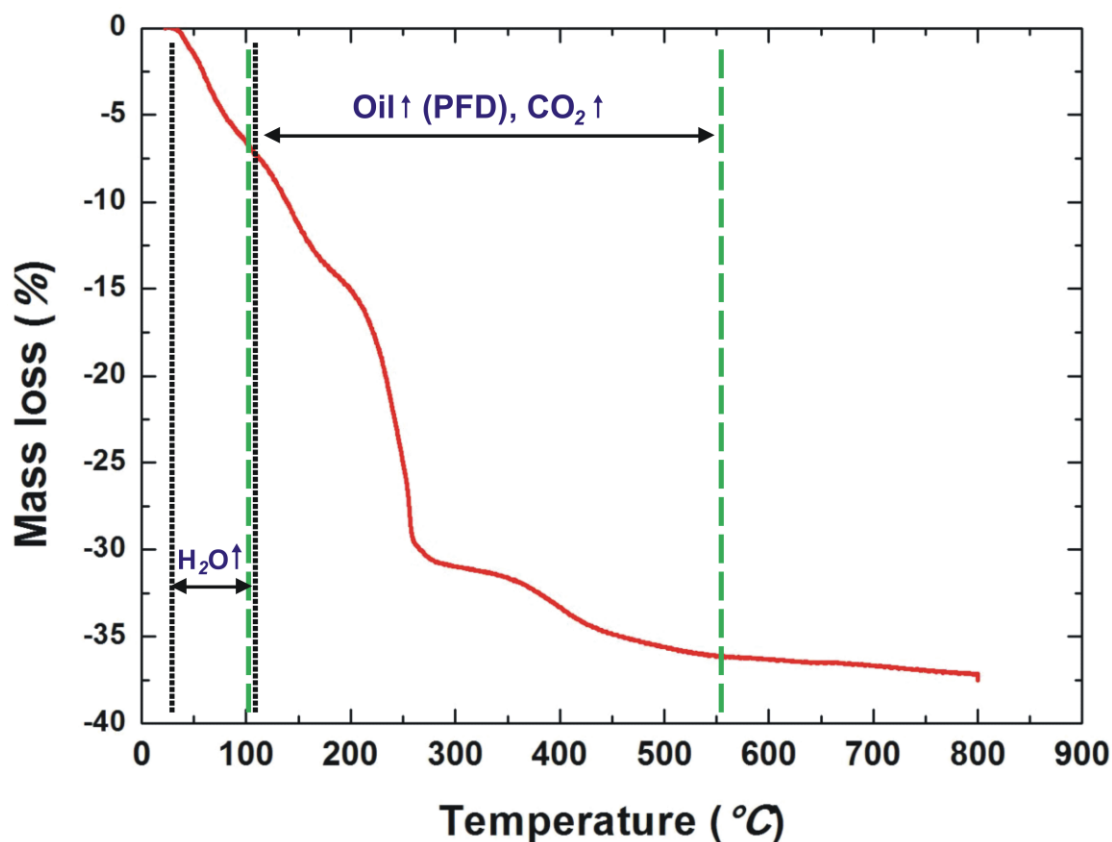
Figure 37. *Thermo-Gravimetric Analysis (TGA) curve of the silica particles produced.*

The particles and their surface structure after calcination are imaged by scanning electron microscopy SEM. The monodispersity of the calcined particles does not resemble the precisely controlled volume of the droplets (see Fig. 38). This is not due to any unwanted coalescence effects or insufficient control of the microfluidic process but is due to the massive volume change during the calcination process which differs slightly between the individual gel particles. The close-up of these silica particles (Fig. 39) shows that the particles are almost perfectly round rarely showing small raised surface corrugations. Furthermore, they have a cloudy surface morphology, reminiscent of a crumble topping.
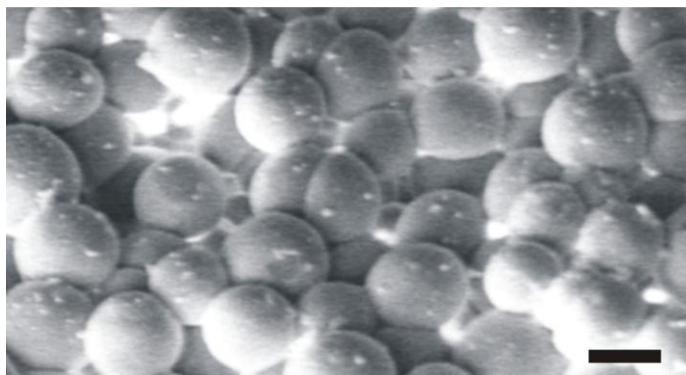
Figure 38. *Scanning electron micrograph of a lager accumulation of silica particles after calcination. Scale bar: 5 μm.*
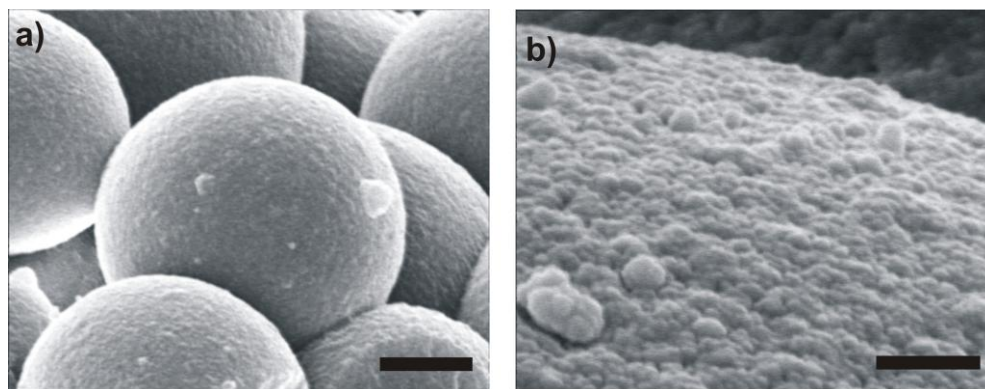
Figure 39. *Scanning electron micrographs of the silica spheres after calcination: a) Silica spheres. Scale bar: 1 μm. b) Surface structure of silica spheres. Scale bar: 100 nm.*

The porosity and the pore volume of the synthesized silica particles are investigated by a BET (Brunauer, Emmett, and Teller) analysis (section 4.3) using nitrogen as adsorbate. A typical Nitrogen adsorption-desorption isotherm for the microfluidically synthesized silica particles is shown in Fig. 40a. It shows a steep rise in the low-pressure region at a normalized pressure of about $p/p_0 < 0.05$ which is interpreted as indication for the presence of micropores in the analyzed silica samples. At larger partial pressure a characteristic hysteresis loop appears, between a relative pressure of $p/p_0 = 0.40$ and $p/p_0 = 0.85$. According to IUPAC [124-126] this type of isotherm can be classified as type IV and indicates the presence of mesopores (pore size 2-50 nm). Moreover, with the shape of the hysteresis, it can be understood that the silica gel particles have cylindrical pores with bimodal pore openings [127, 128]. The pore size distribution (PSD) is calculated from this adsorption isotherm. As seen in Fig. 40b, PSD is narrow and has a distribution maximum at 2.4 nm pore radius. The specific surface area of the produced silica particles averaged over several production runs and for various measurements was determined to 820 m^2/g ($\pm$ 20 m^2/g) with a cumulative pore volume of 0.61 cm^3/g ($\pm$ 0.02 cm^3/g). The surface area of the spheres itself is just about 1 m^2/g which is negligible with respect to its measured internal surface area.

Comparing these results with the specific surface area and the pore structure of silica prepared by sol-gel bulk synthesis under strong acidic (pH < 2) or strong basic (pH > 12) conditions reveal significant differences. Both types of bulk synthesis usually lead to silica with specific surface areas in the range of 200 – 600 m^2/g. Silica prepared under acidic conditions is normally microporous and exhibits a fairly high surface area whereas the silica obtained under strong basic conditions (Stöber conditions [129]) has a low surface area and is nonporous (pseudo mesoporous) [130]. The silica particles synthesized by our microfluidic approach are mesoporous as expected for a base catalyzed condensation at pH about 6 and consequently far away from the Stöber conditions. Using the same chemical route for bulk synthesis we achieved an internal surface area below 600 m^{2}g^{-1} of the produced silica (see Fig. 41). Thus, the internal surface area of the silica particles synthesized *via* the microfluidic scheme is about 40% more than the bulk synthesized material.
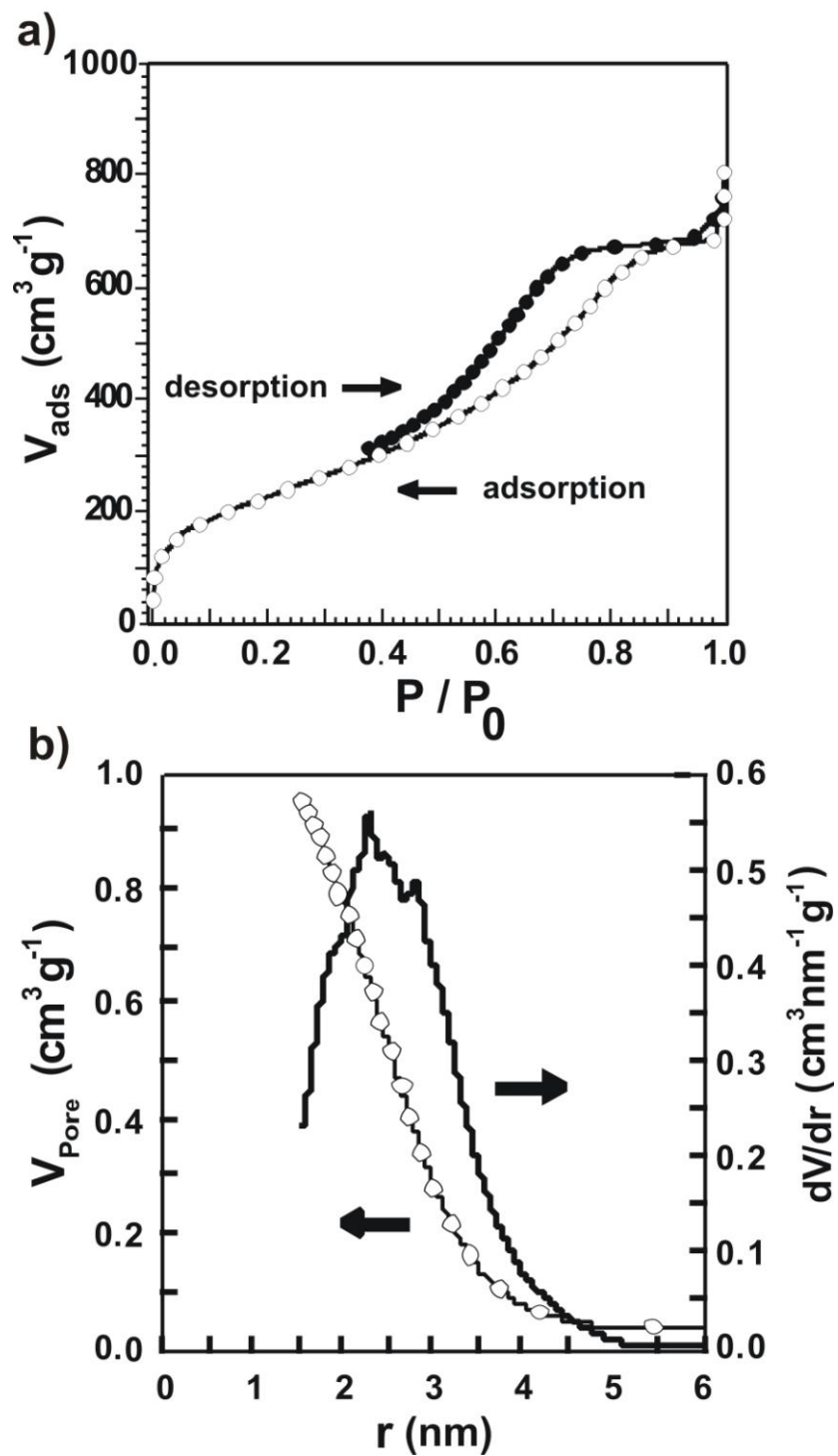
Figure 40.   *a) BET Nitrogen adsorption-desorption isotherm of silica spheres synthesized through microfluidics. b) Pore size distribution. V_{ads} = adsorbed volume, p/p_0 = reduced pressure, V_{pore} = pore volume, r = pore radius.*
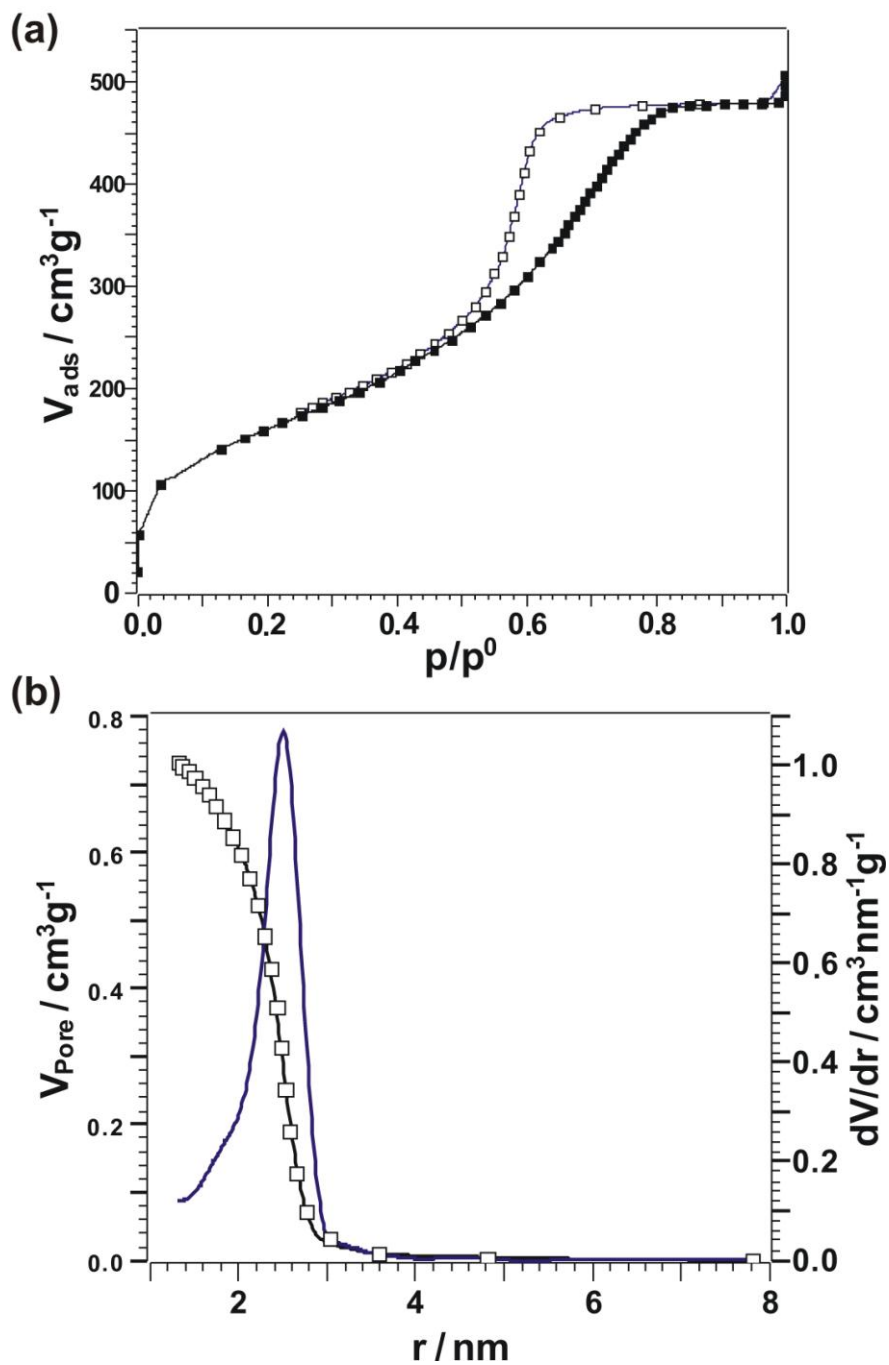
Figure 41. (a) *BET Nitrogen adsorption-desorption isotherm of silica synthesized in bulk* (b) *Pore size distribution.* V_{ads} = *adsorbed volume,* p/p_0 = *reduced pressure,* V_{pore} = *pore volume,* r = *pore radius.*

In order to further emphasize the superior results in term of the internal surface area due to the optimized microfluidics reaction control, let us compare the properties of our produced silica particles also to other recent microfluidics synthesis routes by Carroll *et al.* [131], Lee *et al.* [132], Chen *et al.* [133]. In all of these approaches the content of the sol-gel solution is completely mixed outside the device and microfluidics is just used for the droplet production through which inlet clogging becomes unavoidable. Moreover, the formation of mesoporous silica particles is supported by templates. Carroll *et al.* [131] estimated the internal surface area of their produced silica particles to about 500 m^2g^{-1} based on results from batch processing using the identical chemical route [134], whereas no value is given by Lee *et al.* [132]. Chen *et al.* [133] used an approach similar to Caroll *et al.* [50] but on a significantly larger scale and determined the internal surface areas of the produced silica particles to 550 – 675 m^2g^{-1} and the total pore volume to 1.1 – 2.6 cm^3g^{-1}, depending on exact experimental parameter. However, to date no microfluidic synthesis route had been reported for the production of mesoporous silica spheres with very high specific surface area by explicitly analyzing the microfluidically produced particles. This might be a result of the limited operation time of the microfluidics device due to clogging. But even comparing our results to the assumptions and results from ref. [131] and [133], we achieved a 50 % larger internal surface area even without surfactant templating due to the optimized droplet-based microfluidic reaction scheme. These improved qualities might be a result of the faster mixing of reagents inside the droplets and much shorter diffusion ways for the liquids in the droplets during the drying process

5.2   Microfluidic synthesis of Precious Metal Catalysts

Due to the enormous internal surface area and narrow pore size distribution of the silica particles produced through our microfluidic synthesis scheme, they would be ideal supports for catalytically active elements. Platinum (Pt) or palladium (Pd) doped silica catalysts [135] are highly active for catalytic combustion of hydrocarbon and other organic exhausts. Here we try to focus on propane oxidation reaction as model hydrocarbon. Yao et al. [136] investigated propane oxidation reactions and found Pt doped materials to be a better catalysts than Palladium and Rhodium doped materials for this reaction. Thus, we focus on the production of Pt doped silica spheres in our microfluidic approach.

Platinum compounds were readily dissolved in aqueous phase and can thus be in a straight forward manner applied to the platinum doped silica sphere production from the microfluidic sol-gel synthesis scheme mentioned in section 5.1. This microfluidic scheme is quite universal and therefore, the recipe (e.g. reagents for the chemical reaction) could be changed without any changes in the microfluidic scheme. In order to realize the production of metal catalysts through our microfluidic scheme, we added $Pt(NO_3)_2$ to the aqueous phase containing TMOS. Platinum contents up to about 7 mol.% (46 wt. %) can be dispersed along with the silica precursor tetramethoxysilane, TMOS ($Si(OCH_3)_4$, ABCR GmbH & Co. KG) in a mixture of methanol (Merck KGaA, Darmstadt, Germany) and water (Millipore^{TM}) at a volumetric ratio of 60/40 in the aqeuous phase A. The second type of aqueous phase B contains ammonia (Merck KGaA, Darmstadt, Germany) based on the same solvent having the same volumetric content (methanol/water, 60/40). Following the above mentioned microfluidic approach (section 5.1) of producing, merging and post-processing the droplets, Pt doped silica particles were collected outside the microfluidic device. Later, the calcination of these particles were also carried out at 550 °C as before to obtain Platinum doped silica spherical particles (see Fig. 42). A close look at the surface morphology of these particles clearly shows a difference depending on the Pt concentration added. Scanning electron micrographs of platinum doped silica particles revealed a cloudier surface morphology than silica particles without platinum doping as shown in Fig. 39.
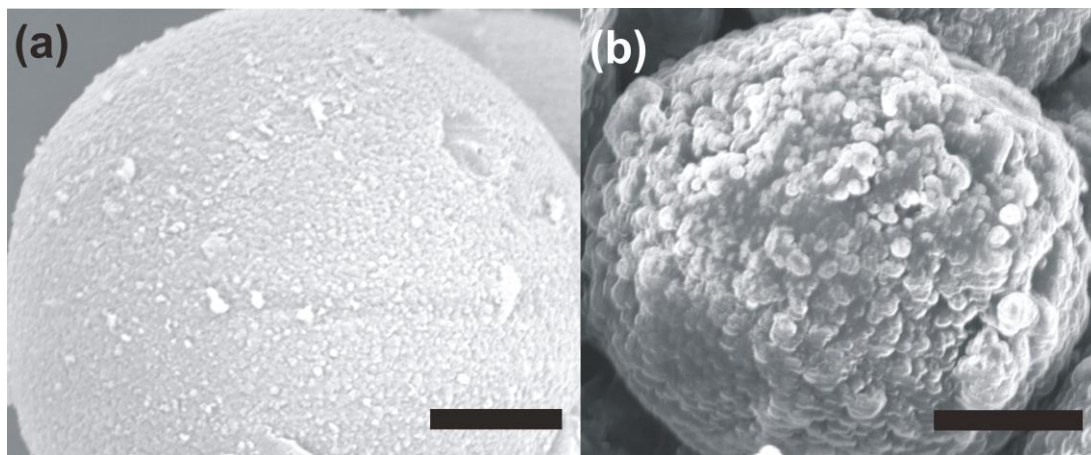
Figure 42. *SEM images of Pt doped silica microspheres: (a) 3 mol. % (20 wt. %), (b) 7 mol. %. (46 wt. %). Scale bar: 1 µm.*

In order to compare the composition and characteristics of the platinum doped silica particles produced via our microfluidic synthesis scheme with a commercially available platinum doped silica sample, we bought a bulk produced platinum doped silica catalyst (ABCR GmbH, Germany). This was used as a reference material for comparison. X-ray fluorescence (XRF) analysis of the samples was carried out to check the platinum content available in the reference material. Results revealed about 30 wt. % of platinum in the reference material. To allow for the quantitative comparisons, the microfluidic synthesis recipe is adjusted accordingly to produce platinum doped silica particles with the same platinum content as the reference material (Table 2). Moreover, Transmission Electron Micrographs (TEM) indicated both the candidates for comparison had metallic platinum arranged in face centered cubic lattice (see Fig. 43).

Material	Specific Surface Area SSA (m^2/g)	Pore radius (nm)	Pt (wt. %)	Si (wt. %)
Pt/SiO_2 – microfluidic synthesis scheme	590 ($\pm$ 20 m^2/g)	1.994	32.07 (4.91 mol. %)	67.93
Pt/SiO_2 – ref. material (ABCR)	138 ($\pm$ 20 m^2/g)	12.468	29.54 (4.43 mol. %)	70.46

Table 2. *Characterization results from the BET isotherms and XRF Analysis.*
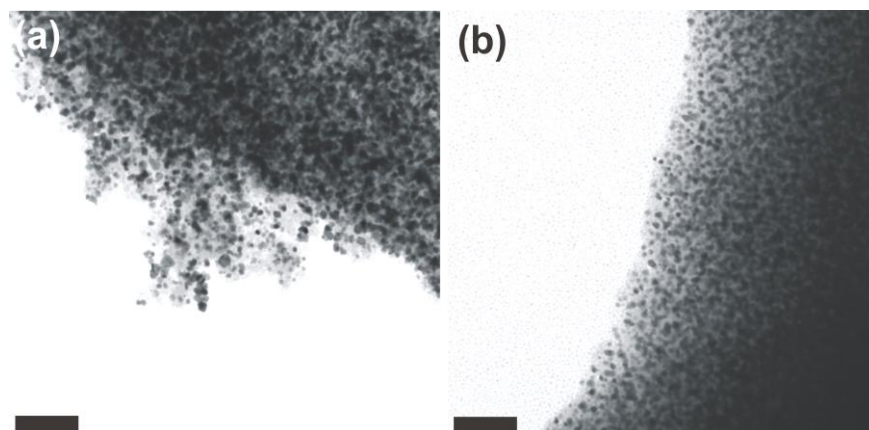
Figure 43. *TEM micrographs for (a) bulk synthesized reference platinum on silica, (b) microfluidically synthesized platinum on silica. Scalebar: 100 nm.*

To investigate if the microfluidically produced platinum doped silica particles have catalytic properties, emissivity corrected InfraRed Thermography (ecIRT) (section 4.4) was used for initial screening of catalyst libraries. The test was done for the propane (C_3H_8) oxidation reaction with the feed gas consisting of $C_3H_8/O_2/N_2$ and with a composition of about 0.4/20/79.6 vol. % at a flow rate of 50 ml/min. ecIRT image of a library is shown in Fig. 44. Commercially available industrial catalyst material Hopcolite (mixture of copper and manganese oxides) (Sigma Aldrich GmbH) was also used as a reference for this screening. It can be inferred from this screening that the platinum doped silica particles were found catalytically active through the resulting differential temperature as discussed in section 4.4 calculated by the software program. To understand the catalytic activity more precisely, conventional fixed bed catalyst testing is carried out.
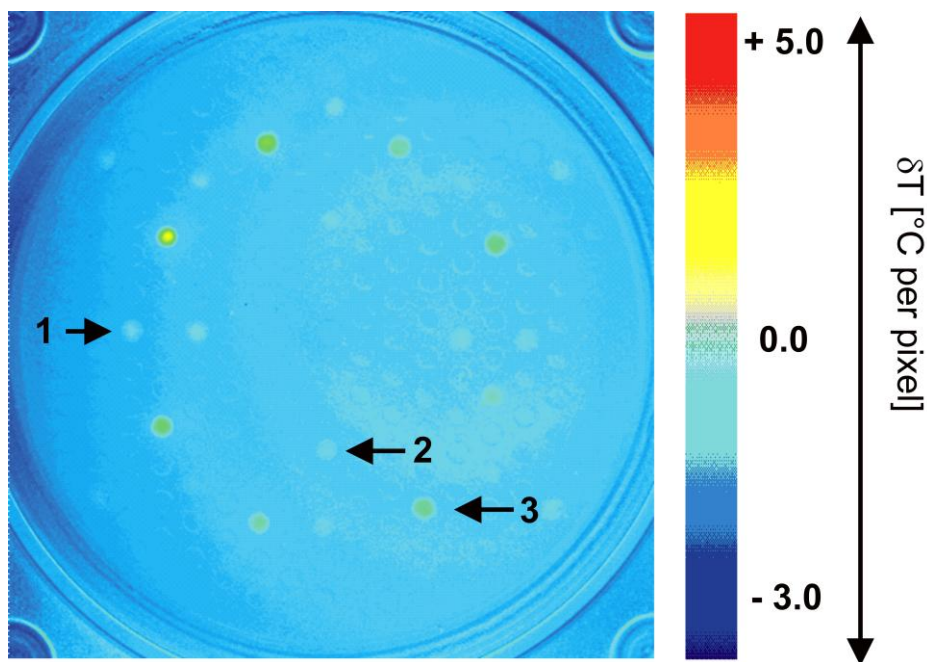
Figure 44. *Emissivity corrected infrared thermography (ecIRT) image for propane oxidation reactions. 1: 3 mol. % (20 wt. %) Pt doped silica, 2: 7 mol. %. (46 wt. %) Pt doped silica, 3: Hopcolite as reference.*

Conventional fixed bed tests were done with platinum doped silica particles produced by our microfluidic synthesis scheme as well as with bulk produced reference material from ABCR for the

propane oxidation reaction. Both the samples were tested in the fixed bed reactor [137] (section 4.4) with a total feed flow rate of 50 ml/min with operating temperature between 150 up to 350°C and a feed gas concentration of $C_3H_8/O_2/N_2 = 0.2/5/94.8$ vol. %. The catalytic behavior of the particles was evaluated by measuring propane conversion versus temperature (see Fig. 45). For best possible catalytic activity, it is very important for this conversion to take place at low temperatures [124]. Accordingly, the temperatures of 50 % conversion (T_{50}) were read out from the curves to compare the combustion activities of the catalysts. T_{50} for the reference ABCR sample (half filled circles in Fig. 45) is about 425 °C and is significantly higher than that of catalysts produced via microfluidic synthesis scheme (295 °C) (half filled diamonds in Fig. 45). For comparison, pure silica particles without platinum doping were also tested and were found with no catalytic behavior as expected (half filled pentagons in Fig. 45). This shows that platinum doped on silica particles produced via microfluidic synthesis scheme is much favorable for propane oxidation reactions than those available commercially.
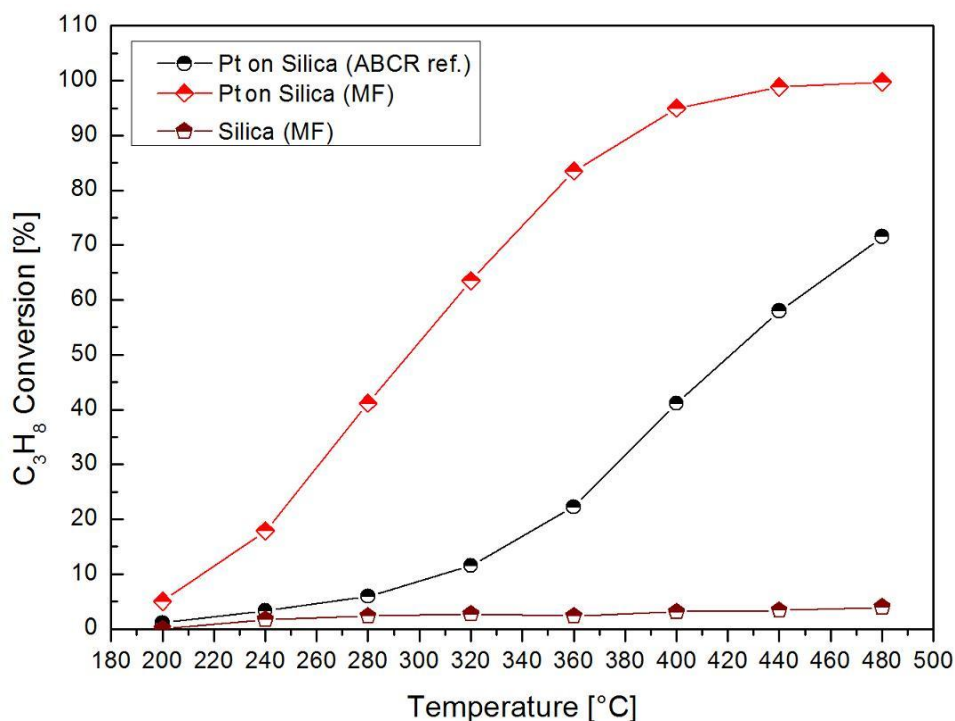
Figure 45. *Temperature dependence of the conversion of propane on Pt/SiO$_2$ in a gas phase flow reactor with reaction in increment order of temperatures from 200°C to 480°C.*

To explain the superior catalytic behavior obtained for catalysts produced via microfluidic synthesis scheme over commercial catalysts with the porosity of the silica particles, BET analysis (section 4.3) was done using nitrogen as adsorbate. The specific surface area of the ABCR reference catalyst particles was determined to be around 138 m^2/g ($\pm$ 20 m^2/g) with a pore size distribution maximum at 11.6 nm ($\pm$ 0.2 nm) pore radius with a cumulative pore volume of 0.28 cm^3/g ($\pm$ 0.02 cm^3/g). The corresponding BET isotherms and pore size distribution are shown in Fig. 46. Similarly, the porosity and the pore volume of the microfluidically synthesized platinum doped silica particles are investigated in a similar manner by a BET analyzer. The specific surface area of the produced catalyst particles averaged over several production runs and for various measurements was determined to be around 590 m^2g^{-1} ($\pm$ 20 m^2/g) with a pore size distribution maximum at 1.9 nm ($\pm$ 0.1 nm) pore radius and a cumulative pore volume of 0.54 cm^3/g ($\pm$ 0.02 cm^3/g). The corresponding BET isotherms and pore size distribution are shown in Fig. 47.
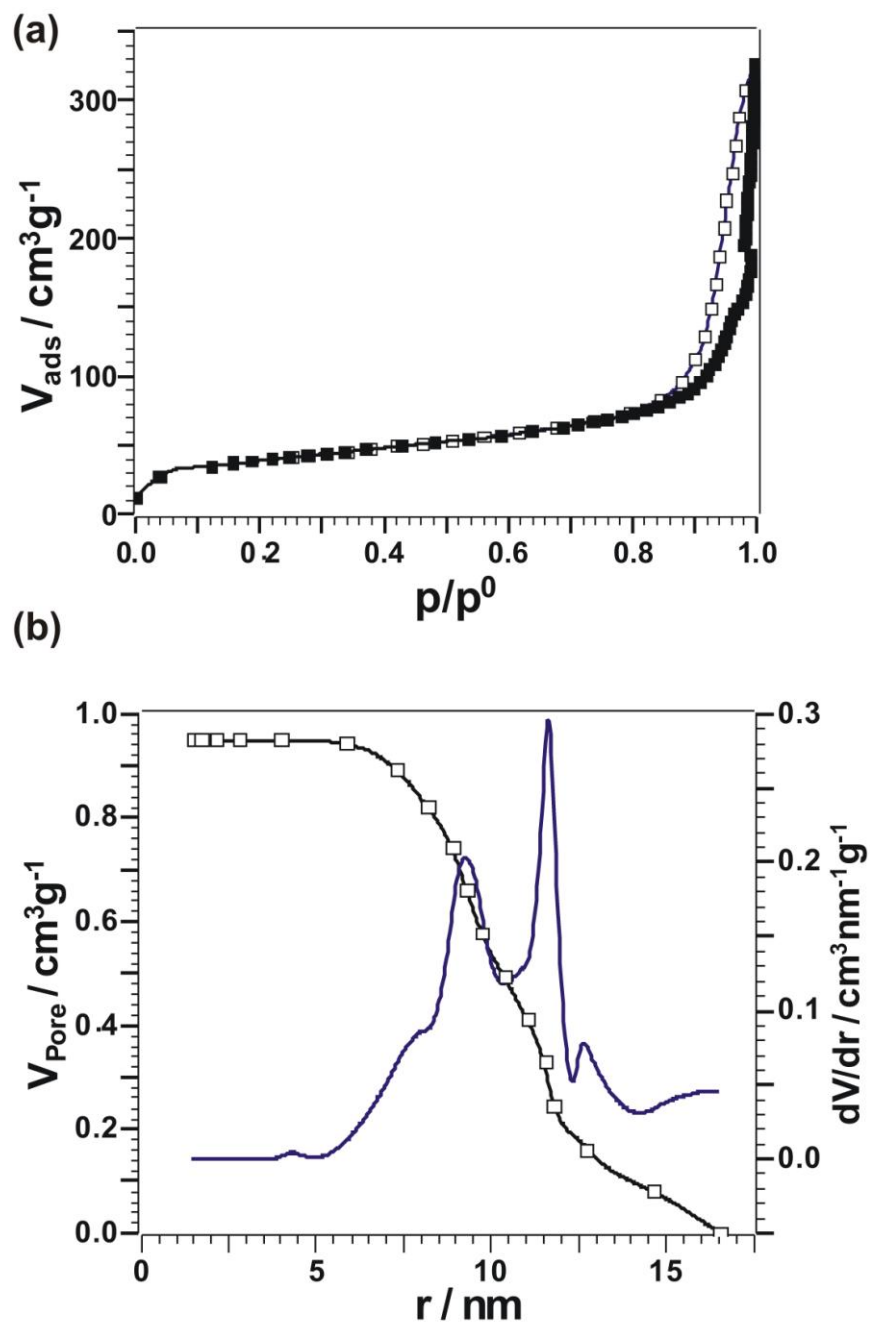
Figure 46. (a) *BET Nitrogen adsorption-desorption isotherm of the reference platinum doped silica catalyst (ABCR GmbH),* (b) *Pore size distribution.* V_{ads} = *adsorbed volume,* p/p_0 = *reduced pressure,* V_{pore} = *pore volume,* r = *pore radius.*
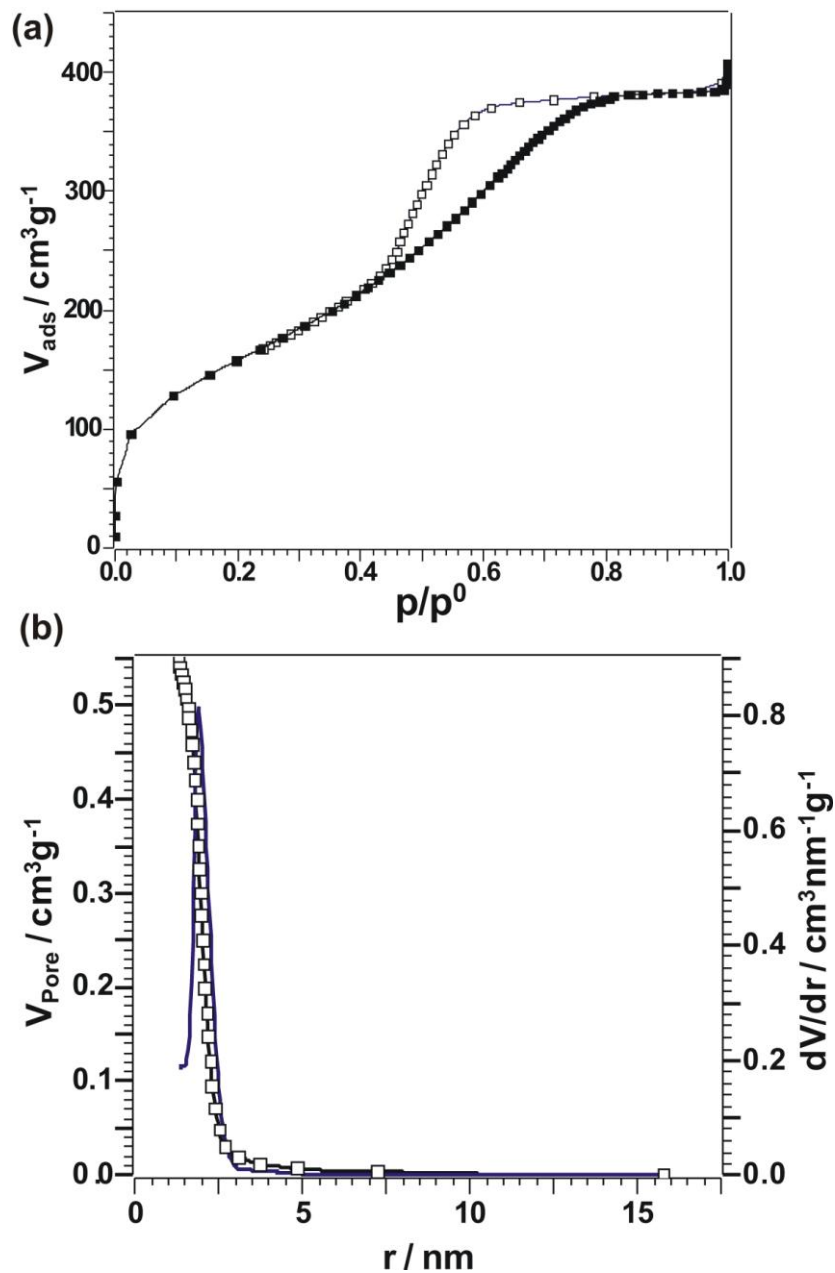
Figure 47. (a) *BET Nitrogen adsorption-desorption isotherm of the platinum doped silica catalyst produced through microfluidic scheme,* (b) *Pore size distribution.* V_{ads} = *adsorbed volume,* p/p_0 = *reduced pressure,* V_{pore} = *pore volume,* r = *pore radius.*

Comparing the surface areas shows a significant difference. Platinum doped silica catalysts prepared via our microfluidic synthesis scheme are superior in surface area by more than 3 times than that of the commercially available platinum doped silica catalysts (reference material). Moreover, our microfluidically produced silica supported catalyst has much smaller pores than the reference material from ABCR. In addition, the mixing inside the droplets and the entire process control is superior through microfluidics which might account for the large internal surface area and thereby influence the better catalytic behavior than the commercial catalysts. From the obtained results it is clear that our novel droplet-based microfluidic sol-gel reaction scheme offers great possibilities to synthesize catalyst materials with superior properties than commercially available catalyst products.

SUMMARY

We have presented a novel droplet-based microfluidic reaction scheme to perform chemical reactions with precise volume and process control that allows for fast reactions even forming gels or precipitates. The important steps developed for this scheme are the synchronized production of droplet pairs containing different reactants, controlled merging of the droplet pairs and mixing of the reactants inside the merged droplets. We proved this microfluidic scheme by performing sol-gel reactions to produce silica particles and platinum doped silica particles with superior properties.

To achieve the synchronized production of droplet pairs, we have presented step-emulsifying microfluidic devices produced by photo-lithography. We combined two of these devices into one double step-emulsification device which results in the production of pairs of droplets in a strictly alternating way. Several droplets with precise volume control and adjustable production frequency can be produced. The synchronization mechanism is very robust and makes the step-emulsification devices ideal for complex chemical reactions.

After the production of droplet pairs, the reaction is started by merging pairs of droplets by a geometrical constriction. After the merging, the reactive mixture is enclosed in the merged droplet that acts as a reaction container and never touches the microfluidic channel walls. Subsequent mixing of the reactants inside the merged droplets is very fast due to the flow induced convective motion. By this merging technique, chemical reactions forming gels or precipitates are possible for long operation times through our microfluidic scheme.

We demonstrated the power of our droplet-based microfluidic reaction scheme explicitly by producing monodisperse silica particles using sol-gel chemistry. For that an additional delay line and a thermal post processing line are included into the microfluidic device. The long and stable operational conditions allow for the first time to produce sufficient quantities of silica particles to perform quantitative analysis of their physical and chemical properties. We achieved mesoporous silica particles with a superior surface area of 820 m^2g^{-1} ($\pm$ 20 m^2g^{-1}) which is about 40 % more than typical bulk synthesis methods and a narrow pore radius distribution of around 2.4 nm. Efficient mixing of reagents within the droplet and shorter diffusion paths for the liquids in the droplets during the drying process help to achieve this improved quality. These superior properties obtained via microfluidic sol-gel synthesis scheme are further extended to produce platinum doped silica catalyst particles by slightly adjusting the sol-gel recipe. The results proved that the catalysts produced via microfluidic sol-gel synthesis scheme have superior surface area properties and therefore resulted in better catalytic behavior than the commercially available industrial catalysts.

From the obtained results we can conclude that the droplet-based microfluidic reaction scheme developed within the framework of this thesis offers great possibilities to perform complex chemical reactions and to synthesize materials with superior properties that were not possible with any existing microfluidic approach. This type of droplet-based microfluidic scheme is thus expected to have a large potential not only for synthesizing reactions but also for drug screening purposes or even combinatorial approaches when being combined with techniques to manipulate, redistribute and split merged droplets.

APPENDIX

Recipe for photolithographic devices

A.1   Underlayer

1. Rinse round glass slides with isopropanol (2-propanol), dry in nitrogen stream

2. Bake at 200◦C for 3-5 minutes

3. Spincoat OMNICOAT at 3000 rpm

4. Bake at 200◦C for > 2min

5. Cool hotplate to 95◦C (WAIT before continuing)

6. Spincoat SU8-2005 at 5000 rpm

7. Bake at 65◦C for 1min

8. Bake at 95◦C for 3min

9. Expose entire wafer (ie. no mask, soft contact) at 15 mW/cm2 for 20 sec

10. Bake at 65◦C for 1min

11. Bake at 95◦C for 1min

12. Plasma on 'HI' for 30 sec (samples upside down to avoid dust settling on layer).

A.2   Channel structures

A.2.1   Resist Structure: 30 μm channel height

1. Spincoat SU8-50 at 2000 rpm

2. Soft bake at 65◦C for 4min

3. Soft bake at 95◦C for 13min

4. Expose (through mask, HP contact mode) at 15 mW/cm2 for 30 sec

5. Post expose bake at 65◦C for 1min

6. Post expose bake at 95◦C for 2min

7. Develop for 2 min in SU8 developer on mechanical shaker.

A.2.2   Resist Structure: 50 μm channel height

1. Spincoat SU8-50 at 1500 rpm

2. Soft bake at 65◦C for 5min

3. Soft bake at 95◦C for 15min

4. Expose (through mask, HP contact mode) at 15mW/cm2 for 30 sec

5. Post expose bake at 65◦C for 1min

6. Post expose bake at 95◦C for 2min

7. Develop for 5min in SU8 developer on mechanical shaker.

A.2.3   Resist Structure: 80 μm channel height

1. Spincoat SU8-100 at 2000 rpm

2. Soft bake at 65◦C for 10min

3. Soft bake at 95◦C for 30min

4. Expose (through mask, HP contact mode) at 15mW/cm2 for 30 sec

5. Post expose bake at 65◦C for 1min

6. Post expose bake at 95◦C for 5min

7. Develop for 5min in SU8 developer on mechanical shaker.

A.2.4   Resist Structure: 120 μm channel height

1. Spincoat SU8-100 at 1700 rpm

2. Soft bake at 65◦C for 13min

3. Soft bake at 95◦C for 37min

4. Expose (through mask, HP contact mode) at 15 mW/cm2 for 30 sec

5. Post expose bake at 65◦C for 1min

6. Post expose bake at 95◦C for 7min

7. Develop for 8 min in SU8 developer on mechanical shaker.

A.3   Preparation of PMMA coated cover plate

1. Rinse round glass slides with isopropanol (2-propanol), dry in nitrogen stream

2. Bake at 180◦C for 3-5 minutes

3. If needed, gold electrodes were thermally vapor deposited at 10−6 mbar onto the cover

plate, with an underlying chromium adhesion layer.

4. Prepare the wires for electrode using CW2400 Conductive Epoxy Glue (ITWChemtronicsr)

5. Spincoat PMMA Photoresist (A11) at 1500 rpm

6. Bake at 180◦C for > 2 min

7. Check layer to ensure NO bubbles etc.

A.4 Thermal bonding of the channels and the cover plate

1. Drill the holes for the tubing connections through the supporting glass substrate

2. Clean the channels by nitrogen stream

3. Bond the cover plate coated with PMMA and the channel system at 160◦ at the thermal

bonding device by applying the pressure (max 0.6 bar) 2-3 times repeatedly to achieve

a good bonding.

A.5 Nanoport bonding

1. Prepare the bonding surfaces of both the Port and the microdevice by cleaning with isopropanol

2. Bond the Nanoport Flat Bottom Port to the microdevice using heat activated adhesive film tape
(FST 3M 583)

3. Clamp the Port to the microdevice. Place clamped Ports in oven at 120◦ for 90 mins to develop a
complete bonding

4. Connect the microchannel with teflon tubing using Nanoport Nut FT PEEK and Ferrule.

BIBLIOGRAPHY

[1]   Mohamed Gad-el-Hak, ed., The MEMS Handbook, CRC Press, 2001, ISBN 0-8493-00770.

[2]   Nadim Maluf, An introduction to Microelectromechanical Systems Engineering, Artech House Publishers, Norwood, 2000, ISBN 0-89006-581.

[3]   Pasi Kallio, Johanna Kuncova, Microfluidics, National Technology Agency, Technology Review 158/2004, Helsinki, 2004.

[4]   C-M Ho, Fluidics - The Link between Micro and Nano Sciences and Technologies, IEEE, 2001, 0-7803-5998-4/01.

[5]   Mohamed Gad-el-Hak, Journal of fluids engineering, Vol. 121, pg. 5-33, 1999.

[6]   D. R. Reyes, D. Iossifidis, P.-A. Auroux and A. Manz, Analytical Chemistry, 2002, 74, 2623-2636.

[7]   R. Jäggi, R. Sandoz and C. Effenhauser, Microfluidics and Nanofluidics, 2007, 3, 47-53.

[8]   R. Huang, T. A. Barber, M. A. Schmidt, R. G. Tompkins, M. Toner, D. W. Bianchi, R. Kapur and W. L. Flejter, Prenatal Diagnosis, 2008, 28, 892-899.

[9]   H. Bruus, Theoretical Microfluidics, Oxford University Press, USA, 2007, ISBN 0199235090.

[10]   H. A. Stone, A. D. Stroock and A. Ajdari, Annual Review of Fluid Mechanics, 2004, 36, 381-411.

[11]   S.-Y. Teh, R. Lin, L.-H. Hung and A. P. Lee, Lab on a Chip, 2008, 8, 198-220.

[12]   H. Kinoshita, S. Kaneda, T. Fujii and M. Oshima, Lab on a Chip, 2007, 7, 338-346.

[13]   I. Mezic, I, J. Fluid Mech, 2001, 431, 347-370.

[14]   G. Taylor, Proceedings of the Royal Society of London. Series A. Mathematical and Physical Sciences, 1954, 225, 473-477.

[15]   A. Günther, S. A. Khan, M. Thalmann, F. Trachsel, K. F. Jensen, Lab on a Chip, 2004, 4, 278-283.

[16]   S. A. Khan, A. Gunther, M. A. Schmidt and K. F. Jensen, Langmuir, 2004, 20, 8604–8611.

[17]   A. Günther and K. F. Jensen, Lab Chip, 2006, 6, 1487–1503.

[18]   H. Song, J. D. Tice and R. F. Ismagilov, Angew. Chem. Int. Edt., 2003, 42, 768-772.

[19]   L. Li, J. Q. Boedicker, R. F. Ismagilov, Anal. Chem., 2007, 79, 2756.

[20]   H. Song and R. F. Ismagilov, J. Am. Chem. Soc. 2003, 125, 14613.

[21]   J. Atencia and D. J. Beebe, Nature, 2005, 437, 648–655.

[22]   P.Tabling, Introduction to Microfluidics, Oxford University Press., ISBN: 0198568649.

[23]   Chen, D. L.; Gerdts, C. J.; Ismagilov, R. F. J. Am. Chem. Soc. 2005, 127, 9672.

[24]   H. Song, D. L. Chen, R. F. Ismagilov, Angew. Chem. Int. Ed., 2006, 45, 7336.

[25]   A. M. Thayer, Chem. Eng. News 2005, 83, 43.

[26]   I. Shestopalov, J. D. Tice, R. F. Ismagilov, Lab on a Chip, 2004, 4, 316-321.

[27]   E. R. Delsman, M. H. J. M. de Croon, G. D. Elzinga, P. D. Cobden, G. J. Kramer, J. C. Schouten, Chem. Eng. Technol., 2005, 28, 267-273.

[28]   E. Surenjav, C. Priest, S. Herminghaus and R. Seemann, Lab Chip, 2009, 9, 325–330.

[29]   S. Hutzler, N. Peron, D. Weaire and W. Drenckhan, Eur. Phys. J. E, 2004, 14, 381–386.

[30]   E. Surenjav, S. Herminghaus, C. Priest and R. Seemann, Appl. Phys. Lett., 2009, 95, 154104.

[31]   D. R. Link, S. L. Anna, D. A. Weitz and H. A. Stone, Phys. Rev. Lett., 2004, 92, 054503.

[32]   G. K. Batchelor, An Introduction to Fluid Dynamics, Cambridge University Press, 1967, ISBN 0521663962.

[33]   J. M. Ottino and S. Wiggins, Phil. Trans. R. Soc. Lond. A, 2004, 362, 923–935.

[34]   M. R. Bringer, C. J. Gerdts, H. Song, J. D. Tice and R. F. Ismagilov, Phil. Trans. R. Soc. Lond. A, 2004, 362, 1087–1104.

[35]   B. Zheng, L. S Roach, and R F. Ismagilov, J. Am. Chem. Soc., 2003, 125, 11170-11171.

[36]   J. M. Ottino, The kinematics of mixing: stretching, chaos, and transport. Cambridge University Press, 1989, ISBN: 0521368782.

[37]   S. Bashforth, J.C. Addams, Cambridge Unitersity Press and Deighton, Bell and Co, London, 1882, ISBN: 114497397X.

[38]   P. G. de Gennes Rev. Mod. Phys., 1985, 57, 827-863.

[39]   T. Young, Phil. Trans. Royal Soc., 1805, part I, 65.

[40]   S. Safran, Statistical Thermodynamics of Surfaces, Interfaces And Membranes, Addison-Wesley Publishing Company: New York, 1994, ISBN: 0201626330.

[41]   M. Schick, Liquids at Interfaces, Elsevier Science, Amsterdam, 1889, ISBN: 0444884505.

[42]   C. Domb, Phase Transition and Critical Phenomena, Vol. 12, Academic Press, London, 1988, ISBN: 0122203208.

[43]   T. Young, Phil. Trans. Royal Soc., 1805, part I, 65.

[44]   G. L. Hasenhuett, R. W. Hartel , Food Emulsifiers and Their Applications, Springer New York, 2008, ISBN 978-0-387-75283-9.

[45]   F. Nielloud and G. Marti-Meatres, Pharmaceutical Emulsions and Suspensions. Informa Healthcare, 2000, ISBN 0-824-0304-9.

[46]   Water-in-oil emulsion type cosmetics, United States Patent 5015469.

[47]   Water-thin emulsion formed by high pressure homogenization process, United States Patent 5994414.

[48]   K. Landfester, Macromol. Symp. 2000, 150, 171-179.

[49]   G. W. Goodwin, Colloids and Interfaces with Surfactants and Polymers – An introduction, Wiley-VCH Verlag GmbH & Co. KGaA, Weinheim, 2004, ISBN: 0470841435.

[50]   M. S. El-Aasser and E. D. Sudol, J. Coat. Tech. Res., 2004, 1, 21.

[51]   L. L. Schramm, E. N. Stasiuk and D. Gerrard Marangoni, Annu. Rep. Prog. Chem., Sect. C, 2003, 99, 3–48.

[52]   P. Taylor, Adv. Coll. Inter. Sci. 1998, 75, 107.

[53]   S. Mun, D. J. McClements, Langmuir 2006, 22, 1551.

[54]   T. F. Tadros, Applied Surfactants, WILEY-VCH Verlag GmbH & Co. KGaA, Weinheim, 2005, ISBN-13: 978-3-527-30629-9.

[55]   K.S. Birdi , Handbook of surface and colloid chemistry, 2003, CRC Press LLC, ISBN 0-8493-1079-2.

[56]   E. Kremer and G. Lagaly, Interfaces, Surfactants and Colloids in Engineering, 1996, Dr. Dietrich Steinkopff Verlag GmbH & Co. KG, Darmstadt, ISBN 3-7985-1057-1.

[57]   J.T. Davies, and E.K. Rideal, Interfacial Phenomena, 2nd ed., p 371, Academic Press, London, 1963.

[58]   W. Menz, J. Mohr and O. Paul, Microsystem Technology. Wiley-VCH, 2001. ISBN: 3527296344.

[59]   H. Lorenz, M. Despont, N. Fahrni, J. Brugger, P. Vettiger, and P. Renaud, Sens. Actuators A, 1998, 64, 33–39.

[60]   B. Xu, F. Arias, S. T. Brittain, X.-M. Zhao, B. Grzybowski, S. Torquato, and G. M. Whitesides, Adv. Mater., 1999, 11, 1186–1189.

[61]   J. H. Xu, S. W. Li, J. Tan, Y. J. Wang and G. S. Luo, Langmuir, 2006, 22, 7943-7946.

[62]   N. T. Nguyen, S. Lassemono, F. A. Chollet, Sensors and Actuators B 117, 2006, 431–436.

[63]   H. Lorenz, M. Despont, N. Fahrni, N. LaBianca, P. Renaud and P Vettiger, J. Micromech. Microeng., 1997, 7, 121–124.

[64]   H. Sato, H. Matsumura, S. Keino and S. Shoji, J. Micromech. Microeng., 2006, 16 2318–22.

[65]   M. G. Jenke, C. Schreiter, G. M. Kim, H. Vogel and J. Brugger, Microfluid. Nanofluid., 2007, 3, 189–94.

[66]   F. Walther, P. Davydovskaya, S. Zürcher, M. Kaiser, H. Herberg, A. M Gigler and R. W Stark, 2007, J. Micromech. Microeng., 17, 524.

[67]   M. J. Madou, Fundamentals of Microfabrication, 2002, CRC press, 2nd edtion, ISBN 0-8493-0826-7.

[68]   O. Geschke, H. Klank, P. Tellermann, Microsystem Engineering of Lab-on-a-Chip Devices, 2004, Wiley-VCH GmbH & Co. KGaA, ISBN 3-527-30733-8.

[69]   G. Voskerician, M. S. Shive, R. S. Shawgo, H. von Recum, J. M. Anderson, M. J. Cima and R. Langer, Biomaterials, 2003, 24, 1959–1967.

[70]   T. B. Christensen, C. M. Pedersen, K. G. Grondahl, T. G. Jensen, A Sekulovic, D. D. Bang and A. Wolff, J. Micromech. Microeng., 2007, 17, 1527–1532

[71]   Ren Yang, Wanjun Wang, Sensors and Actuators B , 2005, 110, 279–288.

[72]   Y. Xia and G. M. Whitesides, Annu. Rev. Mater. Sci., 1998, 28,153–84.

[73]   Y. Xia and G. M. Whitesides, Angew. Chem. Int. Edt., 1998, 37, 550.

[74]   I. Wong and C.-M. Ho, Microfluidics and Nanofluidics, 2009, 7, 291.

[75]   M. Eddings, M. Johnson, and B. Gale, J. Micromech Microeng., 2008, 18, 067001.

[76]   G. M. Whitesides, E. Ostuni, S. Takayama, X. Jiang, and D. E. Ingber, Annu. Rev. Biomed. Eng., 2001, 335–373.

[77]   D. Ganguli and M. Ganguli, Inorganic Particle Synthesis via Macro- and Microemulsions, Kluwer Academic/Plenum Publishers, New York, 2003, ISBN: 0306478773

[78]   T. Nisisako, T. Torii, T. Takahashi and Y. Takizawa, Adv. Mater., 2006, 18, 1152-1156.

[79]   K. Jensen and A. P. Lee, Lab on a Chip, 2004, 4, 31N–32N.

[80]   D. Belder, Angew. Chem. Int. Edt., 2005, 44, 3521–3522.

[81]   I. Kobayashi, K. Uemura and M. Nakajima, Colloids Surf., A, 2007, 296, 285–289.

[82]   T. Thorsen, R. W. Roberts, F. H. Arnold and S. R. Quake, Phys. Rev. Lett., 2001, 86, 4163.

[83]   T. Thorsen, R. W. Roberts, F. H. Arnold and S. R. Quake, Phys. Rev. Lett., 2001, 86, 4163–4166.

[84]   T. Nisisako, T. Torii and T. Higuchi, Lab Chip, 2002, 2, 24–26.

[85]   S. Marre, C. Aymonier, P. Subra, and E. Mignard, Appl. Phys. Lett., 2009, 95, 134105.

[86]   T. Nisisako, S. Okushima and T. Torii, Soft Matter, 2005, 1, 23–27.

[87]   A. S. Utada, E. Lorenceau, D. R. Link, P. D. Kaplan, H. A. Stone and D. A. Weitz, Science, 2005, 308, 537–541.

[88]   B. Zheng, J. D. Tice, L. S. Roach, R. F. Ismagilov, Angew. Chem. Int. Edt., 2004, 43, 2508.

[89]   B. Zheng, R. F. Ismagilov, Angew. Chem. Int. Edt.., 2005, 44, 2520.

[90]   P.Garstecki, M. J. Fuerstman, H. A. Stone and G. M. Whitesides, Lab on a Chip, 2006, 6, 437 – 446.

[91]   L. D. Landau and E. M. Lifshitz, Fluid Mechanics, Pergamon, London, 1959, 1st ed., ISBN: 0750627670.

[92]   G. I. Taylor, Proc. R. Soc. London A 146, 501 (1934).

[93]   Z. T. Cygan, J. T. Cabral, K. L. Beers and E. J. Amis, Langmuir, 2005, 21, 3629–3634.

[94]   S. L. Anna, N. Bontoux and H. A. Stone, Appl. Phys. Lett., 2003, 82, 364-366

[95]   P. Garstecki, I. Gitlin, W. DiLuzio, G. M. Whitesides, E. Kumacheva, and H. A. Stone, Appl. Phys. Lett., 2004, 85, 2649.

[96]   G. M. Whitesides , Nature 442, 368-373, 2006.

[97]   A. M. Gañan-Calvo, L. Martin-Banderas, R. G. Prieto, T. Berdun-Alvarez ; A. Cebolla, S. Chavez and M. Flores-Mosquera, M., Int. Jour. Pharm, 2006, 19, 324.

[98]   C. H. Lee, S. K. Hsiung and G. B. Lee, J. Micromech. Microeng., 2007, 17, 1121–1129.

[99]   F. Malloggi, S. A. Vanapalli, H. Gu, D. van den Ende and F. Mugele, J. Phys.: Condens. Matter, 2007, 19, 462101.

[100]   C. Priest, S. Herminghaus and R. Seemann, Appl. Phys. Lett., 2006, 88, 024106-024103.

[101]   V. Srinivasan, V. K.Pamula, and R. B. Fair, Analytica Chimica Acta, 2004, 507, 145-150.

[102]   N. Nguyen, S. Lassemono, F. A. Chollet, Sens. Actuators B, 2006, 117, 431.

[103]   V. Chokkalingam, S. Herminghaus and R. Seemann, Appl. Phys. Lett., 2008, 93, 254101-254103.

[104]   M. J. Fuerstman, A. Lai, M. E. Thurlow, S. S. Shevkoplyas, H. A. Stone and G. M. Whitesides, Lab on a Chip, 2007, 7, 1479-1489.

[105]   M. Chabert, K.D. Dorfman, and J.-L. Viovy, Electrophoresis, 2005, 26, 3706.

[106]   C. Priest, S. Herminghaus and R. Seemann, Appl. Phys. Lett., 2006 89, 134101 (2006)

[107]   S. Herminghaus, 1999, Phys. Rev. Lett., 83, pp. 2359-2361.

[108]   D. A. Sessoms, M. Belloul, W. Engl, M. Roche, L. Courbin and P. Panizza, Physical Review E, 2009, 80, 016317.

[109]   C. J. Brinker, G. W. Scherer, Sol-Gel Science: The Physics and Chemistry of Sol-Gel Processing, 1990Academic Press, Inc., Boston, ISBN: 0121349705.

[110]   K T. Anderson, James E. Martin, Judy G. Odinek, and Paula P. Newcomer Chem. Mater. 1998, 10, 311-321.

[111]   S. Brunauer, P. H. Emmett and E. Teller, Journal of the American Chemical Society, 2002, 60, 309-319.

[112]   I. Langmuir, J. Am. Chem. Soc., 1917, 39 (9), 1848-1906.

[113]   S. Brunauer, P. H. Emmett and E. Teller, Journal of the American Chemical Society, 2002, 60, 309-319.

[114]   E. P. Barrett, L. G. Joyner and P. P. Halenda, Journal of the American Chemical Society, 1951, 73, 373-380.

[115]   Lord Kelvin, Philos. Mag. 42, 1871, 448.

[116]   A. Holzwarth, H. W. Schmidt, W.F. Maier, Angew. Chem. Int. Edt., 1998, 37, 2644–2647.

[117]   A. Holzwarth; W.F. Maier, Platinum Met. Rev., 2000, 44, 16–21.

[118]   G. Kirsten, W.F. Maier, High Throughput Screening in Chemical Catalysis; Hagemeyer, A., Strasser, V., Volpe, A. F., Eds.; Wiley-VCH: Weinheim, Germany, 2004. ISBN: 978-3-527-30814-9.

[119]   J. C. Pouxviel, J. P. Boilot, J. C. Beloeil and J. Y. Lallemand, Journal of Non-Crystalline Solids, 1987, 89, 345-360.

[120]   R. K. Iler, The Chemistry of Silica Wiley, New York, 1979, ISBN: 978-0-471-02404-0.

[121]   V. Chokkalingam, B. Weidenhof, M. Krämer, W. F. Maier, S. Herminghaus and R. Seemann, Lab Chip, 2010, 10, 1700-1705.

[122]   J.-P. Bégué, D. Bonnet-Delpon, B. Crousse, Synlett, 2004, 1, 18–2905.01.204.

[123]   H. M. Evans, E. Surenjav, C. Priest, S. Herminghaus, R. Seemann and T. Pfohl, Lab on a Chip, 2009, 9, 1933-1941.

[124]   S. Storck, H. Bretinger and W. F. Maier, Applied Catalysis A: General, 1998, 174, 137-146.

[125]   K. S. W. Sing, Pure and Applied Chemistry. 1985, 57, 603.

[126]   S. Lowell, J. E. Shields, M. A. Thomas, M. Thommes, Characterization of Porous Solids and Powders: Surface Area, pore Size and Density, Springer, Dordrecht, 2006.

[127]   J. C. P. Broekhoff and J. H. de Boer, Journal of Catalysis, 1968, 10, 368-376.

[128]   V. Chokkalingam, B. Weidenhof, M. Krämer, S. Herminghaus, R. Seemann and W. F. Maier, Chemphyschem, 2010, 11, 2091 - 2095.

[129]   W. Stöber, A. Fink, E. Bohn, J. Colloid Interf. Sci. 1968, 26, 62-69.

[130]   I. C. Tilgner, P. Fischer, F. M. Bohnen, H. Rehage, W. F. Maier, Microporous Mater. 1995, 5, 77-90.

[131]   N. J. Carroll, S. B. Rathod, E. Derbins, S. Mendez, D. A. Weitz and D. N. Petsev, Langmuir, 2008, 24, 658-661.

[132]   I. Lee, Y. Yoo, Z. Cheng, H.-K. Jeong, Adv. Funct. Mater. 2008, 18, 4014-4021.

[133]   Y. Chen, Y. J. Wang, L. M. Yang and G. S. Luo, AIChE Journal, 2008, 54, 298-309.

[134]   N. Andersson, B. Kronberg, R. Corkery, P. Alberius, Langmuir 2007, 23, 1459

[135]   Y. Yazawa, N.Takagi, H.Yoshida, S.I.Komai, A. Satsuma, T. Tanaka, S. Yoshida, T. Hattori, Appl. Catal. A 233,2002, 103.

[136]   Y. F. Yu Yao, Ind. Eng. Chem . Prod. Res. Dev. 19, 1980, 293.

[137]   C. Mirodatos, Y. Schurmann, C. Hayayud, A. Holzwarth, D. Farusseng, T. Richter, European Patent, 2003, 1293772.
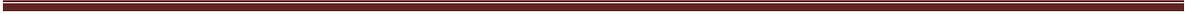
PUBLICATIONS

Platinum Doped Mesoporous Silica Spheres by Optimized Microfludiic Sol-Gel Synthesis Scheme
V. Chokkalingam, B. Weidenhof, W. F. Maier and R. Seemann
Proc. of 8th International ASME Conference on Nanochannels, Microchannels, and Minichannels
(ICNMM), Montreal, Canada, 2010. (accepted)

Template-Free Preparation of Mesoporous Silica Spheres Through Microfluidics
V. Chokkalingam, B. Weidenhof, M. Kraemer, S. Herminghaus, R. Seemann and W. F. Maier
ChemPhysChem, 11, 2091 - 2095, 2010.

Optimized Droplet-based MIcrofluidic Scheme for Sol-Gel Reactions
V. Chokkalingam, B. Weidenhof, M. Kraemer, W. F. Maier, S. Herminghaus and R. Seemann
Lab on a Chip, 10, 1700 - 1705, 2010.

Self-synchronizing Pairwise Production of Monodisperse Droplets by Microfluidic Step-Emulsification
V. Chokkalingam, S. Herminghaus and R. Seemann
Applied Physics Letters 93, 254101, 2008.

Controlled Production of Monodispersed Silica Microspheres Using a Double Step-Emulsification Device
V. Chokkalingam, B. Weidenhof, W. F. Maier, S. Herminghaus and R. Seemann
Proc. of 6th International ASME Conference on Nanochannels, Microchannels, and Minichannels
(ICNMM), Darmstadt, Germany, ISBN: 978-0-7918-4834-0, 1527-1535, 2008.

Self-Synchronizing Droplets with Double Step-Emulsification Devices
V. Chokkalingam, S. Herminghaus and R. Seemann
Proc. of The 12th International Conference on Miniaturized Systems for Chemistry and Life
Sciences (μTAS), ISBN: 978-0-9798064-1-4, 1438-1440, 2008.

Step-Emulsification Microfluidics for Production of Monodispersed High Surface Area Silica
Microparticles
V. Chokkalingam, B. Weidenhof, W. F. Maier, S. Herminghaus and R. Seemann
Proc. of the 1st European Conference on Microfluidics (MicroFlu'08), Bologna, Italy, ISBN 2-906831-76-X, 089, 2008.

Synthesis of Silica Microparticles with Step-Emulsification Microfluidics
V. Chokkalingam, B. Weidenhof, W. F. Maier, S. Herminghaus and R. Seemann
Proc. of The 12th International Conference on Miniaturized Systems for Chemistry and Life
Sciences (μTAS), ISBN: 978-0-9798064-1-4, 444-446, 2008.

Discrete Microfluidics: Production of Silica Particles with Emulsions
V. Chokkalingam, C. Priest, W.F. Maier, S. Herminghaus and R. Seemann
Proc. of The 11th International Conference on Miniaturized Systems for Chemistry and Life
Sciences (μTAS), ISBN 978-0-9798064-0-7, Paris, France, 1534-1537, 2007.

Awards

"Outstanding Research Poster Award" - Gordon Research Conference (GRC) on "Microfluidics, Physics and Chemistry of", Lucca, Italy, 2009.

"Best Poster Award" (1st Prize) - German Research Foundation (DFG) Summer Workshop on "Micro- and Nano- fluidics", Bad Honnef, Germany, 2009.

Scientific talks

Microfluidic Platforms for Rapid Chemical Reactions
Institute for Nanostructural Research and Nanotechnology (Prof. Hartmann), Saarland University, Germany, 04/2010.

Template-Free Preparation of Mesoporous Silica Spheres Through Multiphase Microfluidics
PhD Students' Day, Saarland University, Germany, 02/2010.

Optimized Multiphase Microfluidics for Chemical Synthesis
Winter school: Soft Condensed Matter, Feldberg, Germany, 12/2009.

Micro-Droplets in Action: for Complex Reactions
German-Chinese Summer School for Microsystem Technology [Organized by German Academic Exchange Service (DAAD)] at Science Park, Saarland University, Germany, 09/2009.

Microfluidic Physics of Self-synchronizing Picolitre Droplet Generation
73nd annual meeting of the German Physical Society (DPG'09), Condensed Matter Division, Session: Microfluidic Applications and Devices, Dresden, Germany, 03/2009.

Synthesis of Silica Microspheres with Step-Emulsification Microfluidics
PhD Students' Day, Saarland University, Germany, 02/2009.

Step-Emulsification Microfluidics for Production of Monodispersed High Surface Area Silica Microparticles
1st European Conference on Microfluidics (μFlu'08), Bologna, Italy, 12/2008.

Controlled Production of Monodispersed Silica Microspheres Using a Double Step-Emulsification Device
ASME 6th International Conference on Nanochannels, Microchannels, and Minichannels (ICNMM'08), Darmstadt, Germany, 06/2008.

Droplet Microfluidic Emulsion Technology for Chemical Lab-On-a-Chip Applications
Winter school: Soft Condensed Matter, Feldberg, Germany, 12/2007.

Discrete Microfluidic Emulsion Technology for Chemical Lab-On-a-Chip Applications
Friday-Seminar series, Max Planck Institute for Dynamics and Self-Organisation, Germany, 07/2007.

Discrete Microfluidics: Combinatorial Chemistry with Emulsions
Winter school: Soft Condensed Matter, Feldberg, Germany, 12/2006.

Poster Presentations

Optimized Droplet based Microfluidics for Sol-Gel Synthesis Routes
74th annual meeting of the German Physical Society (DPG'10), Condensed Matter Division,
Session: Micro and Nano Fluidics, Regensburg, Germany; 03/2010.

Self-Synchronizing Microfluidic Droplet Physics for Lab-On-Chip Applications
74th annual meeting of the German Physical Society (DPG'10), Condensed Matter Division,
Session: Micro and Nano Fluidics, Regensburg, Germany; 03/2010.

Step Emulsification Microreactor and its Application for Complex Chemical Reactions
German Research Foundation (DFG) Summer Workshop on "Micro- and Nano- fluidics", 07/2009.

Microfluidics assisted Sol-Gel Preperation of Mesoporous Silica Spheres by Self-Synchronizing
Monodisperse Droplet Pairs
Gordon Research Conference (GRC) on "Microfluidics, Physics & Chemistry Of", Lucca (Barga),
Italy, 06/2009.

Step-Emulsification Microfluidics for the Generation of Spherical Mesoporous Silica Particles
73nd annual meeting of the German Physical Society (DPG'09), Condensed Matter Division,
Session: Colloids and Liquids, Dresden, Germany; 03/2009.

Self-Synchronizing Droplets with Double Step-Emulsification Devices
12th International Conference on Miniaturized Systems for Chemistry and Life Sciences
(μTAS'08), San Diego, USA; 10/2008.

Synthesis of Silica Microparticles with Step-Emulsification Microfluidics
12th International Conference on Miniaturized Systems for Chemistry and Life Sciences
(μTAS'08), San Diego, USA; 10/2008.

Monodisperse silica micro spheres produced with step-emulsification microfluidics
3rd workshop on Pattern Formation & Transport in Complex Systems, Graduate College, Saarland
University, Germany; 09/2008.

Droplet-Based Emulsion Microfluidics for Monodisperse Silica Particle Synthesis
Condensed Matter Division, Session: Micro and Nano Fluidics - migration and flow , Berlin,
Germany; 02/2008.
Discrete Microfluidics: Production of Silica Particles with Emulsions
11th International Conference on Miniaturized Systems for Chemistry and Life Sciences
(μTAS'07), Paris, France; 10/2007.

Discrete Microfluidics: Combinatorial Chemistry with Emulsions
71st Annual Meeting of the German Physical Society (DPG'07), Condensed Matter Division, Regensburg, Germany; 03/2007.

ACKNOWLEDGEMENTS

"When we become more fully aware that our success is due in large measure to the loyalty, helpfulness, and encouragement we have received from others, our desire grows to pass on similar gifts. Gratitude spurs us on to prove ourselves worthy of what others have done for us. The spirit of gratitude is a powerful energizer."

Wilferd A. Peterson

The accomplishment of this thesis would not have been possible without the guidance, contribution and support from many different people.

First of all, I am in great debt to my supervisor **Prof. Dr. Ralf Seemann**. I thank him for giving me the opportunity to conduct this interesting research. Without his enthusiastic guidance, I could not choose this topic and begin the thesis. He has given me all the freedom and independence to work in my own way. Whenever I approached him with a problem, he was always ready to help me out from any kind of situations. I am *blessed* to work with such a supervisor. Also thanks for his patient and careful revisal of this thesis. Furthermore, his kind encouragement made me attend several conferences and present my research work in the scientific community.

I would also like to thank **Prof. Dr. Stephan Herminghaus** for giving me the opportunity to conduct research in his complex fluids group at Max Planck Institute for Dynamics and Self-Organization (MPI-DS). I also have to thank **Prof. Dr. Karin Jacobs** for organizing winter schools together with Prof. Seemann. These schools helped me realize the importance of scientific presentations and helped me improve my presentation skills.

The research atmosphere and flexible environment provided by the rest of the Seemann group both in Göttingen and Saarbrücken helped and inspired me enormously to realize self-fulfillment

during my work. I enjoyed several discussions with *Mario*, *Axel* and *Klaus* who were sharing the office room with me at Göttingen and *Carsten* and *Michael* at Saarbrücken. They helped me a lot with my research and my personal issues. Among their company, I never felt alone, and enjoyed myself during my doctoral life.

I am lucky to have wonderful colleagues and special thanks to all of them: especially *Udo Kraft, Wolf Keiderling, Krishna*, *Enkhtuul*, *Konstantina*, *Shashi and Yas* during my stay in Göttingen; *Somnath*, *JB*, *Carsten*, *Dominik*, *Kamal*, *MJ*, *MH*, *Stefan*, *Hagen* and *Marc* in Saarbrücken. They also helped me whenever I was not comfortable with *my German language* knowledge. I wish them all a good luck for their present and future life. I would specially like to thank **Dr. Craig Priest** for helping me with my very first experiments in Göttingen and always encouraging me with fruitful discussions when we meet in conferences.

It would not end without thanking my *Indian friends* in Göttingen and Saarbrücken for their social support and valuable suggestions. Among them are Anmol, Ratika, Sunil, Manmohan, Priya, Vimal, Harish, Nivethida, Ragav, Rosan, Anant, kalyani, Sravanti, Sweta, Selva, Ramanan, Shiva and Harish. You all have been wonderful friends and I will always cherish my association with you in Germany. Also I would like to thank my badminton and cricket friends Srikanth, Ajaz, Ram and Gawas. I really appreciate all your love and support during all ups and downs in my life.

Last but not least, I wish to express my love and gratitude to my family. I am particularly indebted to my parents. Without their selfless support and encouragement, I can not reach at this stage of my life. I thank them for their countless patience and never-ending support towards achieving this goal. I **dedicate** this thesis to my parents. I can never forget their sacrifices for the betterment of my life. I give a special thanks to my wife, Aarthy. She has been a tremendous support and constant source of encouragement in my life. Also, I would like to thank God for the wisdom and perseverance that he has been bestowed upon me during this research project, and indeed, throughout my life.

CURRICULUM VITAE

Personal Information

Name: Venkatachalam Chokkalingam
Date of Birth: 3rd June 1982
Place of Birth: Chennai, India
Present address: Waldhausweg 19, Apartment 73-01-02, 66123 Saarbrücken, Germany
e-mail: venkat.chona@gmail.com, venkat.chokkalingam@physik.uni-saarland.de
Nationality: Indian

Education

PhD candidate   (Oct 2006 – present)
(Geometry of Fluid Interfaces - Prof. Dr. Ralf Seemann)
    Saarland University, Saarbrücken, Germany,   (Feb 2009 – present)
    MPI for Dynamics and Self Organization, Gottingen, Germany.   (Oct 2006 – Jan 2009)

Master of Science (M.S.) in Microsystem Technology   (August 2006)
    Hamburg University of Technology (TUHH), Hamburg, Germany.

Bachelor of Engineering in Electrical and Electronics   (April 2003)
    Madurai Kamaraj University, Madurai, India.
    Mepco Schlenk Engineering College, Sivakasi, India.

High School Leaving Cerificate   (April 1999)
    AV.M. Higher Secondary School, Chennai, India.

Declaration

I hereby swear in lieu of an oath that I have independently prepared this thesis and without using other aids than those stated. The data and concepts taken over from other sources or taken over indirectly are indicated citing the source. The thesis was not submitted so far either in Germany or in another country in the same or a similar form in a procedure for obtaining an academic title.

Saarbrücken, 23rd July 2010.

(Venkatachalam Chokkalingam)

Eidesstattliche Erklärung

Hiermit versichere ich an Eides statt, dass ich die vorliegende Arbeit selbstÄandig und ohne Benutzung anderer als der angegebenen Hilfsmittel angefertigt habe. Die aus anderen Quellen oder indirekt Äubernommenen Daten und Konzepte sind unter Angabe der Quelle gekennzeichnet. Die Arbeit wurde bisher weder im In- noch im Ausland in gleicher oder Äahnlicher Form in einem Verfahren zur Erlangung eines akademischen Grades vorgelegt.

Saarbrücken, 23rd July 2010.

(Venkatachalam Chokkalingam)